Quantitative risk assessment of the effects of climate change on selected causes of death, 2030s and 2050s

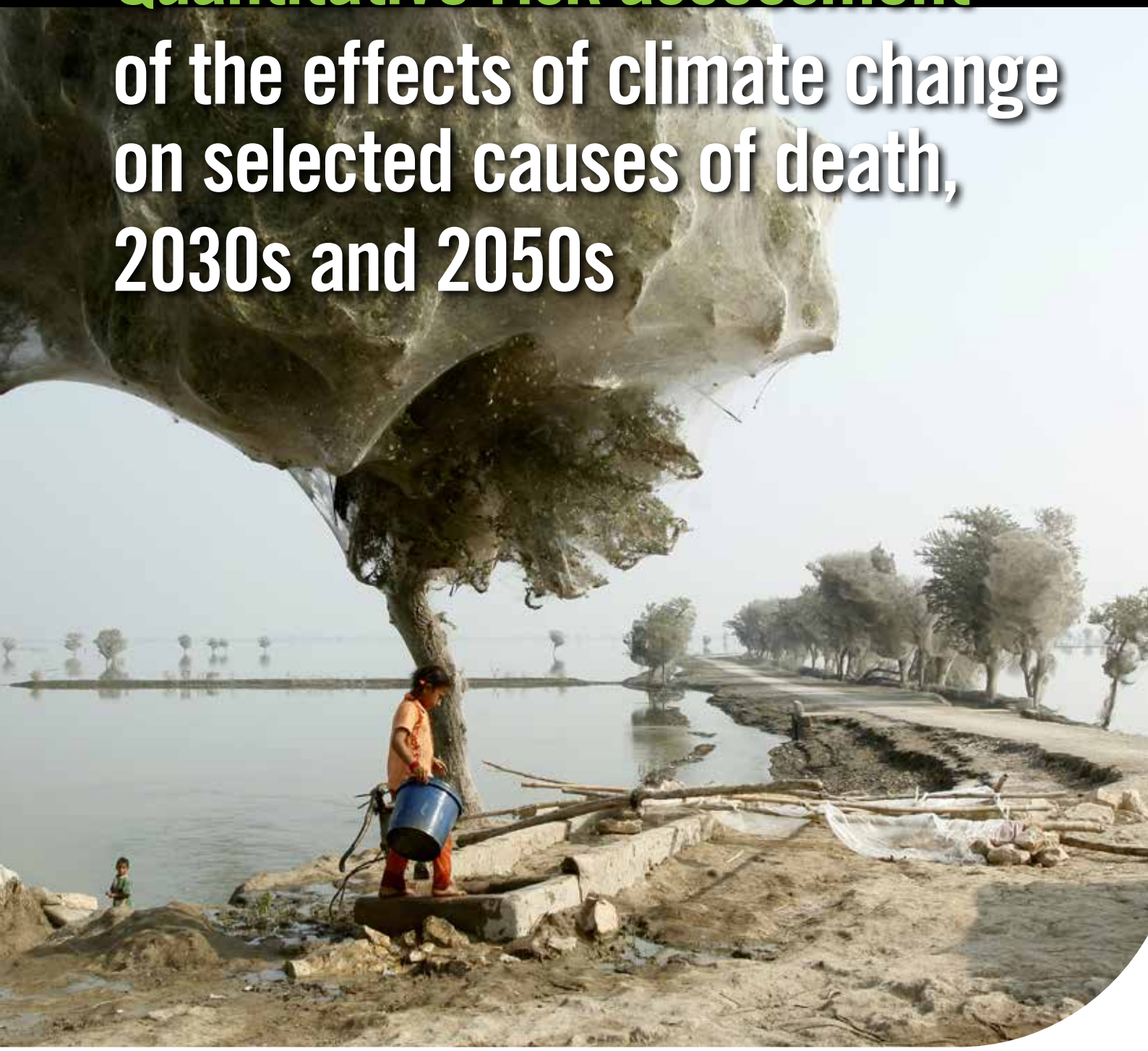

World Health Organization

Editors: Simon Hales, Sari Kovats, Simon Lloyd, Diarmid Campbell-Lendrum

WHO Library Cataloguing-in-Publication Data

Quantitative risk assessment of the effects of climate change on selected causes of death, 2030s and 2050s.
1.Climate Change. 2.Environmental Health. 3.Mortality – trends. 4.Risk Assessment. I.World Health Organization.

ISBN 978 92 4 150769 1 (NLM classification: WA 30.5)

Printed in Switzerland

Cover photo: © Russell Watkins/DFID UK Department for International Development

Photo caption: Flooding following extreme rainfall in Pakistan in 2010, with trees covered in webs made by spiders displaced by rising waters. Climate change is expected to increase temperatures and alter precipitation patterns, leading to a range of risks, from increased risks of water-borne infections, to changing transmission cycles of vector-borne disease, to impacts on agricultural production and malnutrition.

Data source and map production of figure 2.3: Simon Hales

Copyediting and layout: Inis Communication – www.iniscommunication.com

Quantitative risk assessment of the effects of climate change on selected causes of death, 2030s and 2050s

World Health Organization

Acknowledgements

This work was funded by the World Health Organization (WHO), with institutional support for non-funded participants. The work was undertaken by an international consortium coordinated by the London School of Hygiene and Tropical Medicine (United Kingdom of Great Britain and Northern Ireland), the University of Otago (New Zealand) and WHO. Mariam Otmani del Barrio from the Department of Public Health, Environmental and Social Determinants of Health, WHO, was responsible for managing the completion of the assessment and the production of the report.

The climate projections were derived from the ENSEMBLES project, which was funded by the European Union (EU) FP6 Integrated Project ENSEMBLES (contract no. 505539). This research also uses data provided by the Bergen Climate Model project (http://www.bjerknes.uib.no/pages.asp?id=1837&kat=8&lang=2) at the Bjerknes Centre for Climate Research, funded largely by the Research Council of Norway.

The authors would like to thank Ian Harris at the Climate Research Unit, University of East Anglia, for processing and providing the climate model data. We also thank the individual climate modelling groups.

Chapter 2: This study was supported by Environment Research and Technology Development Fund S-8 and S-10 from the Ministry of the Environment, Japan and the Global Research Laboratory (no. K21004000001–10AO500–00710) through the National Research Foundation funded by the Ministry of Education, Science and Technology, Republic of Korea.

Chapter 3: We thank Sally Brown and Robert Nicholls for providing data on coastal flooding exposures from the Dynamic Interactive Vulnerability Assessment (DIVA) model, and for advice on the assessment. For the flood mortality data, we used the International Disaster Database (EM-DAT) at the Centre for Research on the Epidemiology of Disasters, Belgium (http://www.emdat.be).

Chapter 5: We thank Simon Hay and the Malaria Atlas Project team for providing access to the malaria map data (http://www.map.ox.ac.uk/).

Chapter 7: We used data produced by the International Food Policy Research Institute (IFPRI) to accompany the report *Food security, farming, and climate change to 2050* (http://www.ifpri.org/sites/default/files/publications/climatemonograph_advance.pdf).

We also thank the anonymous reviewers for their comments on the report.

Contents

Figures

Tables

Abbreviations

AIDS	acquired immunodeficiency syndrome
CCRA	Climate Change Risk Assessment
CIESIN	Center for International Earth Science Information Network
CRED	Centre for Research on the Epidemiology of Disasters
CRU	Climate Research Unit (University of East Anglia, United Kingdom of Great Britain and Northern Ireland)
CSIRO	Commonwealth Scientific and Industrial Research Organisation
DALY	disability-adjusted life-year
DIVA	Dynamic Interactive Vulnerability Assessment
DSSAT	Decision Support System for Agrotechnology Transfer
EGMAM	ECHO-G Middle Atmosphere Model
EM-DAT	Disaster Events Database
EU	European Union
FAO	Food and Agriculture Organization of the United Nations
GDP	gross domestic product
HIV	human immunodeficiency virus
IIASA	International Institute of Applied Systems Analysis
IFPRI	International Food Policy Research Institute
IMF	International Monetary Fund
IMPACT	International Model for Policy Analysis of Agricultural Commodities and Trade
IPCC	Intergovernmental Panel on Climate Change
MIROC	Model for Interdisciplinary Research on Climate (Japan)
NCEP	National Centers for Environmental Prediction (United States of America)
OECD	Organisation for Economic Co-operation and Development
SRES	Special Report on Emissions Scenarios
UN	United Nations
UNDP	United Nations Development Programme
UNICEF	United Nations Children's Fund
UNISDR	United Nations International Strategy for Disaster Reduction
WHO	World Health Organization

Executive summary

Better evidence is required regarding future risks to health from global climate change in order to inform mitigation (low carbon) and adaptation (public health) policy development. Future climate change is likely to affect proximal and distal (upstream) risk factors for a wide range of health outcomes, but only some of these causal pathways can be modelled using currently available methods and at the global level. This assessment uses scenarios to estimate the effect of climate change on selected health outcomes in the context of uncertain climate and global health futures.

Future cause-specific mortality in 2030 and 2050 (in the absence of climate change) was estimated using regression methods for three development futures: base case, high growth and no growth scenarios. Global climate-health models were developed for a range of health outcomes known to be sensitive to climate change: heat-related mortality in elderly people, mortality associated with coastal flooding, mortality associated with diarrhoeal disease in children aged under 15 years, malaria population at risk and mortality, dengue population at risk and mortality, undernutrition (stunting) and associated mortality. Future climate change was characterized by a medium-high emissions scenario (A1b) run through three climate models. The counterfactual was a future world with population growth and economic development but with baseline (1961–1990) climate. The annual burden of mortality due to climate change was estimated for world regions. For most pathways considered, the results reflect both positive and negative impacts on health. Model uncertainty was assessed for each outcome, as far as technically possible.

Compared with a future without climate change, the following additional deaths are projected for the year 2030: 38 000 due to heat exposure in elderly people, 48 000 due to diarrhoea, 60 000 due to malaria, and 95 000 due to childhood undernutrition. The World Health Organization (WHO) projects a dramatic decline in child mortality, and this is reflected in declining climate change impacts from child malnutrition and diarrhoeal disease between 2030 and 2050. On the other hand, by the 2050s, deaths related to heat exposure (over 100 000 per year) are projected to increase. Impacts are greatest under a low economic growth scenario because of higher rates of mortality projected in low- and middle-income countries. By 2050, impacts of climate change on mortality are projected to be greatest in south Asia. These results indicate that climate change will have a significant impact on child health by the 2030s.

Under a base case socioeconomic scenario, we estimate approximately 250 000 additional deaths due to climate change per year between 2030 and 2050. These numbers do not represent a prediction of the overall impacts of climate change on health, since we could not quantify several important causal pathways.

A main limitation of this assessment is the inability of current models to account for major pathways of potential health impact, such as the effects of economic damage, major heatwave events, river flooding and water scarcity. The assessment does not consider the impacts of

climate change on human security, for example through increases in migration or conflict. The included models can capture only a subset of potential causal pathways, and none account for the effects of major discontinuities in climatic, social or ecological conditions.

Overall, climate change is projected to have substantial adverse impacts on future mortality, even considering only a subset of the expected health effects, under optimistic scenarios of future socioeconomic development and with adaptation. This indicates that avoiding climate-sensitive health risks is an additional reason to mitigate climate change, alongside the immediate health benefits that are expected to accrue from measures to reduce climate pollutants, for example through lower levels of particulate air pollution. It also supports the case for strengthening programmes to address health risks including undernutrition, diarrhoea, vector-borne disease and heat extremes, and for including consideration of climate variability and change within programme design. The strong effect of socioeconomic development on the projections of future risks emphasizes the need to ensure that economic growth, climate policies and health programmes particularly benefit the poorest and most vulnerable populations.

Introduction and key findings

1

Sari Kovats, Simon Hales, Simon Lloyd

Climate change risks are systemic and long term in nature, requiring a different approach to assessment compared with other environmental exposures. Global burden of disease studies have focused on proximal risk factors and historical patterns (Lim et al., 2012), with relatively little attention paid to upstream causes. Burden of disease studies also focus on current exposures rather than future exposure and the long timescales required by climate change assessments. Climate change poses qualitatively different risks to human health, mainly via indirect pathways (McMichael, 1999, 2013). These features result in unique challenges for health risk assessment. There is a need to improve estimates of the effects of climate change on health on a global and regional scale (Campbell-Lendrum et al., 2007; Costello et al., 2009). The latest assessment of the Intergovernmental Panel on Climate Change (IPCC) found significant evidence gaps (Smith et al., 2014). For example, uncertainties about future vulnerability, exposure and responses of interlinked human and natural systems were acknowledged to be large, indicating the need to explore a wide range of socioeconomic futures in assessments of climate change-related risks.

This report summarizes the potential impact of climate change on health metrics and attributable mortality for two future time periods: 2030 and 2050. The assessment is an advance on previous studies (Campbell-Lendrum & Woodruff, 2006), but it is still constrained by limited quantitative information about, and understanding of, causal mechanisms linking climate with health impacts on a global and local scale. We did not assess the current burden of disease due to observed climate change (warming since the 1960s) (WHO, 2009a).

Since the first global risk assessment was published (McMichael et al., 2004), there has been some development of global models to estimate climate change impacts for a range of health issues, particularly for malaria (Caminade et al., 2014) and undernutrition (Nelson et al., 2010; Lloyd et al., 2011).

The health impacts of climate change described in this report are mortality caused by heat, coastal flooding, diarrhoeal disease, malaria, dengue and undernutrition (Figure 1.1). Models were run with a consistent set of climate, population and socioeconomic scenarios, as far as was technically possible. In keeping with current approaches to scenario-based climate impacts assessment, climate and non-climate scenarios were kept separate in the presentation of results. We also assessed, as far as possible, uncertainties associated with each impact model. We assessed the effect of climate model uncertainty by including a range of climate model projections. Estimates were done with and without inclusion of adaptation to climate change, as far as technically feasible (Table 1.1).

Figure 1.1 Models used in this assessment, with output metrics

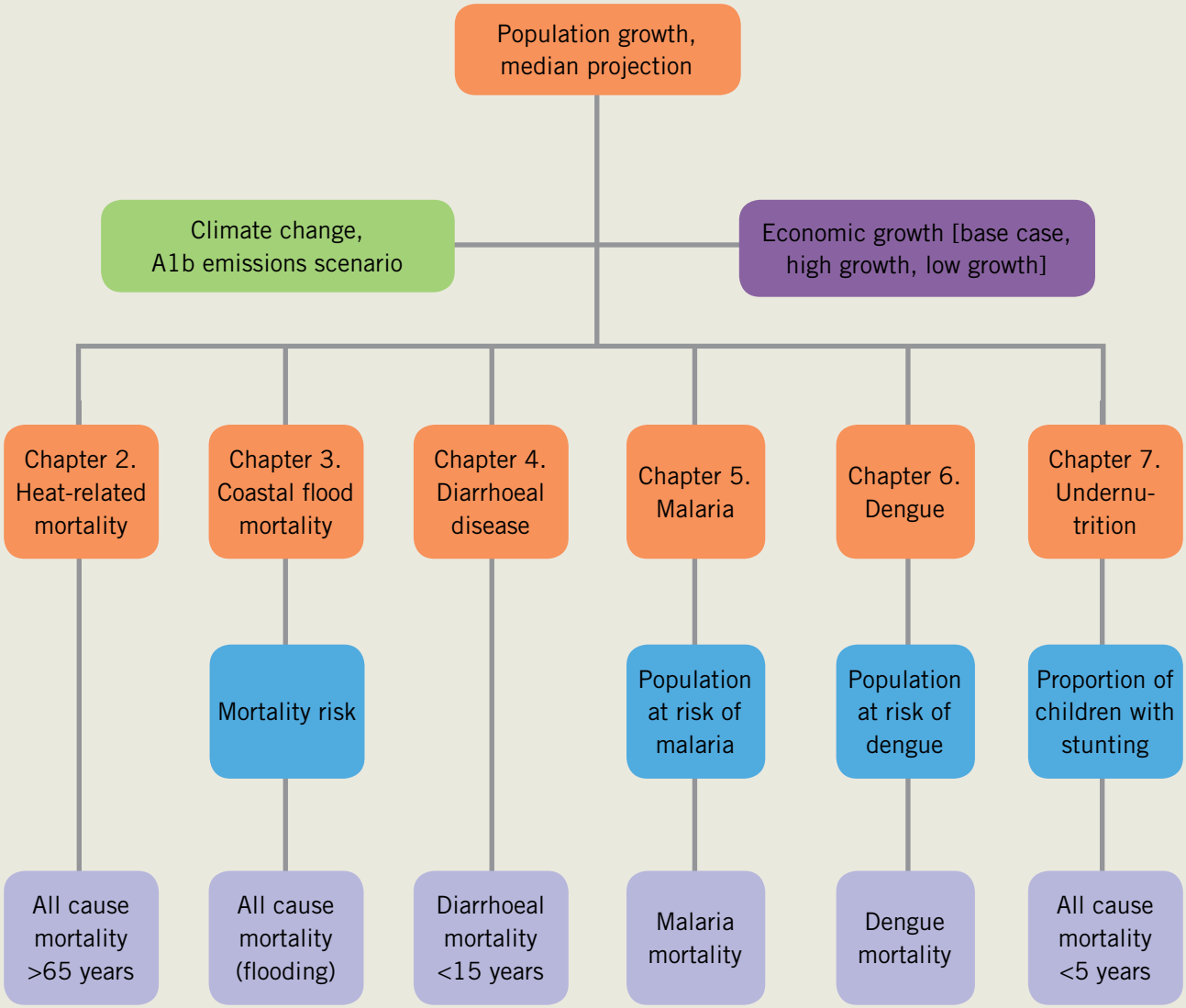

1.1 Methods and data

This assessment, subsequently referred to as the Climate Change Risk Assessment (CCRA), involves the development of outcome-specific models to estimate future climate change-attributable health effects (a range of metrics indicated by blue boxes in Figure 1.1) and future annual mortality (light purple boxes in Figure 1.1). The individual health models are described briefly below and in detail in each chapter.

The overall conceptual framework of this assessment was to model mortality in future worlds with and without climate change. The climate change-attributable impacts were defined as the additional mortality in future years (2030s and 2050s) under climate change scenarios compared with the mortality in the same time periods under the 1961–1990 climate (the counterfactual).

In absolute terms, the future impacts of climate change will depend on underlying health status. Rather than assume no change in future health status, we base our assessment on forecasts of mortality in future decades. Mortality forecasts are based on empirical models of observed mortality trends in relation to major drivers such as socioeconomic development, education and technology, together with projections of the future trajectories of these drivers on a national scale (see below and Chapter 8 for details). It is assumed that recent trends in socioeconomic development, education and technology will continue for the next 15–50 years, resulting in a continued decline in mortality from infectious diseases and undernutrition (Mathers & Loncar, 2006; WHO, 2008, 2012). We acknowledge that the empirical method has limitations, including an inability to account for the subnational distribution of wealth and the optimistic assumption that there will be no major discontinuities in the trajectory of socioeconomic development until at least the middle of the 21st century.

A single greenhouse gas emission scenario, the Special Report on Emission Scenarios (SRES) A1b, was used in this assessment. Because of the long lead times between emission of greenhouse gases and changes in climate, the choice of emission scenario makes little difference to the projected range of climate change in the next few decades (IPCC, 2013). There is, however, strong justification for early emissions reductions, since the level of emissions in future decades has a major impact on the severity of climate alteration beyond the 2050s.

In order to take into account climate modelling uncertainty in future climate projections, five global climate model runs were used to estimate future impacts (see Chapter 8 for details). For some impact pathways, the results of intermediate models were used (for example, undernutrition estimates use outputs from food trade models, and flood mortality estimates use outputs from a coastal flood model). Final results were derived for 21 world regions, based on the regions used in the most recent round of the Global Burden of Disease study (Lim et al., 2012) (see Annex for details) and for two time periods (2030s and 2050s). We also report summary results for 10 world regions (Figure 1.2).

Table 1.1 Adaptation assumptions in the models used in this assessment

	Underlying trends	Adaptation assumptions included in model	Potential options not included in model	Foreseeable limits to adaptation
Heat-related mortality in elderly people	Population growth and ageing; improved health in elderly people due to economic development	Three levels of autonomous adaptation assumed – none, partial and full – based on shifts to optimum temperature	Improved heat health protection measures; early warning systems	Cost and feasibility of active and passive cooling measures in dwellings
Coastal flooding	Coastal population increase; increased vulnerability due to rapid urban development, which then declines	Evolving coastal protection measures	Population relocation	Technical and cost barriers to coastal defences, particularly in atoll countries, deltas and low-lying areas in poor countries
Diarrhoeal disease	Improved mortality outcomes due to technology and economic development	None	Improved water, sanitation and hygiene	Cost of installation and maintenance of water and sanitation facilities. Potential future decreases in water availability
Malaria and dengue	Assumed reductions in mortality rates resulting from socioeconomic development	Assumed reductions in mortality rates resulting from socioeconomic development	Specific novel interventions, e.g. vector control, vaccination, early warning systems	Insecticide or drug resistance
Undernutrition	Population growth; improved population health due to technology and economic development	Crop yield models include adaptation measures	Non-agricultural interventions, e.g. water and sanitation provision; reduced meat consumption in countries with currently high consumption	Limits of maximum productivity of agricultural systems

Table 1.2 Additional deaths attributable to climate change,[a] under A1b emissions and the base case socioeconomic scenario, in 2030

Region	Undernutrition[b]	Malaria	Dengue	Diarrhoeal disease[c]	Heat[d]
Asia Pacific, high income		0 (0 to 0)	0 (0 to 0)	1 (0 to 2)	1488 (1208 to 1739)
Asia, central	473 (–215 to 1161)	0 (0 to 0)	0 (0 to 0)	111 (49 to 150)	740 (364 to 990)
Asia, east	1155 (–5313 to 7622)	0 (0 to 0)	39 (23 to 48)	216 (95 to 298)	8010 (5710 to 9733)
Asia, south	20 692 (–39 019 to 80 404)	1875 (1368 to 2495)	197 (101 to 254)	14 870 (6533 to 20 561)	9176 (7330 to 10 620)
Asia, south-east	3348	550	0	765	2408

[Continues]

[Continued]

Region	Undernutrition[b]	Malaria	Dengue	Diarrhoeal disease[c]	Heat[d]
	(–2635 to 9331)	(398 to 779)	(0 to 0)	(336 to 1105)	(1629 to 3192)
Australasia		0 (0 to 0)	0 (0 to 0)	0 (0 to 0)	93 (58 to 151)
Caribbean		12 (12 to 12)	3 (3 to 3)	72 (31 to 104)	117 (73 to 148)
Europe, central		0 (0 to 0)	0 (0 to 0)	1 (0 to 1)	880 (570 to 1523)
Europe, eastern		0 (0 to 0)	0 (0 to 0)	3 (1 to 4)	1974 (1325 to 2904)
Europe, western		0 (0 to 0)	0 (0 to 0)	2 (1 to 13)	2625 (1152 to 5279)
Latin America, Andean[e]	445 (–327 to 1218)	17 (6 to 37)	2 (0 to 4)	49 (21 to 69)	181 (119 to 241)
Latin America, central[f]	859 (–837 to 2554)	39 (32 to 47)	6 (–1 to 9)	109 (48 to 156)	878 (540 to 1113)
Latin America, southern	14 (–49 to 76)	0 (0 to 0)	0 (0 to 0)	1 (0 to 2)	421 (303 to 686)
Latin America, tropical		95 (87 to 113)	5 (4 to 5)	19 (9 to 27)	739 (623 to 954)
North America, high income		0 (0 to 0)	0 (0 to 0)	2 (0 to 2)	2990 (2297 to 3287)
North Africa/ Middle East	1617 (–2030 to 5264)	14 (14 to 14)	0 (0 to 0)	1323 (582 to 1850)	2,058 (1381 to 2342)
Oceania		44 (44 to 44)	0 (0 to 0)	22 (10 to 32)	13 (9 to 20)
Sub-Saharan Africa, central	14 385 (–27 448 to 56 217)	56 705 (34 908 to 112 719)	0 (0 to 0)	6326 (2774 to 8946)	344 (281 to 389)
Sub-Saharan Africa, eastern	27 999 (–8701 to 64 699)	143 (142 to 143)	6 (5 to 7)	10 997 (4811 to 15 585)	1212 (1064 to 1552)
Sub-Saharan Africa, southern	1245 (–1505 to 3994)	0 (0 to 1)	0 (0 to 0)	489 (215 to 685)	254 (163 to 313)
Sub-Saharan Africa, western	22 944 (–31 728 to 77 616)	597 (597 to 597)	1 (1 to 1)	12 737 (5581 to 18 110)	987 (712 to 1214)
World	95 176 (–119 807 to 310 156)	60 091 (37 608 to 117 001)	258 (136 to 331)	48 114 (21 097 to 67 702)	37 588 (26 912 to 48 390)

a Unless otherwise stated, the central estimate is the mean, based on five global climate model runs, and the uncertainty interval (in brackets) is the lowest and highest estimates; for each region, the first line is the mean estimate and the second line is the lowest and highest estimates

b Undernutrition estimates are for children aged under 5 years; the central estimate is the mean of the probability density function of impact estimates; the uncertainty interval is mean ± 1 standard deviation of the probability density function

c Diarrhoeal disease estimates are for children aged under 15 years; estimates are based on median temperature across the five global climate model runs, with the central estimate based on the mid-estimate of the temperature/diarrhoea coefficient, and the range based on the low and high coefficient estimates

d Heat estimates are for people aged over 65 years; results assume 50% adaptation

e Undernutrition estimate for Andean Latin America and tropical Latin America combined

f Undernutrition estimate for central Latin America and Caribbean combined

1.1.1 Global health futures: population, economic and mortality projections

The health impacts of climate change will depend on the underlying health of affected populations, which will in turn depend on future socioeconomic conditions and other important factors, such as universal health coverage and environmental regulation. Three sets of mortality projections were developed for this project by the World Health Organization (WHO) (see Chapter 8):

- low (economic) growth;
- base case;
- high (economic) growth (consistent with the SRES A1 scenario) (Nakicenovic & Swart, 2000).

The approach built on previous methods (Mathers & Loncar, 2006; WHO, 2008, 2012). The method uses a series of regression equations that quantify the current and historical relationships between mortality and a set of independent variables. The major independent variables related to mortality were gross domestic product (GDP) per capita, years of education and time (which is assumed to be a proxy for health benefits arising from technological developments). In addition, specific assumptions are made regarding future patterns of acquired immunodeficiency syndrome (AIDS), tuberculosis, malaria, smoking and body mass index.

To represent future population totals and spatial patterns, we used the United Nations (UN) 2010 revision, medium variant (UN, 2011). This estimates a world population of around 9 billion people in 2050 that continues to grow and reaches about 10 billion people by 2100. Fertility and life expectancy are presently higher than anticipated in many countries; if this trend continues, then future population totals will exceed those of earlier projections (UN, 2011).

1.1.2 Climate scenarios

We used a single medium-high emissions scenario, SRES A1b, which captures the range of projections regarding global mean temperatures up to the middle of the 21st century (Nakicenovic & Swart, 2000).

We used five climate model runs – BCM2.0, EGMAM1, EGMAM2, EGMAM3 and CM4v1 (see Chapter 8). The climate scenarios were selected based on the availability of climate variables required for individual models.

The climate models chosen did not share a common spatial grid. Grid resolutions ranged from 48 × 96 to 160 × 320. All runs were therefore regridded (interpolated) to a 1° × 1° global grid (180 × 360). The coastal flood impacts were estimated using a sea-level rise scenario driven by SRES A1b (see Chapter 3).

The baseline climate (no anthropogenic climate change) was represented by the average over 1961–1990 from the Climate Research Unit, University of East Anglia TS 2.1 monthly time series. Some analyses have used alternative datasets, such as for heat-related mortality in

Chapter 2. The analysis of undernutrition relied on a model of the effect of climate change on food availability, which used two global climate models – Model for Interdisciplinary Research on Climate (MIROC) and Commonwealth Scientific and Industrial Research Organisation (CSIRO Mk3) – driven by A1 emissions (see below and Chapter 7 for details).

1.1.3 Climate health models

Heat-related mortality

A published temperature–mortality model was used to estimate heat-related mortality based on the observed association between daily mortality and temperature in Japan (Honda et al., 2014). Impacts were restricted to mortality in people aged over 65 years, and a single temperature mortality function was applied universally as the function was validated against other (temperate-zone) populations. The difference in mortality between the optimum temperature and a temperature beyond the optimum is defined as the heat-attributable mortality. Estimates were generated for three assumptions about the level of autonomous adaptation (no adaptation, partial adaptation and complete adaptation), and the optimum temperature was shifted accordingly (see Chapter 2).

Coastal flood mortality

A new global model to estimate the mortality attributable to storm surge was developed (Lloyd et al., 2014). Estimates of future populations exposed to coastal flooding due to sea-level rise were derived from the Dynamic Interactive Vulnerability Assessment (DIVA) global model (Vafeidis et al., 2008). Country-specific mortality from storm surges was estimated from the International Disaster Database (EM-DAT) (CRED, 2011) and used to fit a model, with the baseline exposure from DIVA (which assumes that all countries optimize coastal protection). The effect of economic development was modelled using the Human Development Index. Based on observed associations between disaster mortality and economic development, the model allows for an initial increase in mortality risk as low-income countries develop, followed by a decline in risk as disaster risk reduction is improved (Patt et al., 2010). The model was fitted with observed disaster mortality data using a short and long time series to balance the competing requirements of data completeness and the need to assess average mortality over a long time period. Impact projections were made for sea-level rise projections under the A1b emissions scenario (see Chapter 3).

Diarrhoeal disease

A linear exposure–response function was derived from the published literature that described the association between temperature and diarrhoeal disease. Due to the limited number of observational studies, a range of exposure–response functions was generated (high, median and low estimates). Estimates were restricted to mortality in children aged under 15 years. Climate scenario data were used to estimate the attributable fraction due to higher temperatures, which was then applied to projections of future diarrhoeal disease mortality (see Chapter 4).

Malaria

A published empirical-statistical model was used, which incorporates temperature, precipitation and GDP per capita as predictors of the past, present and future geographical limits of malaria (Béguin et al., 2011). Scenario-based projections of future climate, economic development and population were used to estimate changes in the population at risk of malaria in the years 2030 and 2050. Gridded population data for the A1b scenario were obtained from the International Institute for Applied Systems Analysis (IIASA, 2009) for the years 1990, 2030 and 2050. The population data were used together with the risk areas from the malaria model to estimate the future population at risk and the change in the population at risk from baseline climate. To calculate mortality associated with malaria infections, national current malaria mortality estimates were multiplied by the national ratio of the projected population at risk to the present population at risk (see Chapter 5).

Dengue

An empirical-statistical model was developed using temperature, precipitation and GDP per capita as predictors of the past, present and future geographical limits of dengue (Åström et al., 2012). Scenario-based projections of future climate, economic development and population were used to estimate changes in the population at risk of dengue in the years 2030 and 2050. Changes in the proportion of the national population at risk, along with estimates of current mortality from dengue, were used to estimate changes in mortality attributable to climate change, using the same method as for malaria above (see Chapter 6).

Undernutrition

A previously published model estimated the effect of changes in per capita calorie availability (undernourishment) on undernutrition (stunting) in children aged under 5 years (Lloyd et al., 2011). The undernourishment estimates were derived from the International Model for Policy Analysis of Agricultural Commodities and Trade (IMPACT) integrated assessment model at the International Food Policy Research Institute (IFPRI) (Nelson et al., 2010). The model accounts for food and non-food (socioeconomic) causes of undernutrition. The model was used to estimate child stunting attributable to climate change based on projections of national food availability per capita published by IFPRI. This outcome was used to estimate the attributable burden of mortality in children aged under 5 years using published relative risks for association between stunting and all-cause mortality (Black et al., 2008), which were then applied to mortality projections provided by WHO (see Chapter 7).

1.2 Findings

Climate change is projected to have substantial adverse effects on human health that will be distributed unequally within and between populations.

Figure 1.2 and Tables 1.2 and 1.3 illustrate the regional distribution of annual climate change-attributable mortality in 2030 and 2050 under the base case scenario of economic development. Estimates are the annual impact for the specified year under each scenario, with a single population projection. The central estimates represent the average from five climate scenarios. Climate change may increase the burden of mortality from coastal flooding, but because these impacts are highly uncertain they are not included below.

Figure 1.2 Estimated future annual mortality attributable to climate change under A1b emissions and for the base case socioeconomic scenario in 2030 (blue bars) and 2050 (orange bars), by world region[a] and health outcome, for (a) undernutrition, (b) malaria, (c) diarrhoeal disease, (d) dengue and (e) heat

[a] Asia, C – Asia, central; Asia, E – Asia, east; Asia, S – Asia, south; Asia, SE – Asia, south-east; HIC, high-income countries (includes Asia Pacific, high income; Australasia; Europe, central; Europe, eastern; Europe, western; North America, high income; and Oceania); LAM – Latin America (includes Latin America, Andean; Latin America, central; Latin America, southern; Latin America, tropical; and Caribbean); SSA, C – sub-Saharan Africa, central; SSA, E – sub-Saharan Africa, eastern; SSA, S – sub-Saharan Africa, southern; SSA, W – sub-Saharan Africa, western. Estimates for North Africa/Middle East are not included.

Table 1.3 Additional deaths attributable to climate change,[a] under A1b emissions and the base case socioeconomic scenarios, in 2050

Region	Undernutrition[b]	Malaria	Dengue	Diarrhoeal disease[c]	Heat[d]
Asia Pacific, high income		0 (0 to 0)	0 (0 to 0)	1 (0 to 1)	2504 (1868 to 3046)
Asia, central	314 (66 to 563)	0 (0 to 0)	0 (0 to 0)	26 (12 to 38)	1889 (1077 to 2173)
Asia, east	700 (–427 to 1828)	0 (0 to 0)	31 (25 to 42)	72 (33 to 107)	17 882 (11 562 to 24 576)
Asia, south	16 530 (–1582 to 34 642)	9343 (2998 to 13 488)	209 (140 to 246)	7717 (3522 to 11 421)	24 632 (20 095 to 31 239)
Asia, south-east	3049 (605 to 5494)	287 (265 to 334)	0 (0 to 0)	383 (172 to 575)	7240 (5883 to 10 290)
Australasia		0 (0 to 0)	0 (0 to 0)	0 (0 to 0)	236 (180 to 359)
Caribbean		7 (7 to 7)	0 (0 to 1)	17 (8 to 26)	320 (259 to 380)
Europe, central		0 (0 to 0)	0 (0 to 0)	0 (0 to 0)	1680 (989 to 2769)
Europe, eastern		0 (0 to 0)	0 (0 to 0)	1 (0 to 1)	3218 (2438 to 4807)
Europe, western		0 (0 to 0)	0 (0 to 0)	1 (1 to 2)	5573 (3908 to 9737)
Latin America, Andean[e]	330 (–6 to 665)	1 (1 to 1)	3 (0 to 7)	12 (5 to 17)	597 (477 to 804)
Latin America, central[f]	706 (100 to 1311)	99 (56 to 167)	10 (7 to 14)	27 (12 to 40)	2713 (2137 to 3679)
Latin America, southern	11 (–27 to 49)	0 (0 to 0)	0 (0 to 0)	0 (0 to 0)	884 (624 to 1261)
Latin America, tropical		0 (0 to 0)	20 (15 to 23)	5 (2 to 7)	2007 (1489 to 2993)
North America, high income		0 (0 to 0)	0 (0 to 0)	1 (0 to 2)	6101 (4923 to 7259)
North Africa/Middle East	1167 (–480 to 2813)	209 (157 to 316)	0 (0 to 0)	812 (369 to 1206)	6669 (4731 to 8537)
Oceania		32 (32 to 32)	0 (0 to 0)	15 (7 to 23)	68 (58 to 101)
Sub-Saharan Africa, central	18 273 (–12 372 to 48 918)	0 (0 to 0)	1 (1 to 1)	5473 (2473 to 8174)	1363 (1139 to 1598)
Sub-Saharan Africa, eastern	26 480 (4936 to 48 024)	22 194 (18 747 to 26 002)	5 (4 to 5)	6951 (3138 to 10 392)	4543 (3497 to 5957)
Sub-Saharan Africa, southern	1032 (–516 to 2580)	0 (0 to 0)	0 (0 to 0)	267 (121 to 396)	706 (553 to 857)
Sub-Saharan Africa, western	16 105 (–19 500 to 51 709)	524 (524 to 524)	1 (1 to 1)	11 174 (5039 to 16 723)	3469 (2887 to 4261)
World	84 697 (–29 203 to 163 989)	32 695 (22 786 to 40 817)	282 (195 to 342)	32 955 (14 914 to 49 151)	94 621 (70 775 to 126 684)

a Unless otherwise stated, the central estimate is the mean, based on five global climate model runs, and the uncertainty interval (in brackets) is the lowest and highest estimates; for each region, the first line is the mean estimate and the second line is the lowest and highest estimates

b Undernutrition estimates are for children aged under 5 years; the central estimate is the mean of the probability density function of impact estimates; the uncertainty interval is mean ± 1 standard deviation of the probability density function

c Diarrhoeal disease estimates are for children aged under 15 years; estimates are based on median temperature across the five global climate model runs, with the central estimate based on the mid-estimate of the temperature/diarrhoea coefficient, and the range based on the low and high coefficient estimates

d Heat estimates are for people aged over 65 years; results assume 50% adaptation

e Undernutrition estimate for Andean Latin America and tropical Latin America combined

f Undernutrition estimate for central Latin America and Caribbean combined

An important component of the CCRA is the use of a consistent set of mortality projections with which to estimate future attributable mortality. We have used a range of GDP projections to drive the mortality forecasts.

The final mortality estimate is a combination of reduction in projected mortality in the absence of climate change, population growth in affected regions, and sensitivity of the health outcome to climate change.

Compared with a future without climate change, and in the absence of adaptation, approximately 65 000 additional deaths due to heat exposure in elderly people are projected for the year 2030 (see Chapter 2).

The coastal flooding modelling results show that much of the future burden of flooding can be avoided by adaptation to coastal flooding – assumed to be the construction and maintenance of coastal defences. This is not feasible for some populations, however, and so the results may represent an optimistic assessment of future health impacts. The results are, however, presented for a range of adaptation scenarios.

An additional 48 000 deaths due to diarrhoea and 60 000 deaths due to malaria are projected for the year 2030. There is very little projected increase in deaths due to dengue fever.

Undernutrition is one of the leading causes of death in young children and is likely to remain so in future decades. IPCC estimates suggest that climate change is likely to have significant effects on cereal crop productivity, potentially increasing the risk of undernutrition (Smith at al., 2014). Projected increases in infectious disease morbidity, especially for diarrhoeal illness, would exacerbate climate change effects on child nutrition.

1.3 Discussion

Climate change is projected to have substantial adverse impacts on future mortality, even under optimistic scenarios of future socioeconomic development. Under a base case socioeconomic scenario, we estimate approximately 250 000 additional deaths due to climate change per year between 2030 and 2050. These numbers do not represent a prediction of the overall impacts of climate change on health, since we could not quantify several important causal pathways (see Section 1.3.1).

The results of individual models are broadly consistent with previous published estimates for specific outcomes (see later chapters for details). A major limitation for a climate change risk assessment is the scope of the impacts that can be modelled quantitatively with sufficient confidence. The results reported here indicate that climate change will have an impact on health, even with adaptation and under conditions of high economic growth. Among these, the most substantial impacts of climate change on health are projected to be caused by undernutrition and infectious diseases (diarrhoeal disease and malaria). Impacts are greatest under a low (economic) growth scenario because of higher rates of mortality projected in low- and middle-income countries (see individual chapters). In 2030, sub-Saharan Africa is projected to have the greatest burden of mortality impacts attributable to climate change. By

2050, south Asia is projected to be the region most affected by the health effects of climate change.

Some models resulted in a wide range of uncertainty around the final estimates. Empirical models with improved statistical power can go some way to addressing this in the future. Due to the formulation of the models, uncertainty was estimated using a range of methods (see later chapters for discussion).

The previous estimate of the disease burden of climate change was for the year 2000 (McMichael et al., 2004) as part of the WHO Comparative Risk Assessment (2000–2004). Approximately 150 000 deaths globally were attributed to the climate warming experienced by 2000; most of these deaths were in sub-Saharan Africa and south Asia (Ezzati et al., 2002). In this project, we did not estimate a current burden due to observed climate change. Furthermore, with different models and different underlying assumptions and scenarios, the results of this project are not directly comparable with the previous WHO estimates.

1.3.1 Limitations of the assessment

The main limitation of the CCRA is the inability of current models to account for major pathways of potential health impact, such as the effects of economic damage, major heatwave events, river flooding or water scarcity. The assessment does not consider the impacts of climate change on human security, for example through increases in migration or conflict. The included models can capture only a subset of potential causal pathways, and none accounts for the effects of major discontinuities in climatic, social or ecological conditions.

Extreme events

The health impacts of extreme climate events are not included in this assessment, with the exception of the increase in coastal flooding due to sea-level rise. Extreme events are not well described by climate data averaged over space and time. Flood disasters from storm-surge events are included in the assessment, but an increase in river flooding due to climate change is not included because no global projections of populations at risk of flooding were available. The coastal flood risk assessment assumed no change in the frequency of storm events, apart from the relative change in impact due to rising sea levels. The crop yield models used within the undernutrition framework will include some measure of climate variability but not a scenario that includes multiple extreme drought events. The same methodological issues arise for the temperature-related impacts.

Burden of disease indicators

There are several reasons why mortality is only an incomplete indicator for a health impact assessment. For several outcomes, such as dengue, the health burden from morbidity far outweighs that attributable to mortality. Furthermore, for outcomes such as diarrhoeal disease, significant reductions in mortality rates have not been reflected in reduced morbidity rates. Future work will focus on summary measures of population health, such as disability-adjusted life-years (DALYs), and economic evaluation of impacts. It should be noted that many of the models provide useful intermediate endpoints that are not included here because they cannot be readily aggregated, such as the proportion of the

population stunted and the population at risk of malaria. Several key outcomes included in this assessment are also closely interrelated, for example malaria and diarrhoeal disease are associated with increased mortality from undernutrition and vice versa. Thus estimates of mortality attributable to single diseases may under- or overestimate the true burden from climate change.

Our ability to model the effects of climate change on vector-borne disease is also limited. The models described below estimate the geographical areas within which the combination of average climatic and socioeconomic conditions is conducive to local transmission. Extrapolation to changes in mortality, based on the proportion of national populations at risk, is a crude, if reasonable, assumption. We assume no change in the mortality rate in the population defined as at risk at baseline and in the future.

1.3.2 Benefits of climate change to health

Climate change will have some positive impacts on human health. There are likely to be reductions in cold-related mortality and morbidity in high-income populations. The most recent assessment report of the IPCC concludes, however, that the impacts on health of more frequent heat extremes greatly outweigh the benefits of fewer cold days, and that the few studies of the large developing country populations in the tropics, point to effects of heat, but not cold, on mortality (Smith et al., 2014). The effect of cold temperatures is therefore not modelled in this assessment. Any beneficial effects of climate change on food supply and vector-borne disease distribution are included in the current estimates, which represent the aggregate results at the regional level. At the national or local level, benefits to health may be more apparent.

1.3.3 Incorporating adaptation into the assessment

Some of the impacts on health due to climate change in this assessment can be avoided by adaptation measures. This reinforces the need for strengthened public health measures. The quantification of the burden avoided by adaptation is difficult to assess, however. Adaptation can occur at all stages of the relevant causal pathways, such as disaster risk reduction or increased food production. Table 1.1 describes how adaptation was modelled explicitly for each health outcome.

This study shows that, even with effective adaptation policies, climate change can undermine current and future development programmes. Therefore, in the long term (decades to centuries), development policy is unlikely to succeed unless future global environmental risks are considered.

1.3.4. Implications for policy

The conclusion that climate change is projected to have substantial adverse impacts on future mortality, even considering only a subset of the expected health effects, under optimistic scenarios of future socioeconomic development and with adaptation, does have implications for the international effort to address climate change.

In relation to mitigation policy, the results indicate that minimizing climate-sensitive health risks is an additional reason to act to reduce climate change, alongside the immediate health benefits expected to accrue from measures to reduce climate pollutants (for example, through lower levels of particulate air pollution), and the avoided damages to other human and natural systems.

With regard to policies on climate change adaptation, the CCRA supports the case both for the overall strengthening of programmes to address health risks including undernutrition, diarrhoea, vector-borne disease, and heat extremes, and for explicit consideration of climate risks (both from climate variability and long-term climate change) within programme design.

The results also have implications for the linkages between climate, health and wider sustainable development objectives. The strong effect of socioeconomic development on the projections of many of the health risks emphasizes the need to ensure that overall economic growth, climate policies and health programmes, particularly benefit the poorest and most vulnerable populations.

Heat-related mortality

2

Yasushi Honda, Masahide Kondo, Glenn McGregor, Ho Kim, Yue-Leon Guo, Simon Hales, Sari Kovats

2.1 Background

An increase in future heat-related mortality is seen as one of the most likely impacts of future anthropogenic climate change (Smith et al., 2014). An increase in health effects is projected from both increases in average seasonal temperatures (Huang et al., 2011) and an increase in the frequency and intensity of heatwave events (IPCC, 2012).

An increase in acute mortality associated with high temperatures has been observed in nearly all populations where it has been studied (Curriero et al., 2002; Honda et al., 2007; McMichael et al., 2008). A review of published temperature–mortality relationships has found the relationship to be U- or V-shaped, with an increase in mortality risk observed at both high and low temperatures in populations in temperate and cold climates (Baccini et al., 2008) and tropical and subtropical areas (Egondi et al., 2012; Sung et al., 2013).

Human populations are adapted to their local climates, as indicated by the threshold value above which mortality risk begins to increase (Kovats & Hajat, 2008). Despite this adaptation, mortality risk increases outside a location-specific optimum temperature range. Some mortality from high temperatures may be prevented by improvements to housing and the outdoor built environment, such as increasing green spaces and using albedo (painting roofs white) (Rogot et al., 1992; Silva et al., 2010). Public health measures, such as heat health warning systems, also reduce heat-related mortality (Schifano et al., 2012).

2.2 Model development

A global model was developed to estimate future heat-related mortality due to climate change in people aged over 65 years. The model is derived from epidemiological studies that analysed the effects of ambient temperature on all-cause mortality, including external causes, which includes deaths from heatstroke and heat-related accidents and injuries (Ishigami et al. 2008, Bhaskaran et al., 2013). The model has been used previously to estimate future heat-related mortality due to climate change, based on the temperature–mortality relationship in Japan (Takahashi et al, 2007).

The assessment was limited to the older population (aged 65 years or over) because this is the population considered most at risk of heat-related mortality, and also to avoid double counting with other outcomes, such as diarrhoeal disease mortality.

The climate change-attributable burden was estimated to be the difference between future heat-related mortality under the A1b emissions scenario and future heat-related mortality under the baseline climate (the counterfactual).

2.3 Quantifying the association between temperature and mortality

The model is based on the quantification of the temperature–mortality function developed for a previously published modelling assessment (Honda et al., 2014). The temperature–mortality function was assumed to be V-shaped, and the temperature value at which mortality was lowest was defined as the optimum temperature. For temperatures above the optimum temperature, the mortality difference is defined as the heat-related mortality burden of a given location (Figure 2.1).

Figure 2.1 Schematic graph of relationship between daily mortality and daily temperature

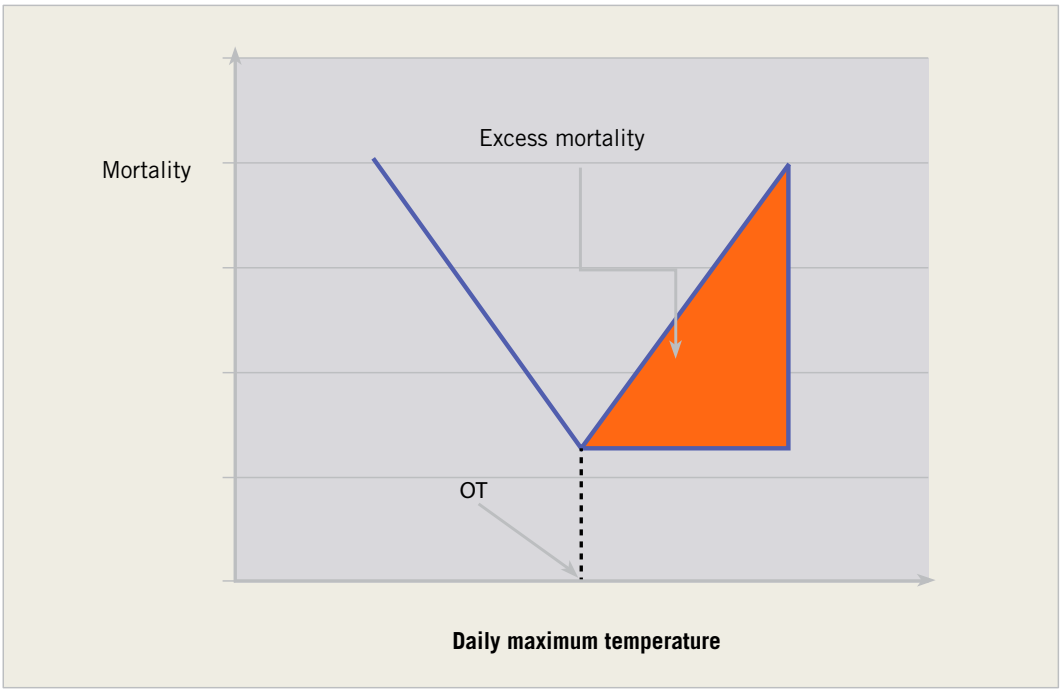

OT – optimum temperature

The majority of observational studies of heat-related mortality are for individual urban populations in Europe, the United States of America and China. There is very limited information on temperature–mortality functions for rural populations and populations in south Asia or Africa. Therefore, the model developed by Honda and colleagues was applied to the global population. Figure 2.2 shows the relationship between a temperature index (daily maximum temperature minus optimum temperature) and the daily number of deaths (relative to the number of deaths at optimum temperature) based on data from 47 Japanese prefectures (Honda et al., 2014). A distributed lag nonlinear model was used to quantify the association (Gasparrini et al., 2010) and controlled for up to 15 days of lag effect. In this regard, short-term mortality displacement has been taken into account to some extent, as the relative mortality risk is cumulative over 15 days. Time trend and age were controlled for in the analysis, but data on other potential confounders such as air pollution were not available. Previous studies have shown that confounding from air pollution usually has little effect on final temperature–mortality relationships (Bhaskaran et al., 2013).

Figure 2.2 Relationship[a] between temperature index (daily maximum temperature minus optimum temperature) and relative mortality for people aged over 65 years

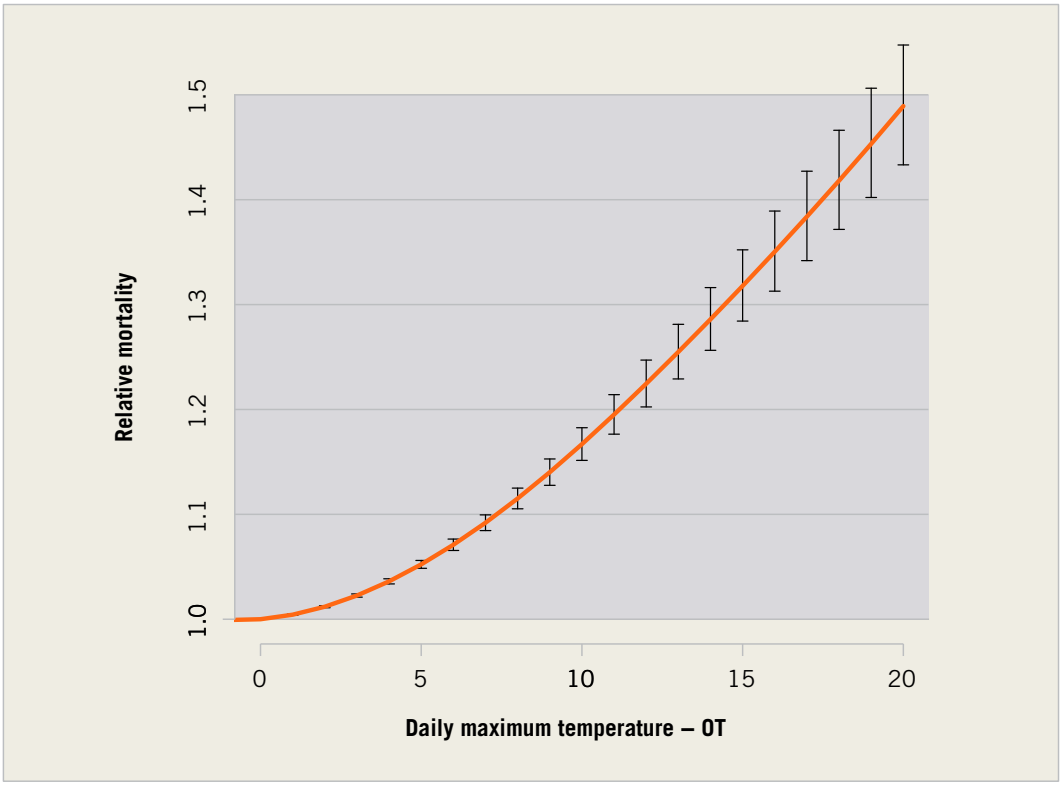

[a] Cumulative effect over 15 days
Reproduced using results from Honda et al. (2014)

Although the model was based on data from Japan, it was tested against other populations and was evaluated as a reasonable model for other countries (Honda et al., 2014).

The optimum temperature was estimated to be the 84th percentile of the daily maximum temperature. Previous work has shown that the relative risk for heat-related mortality is 1.02 in the range between optimum temperature (OT) and OT + 5, and 1.10 for OT + 5 and over (Takahashi et al, 2007). In this assessment, the relative risk for the two categories was averaged to give a single relative risk estimate over the temperature range above the optimum temperature (Takahashi et al, 2007). This implies that the estimate for temperatures much higher than OT + 5 would be underestimated, because most of the days with this category were close to OT + 5, and days with a temperature much higher than OT + 5 (at which mortality is higher than that at OT + 5) would increase in the future. In practice, the relative risk varies between countries, and the heat effect on human health is influenced by socioeconomic factors such as income and education (O'Neill et al., 2003); however, there was no systematic difference among middle-income countries in previous studies (Bell et al., 2008; McMichael et al., 2008). Rather, because there are only a few days with extremely high temperatures in each area, the statistical power to detect between-study differences is limited. To obtain heat-related mortality, it was necessary to use the daily mortality value at optimum temperature as the reference; however, the available mortality information is the annual mortality. Therefore, the mortality at optimum temperature was estimated using the following formula:

Mortality at optimum temperature = 0.88 × (annual mortality/365.25)

Annual mortality divided by 365.25 yields the average daily mortality, and 0.88 is the ratio of mortality at optimum temperature to average daily mortality estimated using Japanese data. The differences in age distribution and mortality pattern could affect the ratio; however, the largest 20 cities in the United States and some selected cities in the Republic of Korea, China (Province of Taiwan) and Europe showed similar ratios across a wide variety of countries (Honda et al., 2014).

Heat-related deaths were calculated on a daily timescale and at the spatial scale of 0.5° × 0.5° grid cells, as follows. For each day, and for each grid location, if the temperature index (daily maximum temperature minus optimum temperature) exceeds 0, then the estimated number of deaths due to heat is:

Heat-related deaths = $D_{av} \times 0.88 \times (RR_t - 1)$

where D_{av} is the daily average number of deaths (in people aged 65 years and over); and RR_t is the ratio of mortality at temperature index t, compared with mortality at the optimum temperature. The daily heat-attributable deaths are then summed up for the year (to provide an annual total). Final results were aggregated for 21 world regions (see Annex).

2.4 Scenario data

A daily maximum temperature distribution for each grid cell was required for this analysis. The baseline (observed) climate was derived from the US National Centers for Environmental Prediction (NCEP) dataset, as corrected by the Climate Research Unit, University of East Anglia, United Kingdom (CRU) (Ngo-Duc et al., 2005), which was based on gridded data from the NCEP/National Center for Atmospheric Research reanalysis project (ESRL, 1996). The NCC dataset provides 6-hour average temperatures. The daily maximum temperature was estimated using the highest of the 6-hour average temperature measurements in a day.

The model was run with the five climate scenarios (see Chapter 8) under the A1b emissions scenario – BCM2, EGMAM1, EGMAM2, EGMAM3 and IPCM4.

For future time periods (2030 and 2050), we assumed month-specific temperature distribution to be identical to the baseline. Using the month-specific temperature change projections, we estimated the daily maximum temperature as follows:

$$T_{mx(p2030)ijk} = T_{mx(b)ijk} + T_{diff(p2030)ij}$$

where $T_{mx(p2030)}$ is the daily maximum temperature for the 2030 projection; $T_{mx(b)}$ is the daily maximum temperature for the baseline (1961–1990); and $T_{diff(p2030)}$ is the difference in temperature between the baseline and 2030 projection for the ith grid, for the jth month and for the kth day.

An identical procedure was applied to data for the 2050s.

2.5 Mortality projections

The model used projected all-cause mortality in people aged 65 years and over (see Chapter 8). For future projections of heat-related deaths, we used future mortality estimates and the corresponding future climate. All-cause mortality in people aged over 65 years is projected to increase due to population growth in all world regions. A single mortality projection – the base case – was used (see Chapter 8). The mortality estimates were gridded based on the current spatial distribution of national populations.

2.6 Adaptation assumptions

Populations will acclimatize and adapt to higher temperatures and warming climates. There is little evidence, however, regarding the rate or extent of adaptation. We made the following assumptions:

At baseline, the optimum temperature is equal to the 84th percentile of daily maximum temperature. Adaptation was incorporated into the assessment by changing the optimum temperature in the future time periods (reflecting population adaptation). There is some evidence that such a shift has occurred following observed climate change in Japan (Honda et al., 2006), but no information is available concerning how fast the shift occurs in other settings. In this assessment, three possible adaptation scenarios were assumed:

- 0% – no adaptation: optimum temperature based on the current climate (1961–1990).
- 50% – some adaptation: midpoint of the 0% adaptation optimum temperature and the 100% adaptation optimum temperature.
- 100% – complete adaptation: optimum temperature based on future climate scenario.

2.7 Results

Climate change is associated with a significant increase in heat-related mortality. The global estimate for increases in heat-related deaths (annual estimate) is 92 207 (64 458–121 464) additional deaths in 2030 and 255 486 (191 816–364 002) additional deaths in 2050 (assuming no adaptation). The increases are not distributed evenly: impacts are greatest in the south, east and south-east Asia regions (Figure 2.3).

Table 2.1 shows the climate change-attributable heat-related deaths by world region. The relative increase in excess deaths from 2030 to 2050 is large in sub-Saharan African regions, Latin America, and south and south-east Asia.

Figure 2.3 Estimated annual counts of heat-related deaths in people aged 65 years and over, by 0.5° grid cell, for BCM2 in 2050, with no adaptation assumed

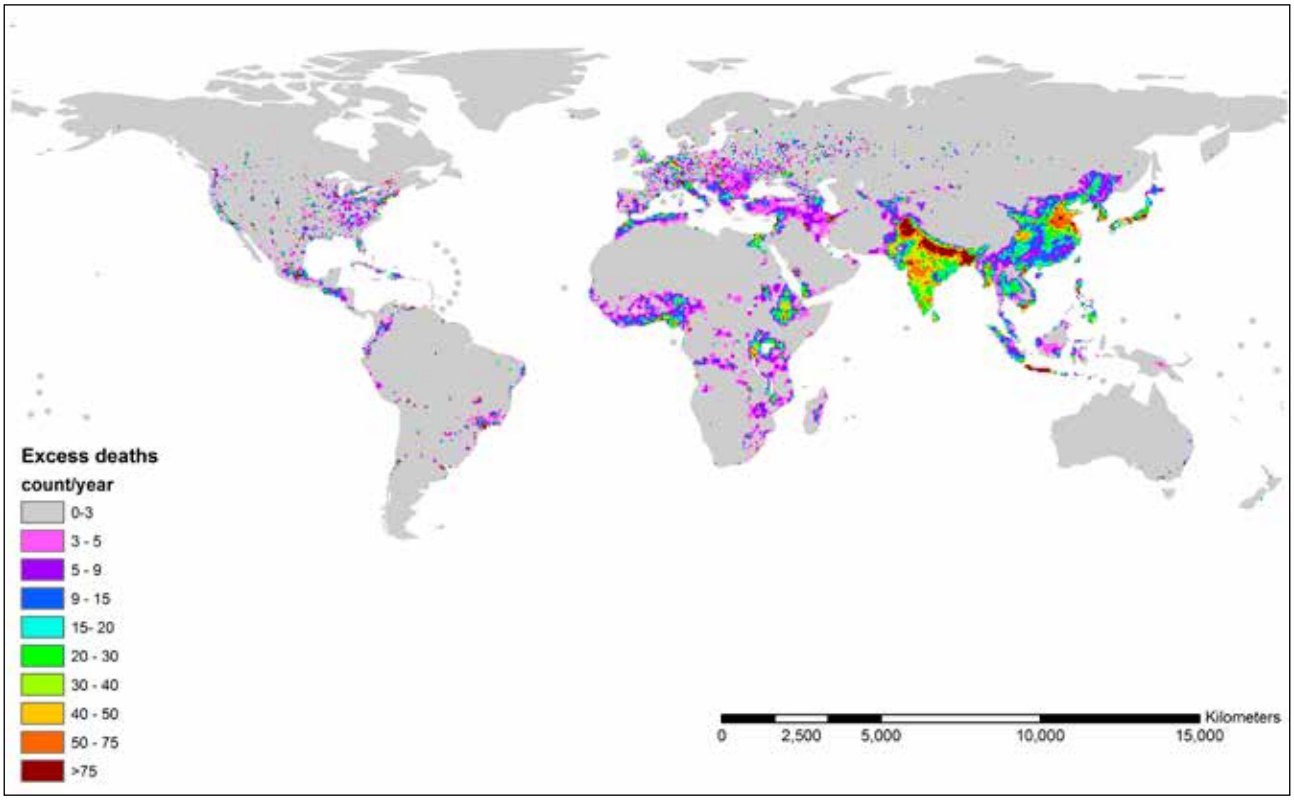

Mortality counts shown for 0.5 degree grid cells.

Table 2.1 Climate change-attributable heat-related excess number of deaths by region, without adaptation[a]

Region	2030	2050
Asia Pacific, high income	3383 (2375 to 4106)	6221 (4339 to 8280)
Asia, central	1752 (847 to 2282)	4886 (2850 to 5656)
Asia, east	19 323 (13 080 to 23 740)	47 367 (29 689 to 70 528)
Asia, south	21 648 (15 974 to 25 653)	62 821 (48 133 to 83 447)
Asia, south-east	6739 (4269 to 9089)	22 517 (17 174 to 32 887)
Australasia	217 (132 to 345)	605 (434 to 980)
Caribbean	281 (193 to 431)	862 (550 to 1314)
Europe, central	2279 (1563 to 4244)	4373 (2461 to 8184)
Europe, eastern	4988 (2899 to 8185)	8745 (5576 to 14 469)
Europe, western	6261 (2644 to 12 412)	14 148 (8942 to 25 840)
Latin America, Andean	540 (332 to 753)	2142 (1689 to 3100)
Latin America, central	2293 (1481 to 2989)	7704 (6138 to 11 251)
Latin America, southern	972 (690 to 1612)	2377 (1769 to 3386)
Latin America, tropical	1808 (1330 to 2707)	5912 (3727 to 10181)
North America, high income	7288 (4986 to 8609)	16 076 (12 488 to 21 152)

[Continues]

[Continued]

Region	2030	2050
North Africa/Middle East	4997 (3184 to 5837)	18 688 (12 122 to 22 936)
Oceania	52 (44 to 71)	217 (177 to 341)
Sub-Saharan Africa, central	921 (717 to 1119)	4107 (3399 to 5277)
Sub-Saharan Africa, eastern	3266 (2828 to 4448)	13 713 (10 055 to 19 295)
Sub-Saharan Africa, southern	671 (384 to 911)	1970 (1469 to 2700)
Sub-Saharan Africa, western	2529 (1716 to 3391)	9971 (7890 to 13 365)
World	92 207 (64 458 to 121 464)	255 486 (191 816 to 364 002)

a ENSEMBLE means, with low and high estimates in brackets

As expected, the estimates are reduced when adaptation is assumed, and the attributable mortality is zero when 100% adaptation is assumed. Table 2.2 shows the adaptation effect on climate change-attributable heat-related excess deaths based on a single model scenario (BCM2). For full results with 50% adaptation, see also Tables 1.2 and 1.3.

Table 2.2 Climate change-attributable heat-related excess number of deaths by adaptation level for the BCM2 model scenario

Region	2030		2050	
	0%	50%	0%	50%
Asia Pacific, high income	2375	1208	4339	1868
Asia, central	847	364	2850	1077
Asia, east	13 080	5710	29 689	11 562
Asia, south	15 974	7330	48 133	20 095
Asia, south-east	4269	1629	17 174	5883
Australasia	251	111	681	268
Caribbean	193	73	550	259
Europe, central	2135	967	4338	1940
Europe, eastern	4642	1939	8739	3114
Europe, western	2644	1152	8942	3908
Latin America, Andean	332	119	1689	477
Latin America, central	1481	540	6138	2137
Latin America, southern	690	303	1769	624
Latin America, tropical	1686	701	5983	1982
North America, high income	4986	2297	12 488	4923
North Africa/Middle East	3184	1381	12 122	4731
Oceania	44	11	187	60
Sub-Saharan Africa, central	717	281	3569	1207
Sub-Saharan Africa, eastern	2828	1064	13 055	4381
Sub-Saharan Africa, southern	384	163	1491	553
Sub-Saharan Africa, western	1716	712	7890	2887
World	64 458	28 055	191 816	73 936

Results are consistent with a previous study that used this modelling approach (Takahashi et al, 2007). The present model has the following improvements: risk function is nonlinear with 95% confidence bands rather than wide category point estimates; we addressed mortality displacement; and the model is based on a longer observation period.

The 84th percentile value of the daily maximum temperature was a good approximation of optimum temperature in the data for the Republic of Korea, China (Province of Taiwan), Europe, the United States and Japan (Honda et al., 2014).

2.8 Uncertainty

Uncertainty was assessed in the future projections using two methods:

- changes to the optimum temperature as an indicator of adaptation;
- statistical uncertainty relating to the underlying temperature mortality function.

The 95% confidence interval around the relative risk estimate was calculated to indicate statistical variation in the underlying temperature–mortality association. In terms of the model, a natural cubic spline was used to draw the risk function curve shown in Figure 2.2. This is because, following Armstrong (2006), it assumes linear relations for temperatures outside the data range and so is more conservative compared with, for example, quadratic curves.

In addition, uncertainty about future climate change was estimated using a range of climate scenarios.

2.9 Discussion

This is a global assessment of future heat-related mortality due to climate change. The results indicate a significant burden on mortality. Hot weather is also known to affect morbidity and mortality in other age groups, and this may indicate that the results are an underestimate of the total burden on health.

There remains some uncertainty about the mortality burden of heat-related mortality in terms of years of life lost. Studies from Europe have shown that there is mortality displacement in heat-related mortality that would reduce the burden in terms of years of life lost. Future assessments should consider using metrics other than age-specific mortality that are better able to describe the burden of disease due to high temperatures. However, the underlying model in this assessment is based on a distributed lag model, which does account, to some extent, for mortality displacement.

There are several limitations to this assessment. First, the exposure of interest is the daily distribution of temperature rather than individual extreme heatwave events. Such events are not well captured by climate assessments (even when daily temperature distributions are included), as 30-year averages are used in the baseline and projections. Many factors that affect heatwave mortality risk were not able to be considered using this method, such as the seasonal timing (Barnett et al., 2012) or duration (Rocklöv et al., 2011) of heatwaves.

Second, there is a lack of evidence regarding the rate of autonomous adaptation in different populations around the world (see above). In previous studies, two types of population-level adaptation (flattening of the V-shaped curve and right shift of the optimum temperature) have been described (Kinney et al., 2008). Although Kinney and colleagues reported that the flattening tendency occurred in the United States, and that some United States cities showed a monotonic relationship between mortality and temperature (lower mortality for higher temperature), this type of adaptation was not included in the model for two reasons: the slope is strongly affected by the mortality on the days with very high temperature, but days with very high temperature are inherently rare – thus, we chose to pool the data to obtain statistical stability; and there is currently no good model of this type of adaptation that can be used for future projection.

Third, weather factors other than temperature may also be important in determining future mortality risk. High humidity is known to increase risks because physiological responses for heat dispersion such as sweating are limited. Humidity has been included in the models in some reports (Iniguez et al., 2010), but the effect of humidity on the temperature–mortality relation was reported to be negligible (Honda et al., 2000).

Fourth, there is some evidence that temperature–mortality functions are heterogeneous in populations around the world (Hajat & Kosatky, 2010). Not all temperature–mortality relations are V-shaped: W-, J- and U-shapes were also reported in previous studies (Bai et al., 2014). In some southern cities in the United States, heat-related deaths were not observed (Kinney et al., 2008), which is assumed to be due to the high penetration of air-conditioning.

A universal relative estimate of optimum temperature may not be valid for all populations, particularly those outside temperate zones. For the optimum temperature estimation, analysis of the US, Europe, the Republic of Korea, China (Province of Taiwan) and Japan in our model paper showed reasonably good agreement between the optimum temperature and the 84th percentile value of daily maximum temperature. As mentioned, however, some southern cities in the United States did not show a V-shaped relation (no optimum temperature was observed). A previous analysis showed that the 84th percentile hypothesis worked well across countries with various income levels (Honda et al., 2014). Sub-Saharan African and south Asian regions are possibly the regions most affected by high heat exposure, but empirical data for these areas are not available and could not be included in model development. Future studies should address this limitation.

Coastal flood mortality

3

Simon Lloyd, Sari Kovats, Zaid Chalabi

3.1 Background

Around 120 million people are exposed to coastal floods associated with tropical cyclones and storm surges each year, causing an estimated 250 000 deaths between 1980 and 2000 (Nicholls et al., 2007). This gives an average of about 12 000 deaths per year (Shultz et al., 2005). A single disaster event may cause considerably higher mortality. For example, Cyclone Nargis caused around 138 000 deaths in Myanmar in 2008 (Fritz et al., 2009). National wealth and adequately implemented warning and protection measures may mitigate mortality impacts, but populations remain vulnerable: Hurricane Katrina, for instance, caused around 1800 deaths in the United States in 2005 (Knabb et al., 2006).

As well as mortality, flood events are known to cause injuries, infection, mental health problems (Ahern et al., 2005), loss of income and crops, and infrastructure damage. Such impacts are not necessarily direct and immediate; they may occur via indirect pathways (for example, damaged water and sanitation facilities may spread infectious diseases) and may be delayed (such as mental health impacts). Few studies have quantified the full health impacts of floods or specific events (Collier, 2007; Fewtrell & Kay, 2008). The economic impacts of cyclones are potentially large and appear to be growing. Estimates suggest that between 1970 and 2010, the proportion of global GDP exposed to cyclones increased from 3.6% to 4.3%; although this appears to be a small change, rapid economic growth over the period means that in absolute terms this accounts for a tripling from around US$ 500 billion to US$ 1.6 trillion (UNISDR, 2011).

In the future, climate change is expected to worsen coastal flood hazards through sea-level rise (Brown et al., 2013) and an anticipated increase in the intensity (but not frequency) of cyclone events (Emanuel, 2005; IPCC, 2012). Rising temperatures are expected to bring sea-level rise due to thermal expansion of oceans and land-ice melt, which will deepen flood waters and potentially affect greater areas of land. The IPCC Fifth Assessment Report estimates that under high emissions (RCP8.5), sea levels may rise between 0.52 m and 0.98 m by 2100 (Church et al., 2013). Under the most optimistic emissions scenario (RCP2.6), the sea-level rise is expected to be 0.26–0.55 m. For the emissions scenarios considered in this assessment, the IPCC estimated sea-level rise would be between 0.26 m and 0.59 m by 2100 under an A1FI scenario (Meehl et al., 2007). More recent studies have estimated higher rates of change, although uncertainty remains large (Ramsdorf, 2010).

A number of non-climate factors will also affect future coastal flood risk due to changes in population exposure and vulnerability. For exposure, coastal mega-cities and other population centres are growing rapidly; many of these are in low-income countries, where vulnerability to disasters is highest (Wisner et al., 2004; McGranahan et al., 2007). Although there has been a general decrease in vulnerability in recent decades due to improved disaster

preparedness, vulnerability remains 225 times greater in low-income than in higher-income countries (UNISDR, 2011). Risk does not decline linearly with economic development: observations suggest that as low-income countries develop, risk may initially increase before decreasing (de Haen & Hemrich, 2007; Kellenberg & Mobarak, 2008). The expansion of slums in coastal cities may increase population exposure at a greater pace than can be compensated for by risk-reduction measures.

This combination of changes in hazard, exposure and vulnerability suggests coastal flooding may have significant impacts on human health in the future.

3.2 Quantifying the burden of flood-related disasters

Several assessments have quantified the impact on mortality or the burden of disease from cyclones and coastal floods (e.g. Jonkman, 2005; Dasgupta et al., 2009; UNISDR, 2011; Peduzzi et al., 2012; Lloyd et al., 2014). We are not aware of any global assessment that has quantified the impact on morbidity.

Previous studies of future flood mortality can be classified as one of two types: event-based models (Penning-Roswell et al., 2005; Jonkman et al., 2008; Maaskant et al., 2009) and average mortality models (e.g. McMichael et al., 2004; Peduzzi et al., 2012; Lloyd et al., 2014). Event-based models focus on single flood events and use detailed data describing flood characteristics (such as water depth and flow velocity), area-specific conditions (such as building types and evacuation routes) and the exposed population (such as age distribution and underlying health). The data requirements mean the strategy is not suitable for global-level modelling. Average-mortality models consider a given area such as a grid cell or nation-state and use data on long-term probabilities of events, average population exposure, and (possibly) average socioeconomic conditions to estimate average mortality over a given time period; we adopt this general strategy in this chapter.

To our knowledge, only three papers have attempted to quantify future storm-surge mortality beyond the local level. McMichael and colleagues (2004) used a 20-year mortality data series of all coastal flood events (a geographical rather than an event-type definition). Mortality risk was estimated using national population rather than exposed population as the denominator. For future projections, the changes in population vulnerability were scaled linearly to GDP per capita.

Dasgupta and colleagues (2009) developed a spatially explicit mortality model for 84 countries and 577 coastal cities. They modelled 1-in-100 year storm-surge events and assessed future impacts under climate change accounting for sea-level rise and a 10% increase in event intensity. Despite detailed physical modelling, socioeconomic changes were poorly represented: future country-level impacts assumed no population or socioeconomic changes, and city-level impacts held socioeconomic factors constant but accounted for population change.

Lloyd and colleagues (2014) developed a mortality model that was fitted using event-based definition of coastal flooding and a 40-year time series of mortality data, modelled

vulnerability using the Human Development Index, and allowed for an initial increase in vulnerability when low-income countries developed.

3.3 Objectives

In this assessment, we use the mortality model of Lloyd and colleagues (2014) to estimate future regional-level mortality patterns associated with coastal flooding.

Coastal flooding refers specifically to flooding associated with storm-surge events, where a storm surge is defined as sea water that has been pushed forward and drawn up by a depression (i.e. a cyclone or 'cyclone-like' event) which floods an otherwise dry area along the coastline (NOAA, 2013). Of note, storm surge is generally just one component of a cyclone-like event, which may also cause loss of life due to high-speed winds and heavy rains. We do not consider the health impacts of these winds and rains. Additionally, as the upstream coastal flood model (see Section 3.4) used to drive the mortality model assumes no changes in cyclone frequency or intensity, our estimates likewise adopt this assumption.

In sum, by isolating the storm-surge component, in our climate change-attributable mortality estimates we specifically assess the mortality impacts of future sea-level rise.

Coastal flooding is an indirect health impact of climate change. Climate influences sea level, which then, via coastal flooding and in interaction with social conditions, impacts on health. Consequently, the mortality model is not driven directly by climate scenarios. Rather, climate scenarios are used to drive a coastal flood model (see Section 3.4) that produces estimates of human exposure to storm surge, which then drive the mortality model. As the coastal flood model was run independently of this project, future mortality estimates are based on a different set of scenarios than those used in other chapters (see Section 3.5).

In this chapter, we provide future mortality estimates both with and without climate change and with and without sea-based strategies of adaptation (that is, the raising of sea dikes and beach nourishment – see Section 3.4). Due to the limitations of the mortality model (see Section 3.4.2), rather than quantifying future mortality we present the results as regional level categorical estimates. Additionally, due to these limitations, we do not formally assess uncertainties in the estimates.

3.4 Description of the model

3.4.1 Coastal flood model (DIVA)

DIVA is an integrated biogeophysical model that assesses the impacts of sea-level rise (assuming no increase in storminess), subsidence and socioeconomic change in the coastal zone (Vafeidis et al., 2008; Hinkel & Klein, 2009). Subsidence values were taken from Peltier (2000a,b) and socioeconomic data from IMAGE 2.3 A1 projections (van Vuuren et al., 2007) (see Section 3.5). Patterned scaled climate scenarios used in the model were derived by Pardaens and colleagues (2011), with impact results reported by Brown and colleagues (2011).

We used the DIVA output of country-level average annual number of people at risk of exposure to storm surge (that is, expected number of people flooded per year if they do not evacuate or move to storm shelters). This estimate does not account for the qualities of the floods to which the population is exposed, such as patterns of intensity (for example, whether total exposure was due to one very large, very lethal flood or due to many small, less lethal floods) or duration of flooding.

DIVA makes three key assumptions of relevance to this assessment. First, it is assumed that the national population changes at the same rate in all locations within a country – that is, urban and coastal areas grow or shrink at the same rate as rural and inland areas. Second, it is assumed that the frequency and intensity of future surge events remain at baseline levels – that is, they are held constant over time; however, due to climate change-induced sea-level rise, along with land subsidence, floodwaters associated with a given event are expected to be deeper, potentially flooding a greater land area. Third, it is assumed that the people who are expected to be flooded on average once a year move out of the flood zone; this reduces exposure and hence potential mortality.

DIVA made future exposure estimates with and without adaptation, modelled as sea dikes and/or beach nourishment. We refer to these as "sea-based strategies of adaptation". In futures without sea-based strategies of adaptation, protection is modelled[1] for a common baseline (1995), and it is assumed that this standard of protection is not upgraded as sea-level rise and socioeconomics change. In futures with sea-based strategies of adaptation, dikes are upgraded to reflect changes in population density as the sea level rises and there is beach nourishment in response to erosion. In this assessment, we made estimates of future mortality both with and without sea-based strategies of adaptation.

DIVA does not consider land-based strategies of adaptation such as warning systems, storm shelters and building regulation. These aspects are modelled in the mortality model. In this assessment, all future estimates include land-based strategies of adaptation.

We used DIVA population exposure estimates for the years 2030, 2050 and 2080, both with and without climate change, and with and without sea-based strategies of adaptation. Exposure estimates in futures with climate change were available as median estimates and the 5th and 95th centiles.

3.4.2 Mortality model

We used the storm-surge mortality model of Lloyd and colleagues (2014). When developing this model, the authors found that although coastal flood mortality risk appeared to be amenable to statistical modelling (partly because it generally changes continuously over time), flood mortality – for which the vast majority of deaths are caused by infrequent large events – was predicted poorly by the model (partly because average annual mortality is subject to discontinuities in the face of a large event). Because of this, the authors made a number of suggestions to improve subsequent mortality modelling efforts (Lloyd et al., 2014). As a rough indication of future mortality patterns under climate change, however, regional

[1] DIVA uses a modelled baseline of adaptation because global data for current protection are not available.

mortality at future time points was presented as categories (for example, 10–30 deaths/year and 30–100 deaths/year); it was stressed that the results should be interpreted very cautiously. We adopt the same practice when projecting mortality in this paper, and the results should be interpreted only as roughly indicative of possible future mortality patterns.

The model is a statistical model that attempts to estimate average annual mortality for a given time slice. The general equation is:

$$\ln\left(\frac{M_{i,j}+1}{X_{i,j}} \times 10^6\right) = \beta_1 \ln(E_i + 1) + \beta_2 \ln(P_{i,j}) + \beta_3 H_{i,j} + \beta_4 H_{i,j}{}^2 + k \qquad [3.1]$$

where $M_{i,j}$ is the average annual surge mortality in country i in time slice j; $X_{i,j}$ is the average annual number of people at risk of exposure to storm surge in country i in time slice j; 10^6 scales the equation to per 1 million people exposed; E_i is the average annual number of surge events in country i; $P_{i,j}$ is the national population of country i in time slice j; $H_{i,j}$ is the Human Development Index in country i in time slice j; $\beta 1$, $\beta 2$, $\beta 3$ and $\beta 4$ are fitted model parameters; and k is a constant. (Note that $M_{i,j}$ and E_i were shifted by 1 as these variables may take zero values; in these cases, the logged term would be undefined.)

The values of the beta parameters and the statistical fit (confidence intervals and *P*-values) are shown in Table 3.1.

Table 3.1 Estimate of mortality model parameters, confidence intervals and *P*-values

Parameter	Mean estimate	95% confidence interval	*P*	Variable
$\beta 1$	1.73	0.75 to 2.72	0.001	E_i
$\beta 2$	–0.78	–0.96 to –0.60	0.0001	$P_{i,j}$
$\beta 3$	18.01	7.68 to 28.35	0.001	$H_{i,j}$
$\beta 4$	–13.46	–22.38 to –4.54	0.003	$H_{i,j}{}^2$
k	15.60	11.51 to 19.69	0.0001	

The left-hand side of Equation [3.1] approximates log mortality risk per 1 million (when mortality is high, shifting mortality by 1 has little influence on the estimate of risk). From here on, we refer to the left-hand side of the equation as the log mortality risk. The denominator $X_{i,j}$ is the exposure data provided by DIVA.

Following Patt and colleagues (2010), the variables on the right-hand side of the equation are interpreted as follows. E_i and $P_{i,j}$ represent exposure characteristics. As the number of annual events E_i increases, coping capacity is expected to decrease and hence average mortality risk is expected to increase. Conversely, it is "expected that larger countries are likely to experience disasters over a smaller proportion of their territory or population, and also benefit from potential economies of scale in their disaster management infrastructure" (Patt et al., 2010). Thus, as population $P_{i,j}$ increases, so mortality risk is expected to decrease.

The Human Development Index $H_{i,j}$ is a national-level measure of development that accounts for social and economic factors (UNDP, 2010). The index takes values from 0 to 1, where 0 is the lowest level and 1 is the highest level of development. In the model, the Human Development Index acts as a proxy for land-based strategies of adaptation for reducing disaster risk. As in the original paper, due to data availability, we use an analogue of the Human Development Index (see original paper (Lloyd et al., 2014) and Section 3.5.3).

Generally, as $H_{i,j}$ increases, total mortality risk may be expected to decline. For coastal floods, however, observations suggest that as low-income countries develop, risk initially increases (de Haen & Hemrich, 2007; Kellenberg & Mobarak, 2008). Because of this, the model includes $H_{i,j}$ as a quadratic term.

Equation [3.1] is used to estimate log mortality risk. Following this, mortality is extracted using

$$M_{i,j} = \left[\frac{\exp(RHS) \times X_{i,j}}{10^6}\right] - 1 \qquad [3.2]$$

where

$$RHS = \beta_1 \ln(E_i + 1) + \beta_2 \ln(P_{i,j}) + \beta_3 H_{i,j} + \beta_4 H_{i,j}^2 + k$$

(that is, the right-hand side of Equation [3.1]).

As the final step in extracting mortality is to subtract 1, it is possible to obtain results where $-1 \leq M_{i,j} < 0$. In these cases, results are rounded up to 0. In cases where mortality exceeds the number exposed, mortality is set equal to exposure.

Equation [3.2] moves from the log space to the natural space; in doing so, error is introduced into the mortality estimates. This error, which is combined with the discontinuous nature of flood mortality as described above, introduces further unreliability into the mortality estimates. Consequently we aggregate all mortality estimates to the regional level and present them categorically. We note that categorization does not overcome the possible errors, and results should be interpreted only as broadly indicative of future impacts.

3.5 Scenario data

The DIVA coastal flood model was run independently of this assessment and used a different set of scenarios from other chapters in this report. We outline the details below.

3.5.1 Sea-level rise scenarios

The DIVA estimates were made under A1B emissions as the mean of two Hadley Centre models: HadCM3C and HadGEM2-A0. (Data were provided by the United Kingdom of Great Britain and Northern Ireland Met Office Hadley Centre and use the multi-model climate experiment from the European Commission ENSEMBLES project (Lowe et al.,

2009).) Average global warming was 2.4°C by the 2050s and 3.8°C by the 2090s. This corresponds to global mean sea-level rises of 0.22 m by 2050 and 0.37 m by 2080.

3.5.2 Population data

DIVA estimates were based on IMAGE 2.3 A1 projections (van Vuuren et al., 2007), with global populations of about 7.8 billion, 9 billion and 7.1 billion in 2035, 2055 and 2085, respectively. This contrasts with the continued post-2050 population growth projected in the UN (2011) estimates used in other chapters in this assessment, which suggest the global population will reach about 10 billion by 2100.

For consistency with DIVA, initial national-level mortality estimates were made using IMAGE 2.3. These initial estimates were then rescaled to match the UN projections using:

$$M'_{i,j} = \frac{P\prime_{i,j}}{P_{i,j}} \qquad [3.3]$$

where M',j is the average annual surge mortality rescaled to the UN (2011) population projections in country i in time slice j; $P'_{i,j}$ is the national population as estimated by the UN (2011) projections in country i in time slice j; and $P_{i,j}$ is the national population as estimated in the IMAGE 2.3 projections of country i in time slice j.

By rescaling, we assume that coastal flood mortality increases in proportion to population. Although this is inconsistent with Equation [3.1], it brings the mortality estimates roughly into line with the population scenarios used in other chapters of this assessment. The impact of this inconsistency is reduced as the mortality estimates are presented only as categories.

3.5.3 Projections of the Human Development Index

Data to calculate the Human Development Index $H_{i,j}$ were required. This index is the geometric mean of normalized estimates of log GDP per capita, life expectancy at birth and years of education (UNDP, 2010). For consistency with DIVA, GDP per capita data were taken from IMAGE 2.3 (van Vuuren et al., 2007). We note that GDP per capita data used in other chapters of this assessment are measured as purchasing power parity, while IMAGE 2.3 uses market exchange rate. These metrics are not directly comparable or easily converted from one to the other. We assume that the IMAGE 2.3 estimates are roughly equivalent to the base case scenario used in the remainder of this assessment. It was not possible to make estimates for low-growth and high-growth futures. Data for life expectancy at birth were from the UN (2011) revision medium estimates, and data for years of education were from Barro & Lee (2010).

Finally, the mortality model (Equation [3.1]) also required data for the events variable E_i. This variable was based on estimates from Lloyd and colleagues (2014), which were derived from EM-DAT (CRED, 2011). The number of events was held constant over time, which, consistent with DIVA, assumes that the frequency of tropical cyclones does not increase in the future.

3.6 Assumptions

The key assumptions have been outlined above. The first three assumptions were necessitated by assumptions in the DIVA flood model (see Section 3.4.1):

- Within-country population change is spatially uniform.
- There is no change in storm-surge frequency and intensity from baseline (but floodwaters are deeper with sea-level rise).
- People flooded on average once a year autonomously leave the area and are not at risk of flooding and hence mortality.

The next assumption, based on observations, is an assumption of the flood mortality model (see Section 3.4.2):

- As low-income countries develop, there is an initial rise in risk of flood mortality, but this risk declines with subsequent development.

The final assumption arose from the need to rescale the population projections used to generate the DIVA exposure estimates to the population used in the other chapters of this report (see Section 3.5.2):

- By rescaling from IMAGE 2.3 to UN population projections, it is assumed that mortality changes in proportion to population.

3.7 Results

Figure 3.1 shows regional average annual mortality at baseline and for the 2030, 2050 and 2080 time slices, for the median exposure estimates based on two global climate models under A1B emissions. Mortality is given as categorical estimates. Regions are shown on the vertical axis and time slices on the horizontal axis. For each region there are three horizontal bars. The upper bar shows mortality without climate change and without sea-based strategies of adaptation. The central bar shows a future with climate change but without sea-based adaptation; comparing the central bar with the top bar gives an indication of climate change-attributable mortality. The lower bar shows mortality in futures with climate change and adaptation; comparing the middle and lower bars gives an indication of the mortality burden avoidable via adaptation. (All futures include land-based strategies of adaptation.)

For example, for east Asia, the results suggest that in the absence of climate change and adaptation (upper bar), mortality increases until 2050 (due to population increase and subsidence). Mortality then decreases by 2080 (but remains above baseline level) due to a mix of change in population and land-based strategies of adaptation, as represented by the Human Development Index. With climate change but no adaptation (middle bar), mortality rises rapidly by 2030 and remains high in 2080, despite the presumed implementation of land-based strategies. With climate change and sea-based adaption (lower bar), mortality increases a relatively small amount between 2030 and 2050 and is reduced to roughly baseline levels by 2080; this suggests that affordable sea-based adaptation would bring

Figure 3.1 Estimates of region-level[a] annual average mortality ranges at baseline in 2030, 2050 and 2080, based on median exposure estimates

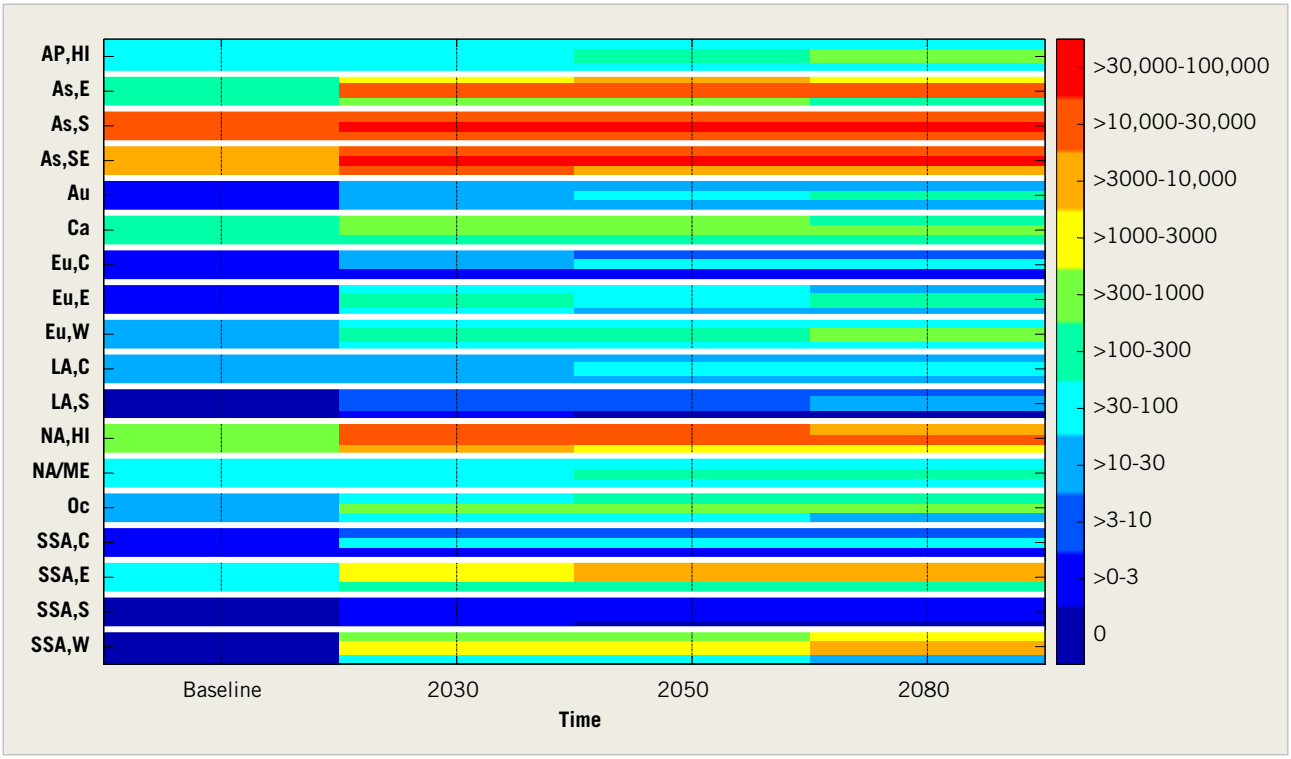

Note: For each region, there are three coloured horizontal bars which, from top to bottom, are (i) a future without climate change or adaptation, (ii) a future with climate change but no adaptation, (iii) a future with climate change and adaptation. The colour of the bar indicates the range of average annual mortality as per the legend on the right.

[a] AP,HI – Asia Pacific, high income; As,E – Asia, east; As, S – Asia, south; As,SE – Asia, south-east; Au – Australasia; Ca – Caribbean; Eu,C – Europe, central; Eu,E – Europe, eastern; Eu,W – Europe, western; LA,C Latin America, central; LA,S – Latin America, southern; NA,HI – North America, high income; NA/ME – North Africa/Middle East; Oc – Oceania; SSA,C – sub-Saharan Africa, central; SSA,E – sub-Saharan Africa, eastern; SSA,S – sub-Saharan Africa, southern; SSA,W – sub-Saharan Africa, western.

significant benefits. Similar patterns are seen in high-income North America, Oceania and parts of sub-Saharan Africa.

In contrast, in south Asia climate change increases mortality, but mortality is high in futures with and without climate change in the absence of adaptation. In a future with climate change and sea-based adaption, mortality decreases but remains high: despite adaptation, storm-surge mortality remains a major threat.

3.8 Discussion

Climate change may increase the burden of mortality from coastal flooding, but the impacts are highly uncertain and depend crucially on adequate coastal defences and disaster preparedness.

The mortality projections agree broadly with the previous assessment (McMichael et al., 2004): that is, climate change is expected to increase storm surge-associated mortality in

many regions of the world, in particular south Asia, high-income North America, Oceania, and east and west sub-Saharan Africa. Sea-based defences could significantly reduce this burden.

The mortality estimates in Figure 3.1 must be treated cautiously. We suggest they may be better interpreted as being indicative future changes in regional mortality risk; that is, the mortality estimates are expected annual averages based on the return periods of storm surges of given magnitudes. The return periods of the most lethal of these events tend to be long, perhaps in the order of 1–100 years. This means that although mortality risk (generally) evolves continuously, risk translates into actual mortality only if an event occurs, which over a timeframe of about 50 years involves an element of randomness (that is, an event may or may not occur). Thus, it is inevitable that mortality projections are often too high or too low over decadal timescales.

Consequently, Figure 3.1 may better illustrate how mortality risk rather than actual mortality may evolve under climate change. Such information is potentially useful, as adaptation (and mitigation) should be (along with other considerations) guided on the basis of mortality risk. Given the potential impact of climate change on storm-surge mortality risk, and the long lead time required for developing sea-based defences, models that assess local risk in areas that are vulnerable should be developed in order to guide policy.

Diarrhoeal disease

4

Sari Kovats, Simon Lloyd

4.1 Background

Many deaths (especially in children) could be prevented if everyone practised good hygiene and had reliable access to good sanitation and drinking water (Bartram & Cairncross, 2010). The modest millennium development goal target for access to safe domestic water has been met, but 2.5 billion people in low- and middle-income countries still lack access to improved sanitation facilities (Dar & Khan, 2011). Diarrhoeal disease is one of several global health problems that is unlikely to be solved by economic development in the near term but may be undermined by environmental changes that damage urban infrastructure (such as climate change and disasters) and reduce the overall availability of water (such as climate change and water resource depletion). A study that evaluated the impact of climate change on household water and sanitation found that very few technologies were resilient to climate change (Howard & Charles, 2010). The authors concluded that although climate change "represents a significant threat to sustainable drinking-water and sanitation services, through no-regrets actions and using opportunities to increase service quality, climate change may be a driver for improvements that have been insufficiently delivered to date".

4.1.1 Sensitivity of diarrhoeal disease to climate variability and climate change

Diarrhoeal disease transmission is known to be affected by temperature and rainfall factors at a range of timescales. Water scarcity (which is a measure of per capita water availability) is associated with a range of health problems, including diarrhoea, in certain populations, although few studies directly quantify this relationship. A study in 18 Pacific islands, considering average weather conditions over a 10-year period, found that all-cause diarrhoea (measured by hospital admissions) increased with decreasing water availability (Singh et al., 2001). An attempt to quantify this relationship using multiple-regression, however, was uninformative, possibly due to a lack of statistical power. A global cross-sectional study found a statistically significant association between low-rainfall locations and diarrhoeal disease prevalence in children (Lloyd et al., 2007).

Several studies have quantified the effect of temporal variation in environmental temperature on human food-related infections, including salmonellosis (d'Souza et al., 2004; Kovats et al., 2004) and campylobacteriosis (Louis et al., 2005; Tam et al., 2006).

The impact of climate scenarios on diarrhoeal diseases was quantified for the WHO Global Burden of Disease project (McMichael et al., 2004). That project developed a global temperature–diarrhoeal disease function based on two papers that quantified the short-term association between temperature and diarrhoeal disease (hospital admissions in Lima (Checkley et al., 2000) and Fiji (Singh et al., 2001)). Since then, more epidemiological

papers have been published that consistently indicate an effect of short-term (daily, weekly, monthly) temperature variability on diarrhoeal disease transmission in a variety of settings.

Few studies have quantified the impacts of climate change on future diarrhoeal disease outcomes. A global study estimated future impacts of climate change on the relative risk function (Kolstad & Johansson, 2011). This assessment is difficult to interpret as it did not relate final results to the actual burden of disease. Furthermore, it did not take into account future factors that would reduce the impact of temperature on diarrhoeal disease transmission.

Some studies have attempted to evaluate the adaptation cost. One study used the Global Burden of Disease estimates to estimate future adaptation costs in treating additional cases of diarrhoeal disease due to climate change (Ebi, 2008).

4.2 Description of model

A new model was developed for this WHO global assessment that could be driven by existing knowledge and the best available data. The first step was to review the literature to assess the current quantitative knowledge of the relationship between climate and diarrhoeal disease. Existing knowledge is limited, and therefore a relatively simple model was constructed. Figure 4.1 describes the framework of the model developed. The model applies gridded estimates of average annual temperature anomalies under climate change to a global-level temperature–mortality risk relationship, combines this with future diarrhoeal disease mortality estimates in children aged under 15 years in futures without climate change, and estimates climate change-attributable diarrhoeal disease deaths at the regional level.

Figure 4.1 Structure of the diarrhoeal disease mortality model

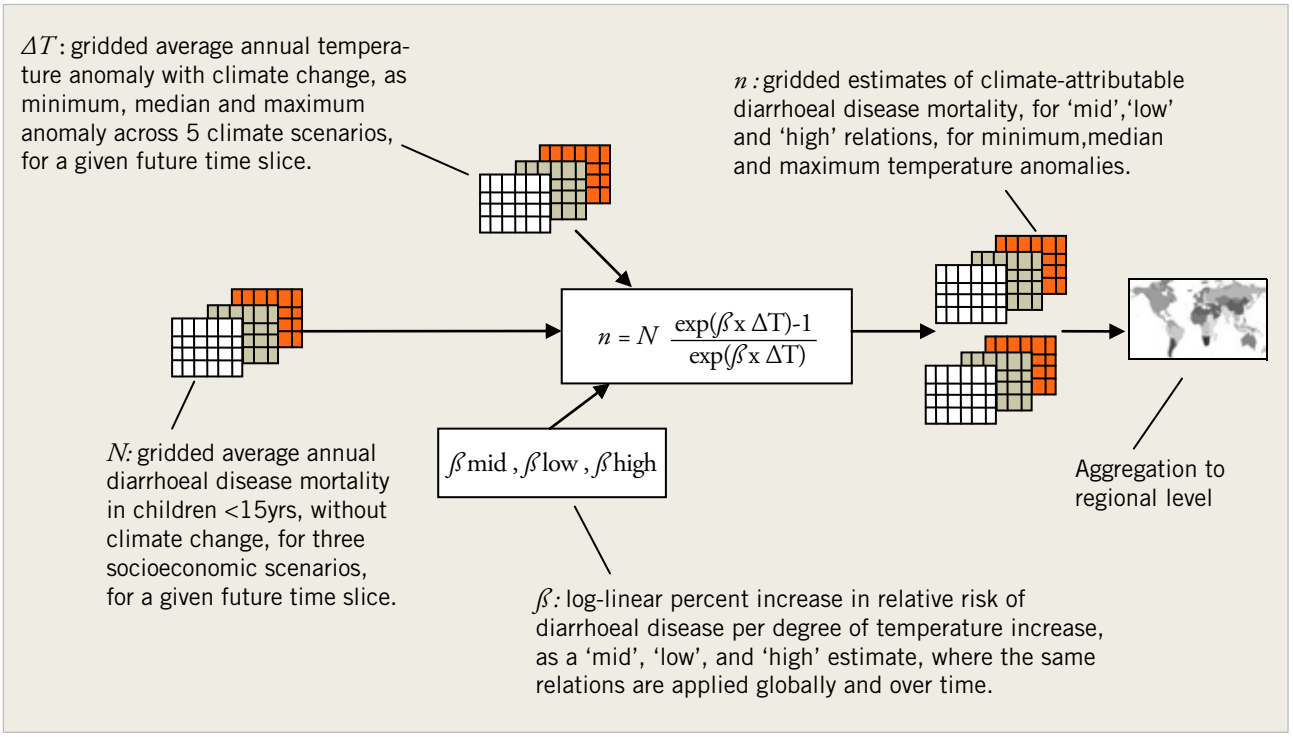

4.2.1 Existing quantifications of the diarrhoea–temperature relationship

To develop the exposure–response functions for this assessment, we conducted a literature review to identify all studies that quantified an association between temperature and diarrhoeal disease using time series regression. We then grouped these studies by world region.

Very few studies were found that quantified the effect of rainfall on diarrhoeal disease outcomes, so we restricted the assessment to temperature effects. We found seven published studies that met our criteria. All the studies focused on morbidity, with no studies assessing mortality (the focus of this assessment). Table 4.1 lists all the studies that met our inclusion criteria.

Table 4.1 Time-series studies quantifying relationship between temperature and morbidity due to diarrhoeal disease, by WHO region

Region	Reference	Location	RR (95% CI) per 1°C above threshold value	Study design	Outcome	Age group	Data period
Asia Pacific, high income	Onozuka et al. (2010)	Japan	0.08 (0.05 to 0.11)	Poisson regression, weekly	Hospital reports of infectious gastroenteritis cases	All ages	1999–2007
Asia, east	Chou et al. (2010)	China, Province of Taiwan	0.04 (0.01 to 0.07)	Poisson regression, monthly	Hospital admissions for all-cause diarrhoea	< 14 years	1996–2007
	Zhang et al. (2008)	Jinan, China	0.10 (0.10 to 0.13)	Monthly time series, SARIMA	Bacillary dysentery	All ages	1987–2000
Asia, south	Hashizume et al. (2007)	Dhaka, Bangladesh	0.06 (0.03 to 0.08)	Poisson regression, weekly	Hospital visits, all non-cholera diarrhoea	All ages	1996–2002
Latin America, Andean	Checkley et al. (2000)	Lima, Peru	0.08 (0.07 to 0.09)	Time series, daily	Hospital admissions, all for diarrhoea	< 10 years	1993–1996
	Lama et al. (2004)	Lima, Peru	0.11 (0.07 to 0.16)	Time series, monthly	Hospital admissions, all for diarrhoea	> 13 years of age	1991–1998
Oceania	Singh et al. (2001)	Fiji	0.03 (0.01 to 0.05)	Poisson regression, monthly	Hospital admissions, all for diarrhoea	All age groups	1978–1989

All studies provided estimates of the percentage increase in the relative risk of diarrhoeal disease per 1°C of temperature increase, and most studies controlled for seasonal variations and long-term trends. Overall, all studies found that diarrhoeal disease risk increases as temperature increases, ranging from a 3% to 11% increase in risk per 1°C of temperature increase. Of note, the timescale over which these relationships apply ranged from daily to monthly. Some studies looked at all ages, while other studies focused on specific age groups. In terms of regional coverage, studies covered only 5 of the 21 regions.

Current knowledge of observed temperature–diarrhoea relationships over time and space is very limited. The age groups varied by study. More significantly, for a global assessment, studies are available for relatively few locations. A further difficulty in generating a valid temperature–health function is the range of pathogens that cause diarrhoeal disease (Table 4.2). Major viral agents such as rotavirus typically peak in the winter seasons in temperate countries and in rainy seasons in tropical countries. Several studies describe climate effects on particular enteric pathogens, but these cannot be used directly to estimate effects on diarrhoeal disease without information on their relative contribution to overall disease incidence, and equivalent data on climate sensitivity and relative prevalence for all other diarrhoea pathogens. There was insufficient information to address this source of bias in the functions (see below).

Table 4.2 Percentage of selected enteropathogens in children with diarrhoea in developing countries

Enteropathogen	Community-based studies		Health facility-based studies	
	Median	Range	Median	Range
Aeromonas sp.	2	<1–13	2.5	<1–42
Campylobacter sp.	6	1–24	7	0–32
Cryptosporidium purvam	4	2–7	4	1–12
Entoamoeba histolytica	<1	<1–9	1	0–7
Enterotoxigenic *Escherichia coli*	14	2–41	11	1–54
Giardia lamblia	10.5	<1–24	2	0–28
Rotavirus	6	2–29	20	5–49
Salmonella sp.	1	0–6	4	0–38
Shigella sp.	4	1–27	5	0–33
Vibrios	<1	0–3	1	0–33

Source: Black et al. (2003)

4.2.2 Model development

There were a number of issues related to choosing and using the available temperature–diarrhoeal disease relationships. First, we wanted to estimate future climate change-attributable diarrhoeal disease mortality, but the available studies focus on morbidity. Because of this, we assumed that for a given percentage change in morbidity in response to temperature, mortality changes by the same percentage and that this is true over space and time.

The second issue was whether there is a threshold above which the temperature begins to increase diarrhoeal disease. The available studies do not specify thresholds. Because of this, we assume that if there is a threshold, then it is below current (baseline) average annual temperatures and that any future temperature increases (anomalies) associated with climate change are above the threshold and contribute to more diarrhoeal disease.

The third issue relates to the unit of time over which the estimates of the temperature–diarrhoeal disease relationship apply. Most studies were analyses of daily or weekly time series data. We applied changes in annual temperature to the temperature-mortality function (see below). We note that as a consequence we are unable to account for seasonal variations in risk.

The fourth issue relates to choosing the exposure–response relationships with which to drive the model. Ideally, particular functions would be derived by meta-analysis by region, age group and pathogen. Given the scarcity of the available data, we assumed that the available relationships apply to all age groups and all-cause diarrhoea. Furthermore, as there is no evident general pattern in the magnitude of the relationships by level of economic development (such as GDP per capita) or climate (such as latitude), we did not attempt to assign particular relationships to particular regions. As the majority of diarrhoeal disease burden falls on children, future estimates were restricted to children aged under 15 years.

Although the relationship between temperature and diarrhoeal disease is likely to vary by pathogen, and is likely to be modified by factors such as general child health and water and sanitation provision, for the purposes of estimating disease burdens across the globe we sought general relationships for all-cause diarrhoeal disease. For reasons described above, it was assumed that the range of estimates in Table 4.1 captures the plausible range in any location at any time, and a low, mid- and high estimate was used for all regions for all time periods (Table 4.3). The mid-estimate is not the best estimate of the relationship: it is merely the middle estimate; both the low and high estimates are equally plausible, and results are presented for mortality based on all three estimates (see Tables 4.4–4.6).

Table 4.3 Estimate of the percentage increase in relative risk of diarrhoeal disease mortality per 1°C increase in temperature

Estimate	Percentage increase in relative risk
Low	3
Mid	7
High	11

Mortality in futures without climate change

We use gridded mortality due to all-cause diarrhoeal disease in children aged under 15 years for three socioeconomic scenarios (base case, low growth and high growth; see Chapter 8).

Estimating future climate change-attributable mortality

We estimated future mortality using the above data and the following formula (Gasparrini et al., 2012):

$$n_{c,y,i,j} = N_{c,y} \frac{\exp[\beta i(\Delta T_{c,y,j})] - 1}{\exp[\beta i(\Delta T_{c,y,j})]} \quad [4.1]$$

where $n_{c,y}$ is the number of climate change-attributable average annual diarrhoea deaths in children aged under 15 years in grid-cell c in time slice y; $N_{c,y}$ is the total number of average annual diarrhoea deaths in children aged under 15 years in a future without climate change in grid-cell c in time slice y; $\Delta T_{c,y,j}$ is the temperature anomaly in grid-cell c at time slice y, where j = 1 for the minimum anomaly, j = 2 for the median anomaly, and j = 3 for the maximum anomaly, across the five climate scenarios; β_i is the log-linear increase in diarrhoeal deaths per degree of temperature increase, where i = 1,2,3 for the low, mid- and high estimates, respectively; and $\beta i = \log(1 + \alpha_i)$, where α_i is the linear increase in diarrhoeal deaths per degree of temperature increase, where i = 1,2,3 for the low, mid- and high estimates, respectively.

The grid cell-level estimates of climate change-attributable mortality are then aggregated to the regional level.

Model output

We estimated future climate change-attributable diarrhoeal disease mortality in children aged under 15 years for an A1b emissions scenario and for the three socioeconomic scenarios. Our main results at the regional level are based on the median temperature anomaly across five climate scenarios and use the low, mid- and high exposure–response function estimates (see Tables 4.4–4.6). We show climate uncertainty at the global level as climate change-attributable deaths for the minimum, median and maximum temperature anomalies, for the three socioeconomic scenarios using the mid-exposure–response relationship.

4.3 Scenario data

4.3.1 Climate data

We used the standard CCRA scenarios – that is, three global climate models driven by A1b emissions. As outlined above, the model was driven by grid-level minimum, median and maximum temperature anomalies from the five climate scenarios.

4.3.2 Diarrhoea mortality projections

We used the mortality projections described in Chapter 8 for estimates of future diarrhoeal disease mortality. Figure 4.2 shows global-level mortality and the crude mortality rate for the three socioeconomic scenarios. There is a clear decline in both the number of deaths and death rates in all three scenarios.

4.4 Assumptions

The central assumptions are as follows:

- The relationship between diarrhoeal disease morbidity and mortality is constant over time.
- The threshold above which temperature increases diarrhoeal disease is equal to or lower than current annual average temperatures – that is, all future temperature increases are above the threshold.
- The available estimates of the exposure–response relationship broadly capture the plausible range of this relationship across time and space.

Figure 4.2 Projections of diarrhoeal mortality: (a) deaths and (b) crude mortality rate for three socioeconomic scenarios

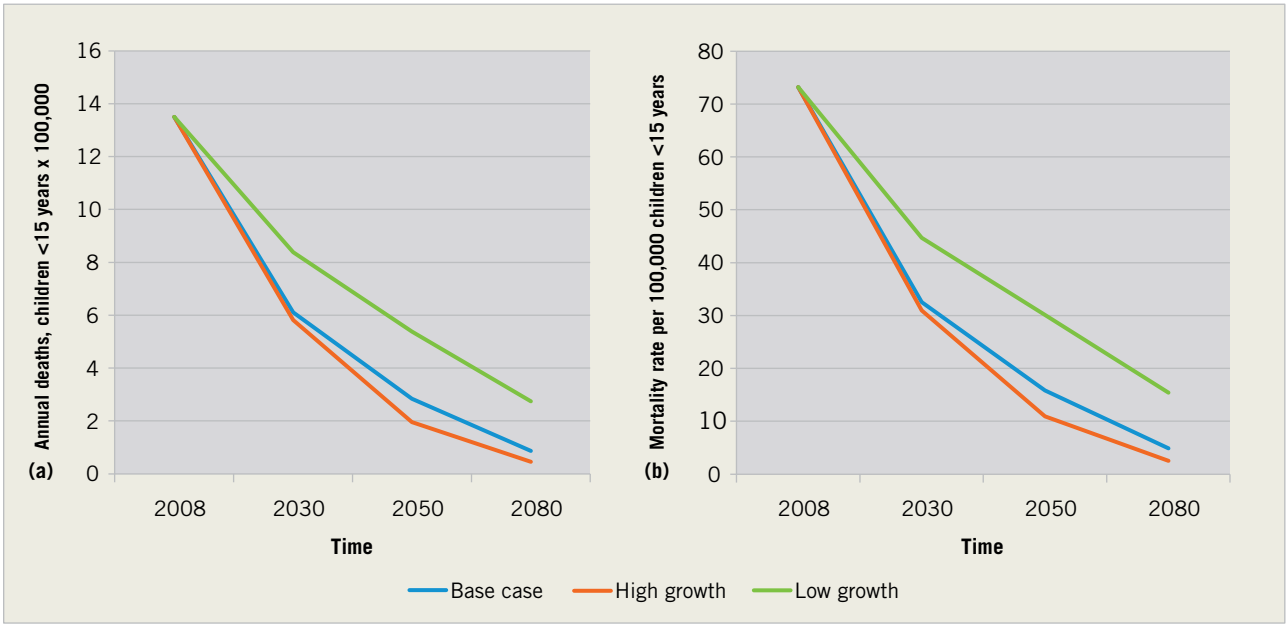

4.5 Results

In the base case scenario, climate change is estimated to cause an additional 48 000 deaths in 2030 and an additional 33 000 deaths in 2050 in children aged under 15 years due to diarrhoeal disease (Table 4.4).

Tables 4.4–4.6 show the results for the base case, high growth, and low growth scenarios. In all scenarios the climate change-attributable burden declines from 2030 to 2050 as the underlying burden of disease declines, despite rising temperatures due to climate change.

Table 4.4 Base case scenario: estimated number of deaths[a] due to diarrhoeal disease in children aged under 15 years by region, for 2008, 2030 and 2050, with and without climate change[b]

Region	2008	2030		2050	
		No climate change	With climate change	No climate change	With climate change
Asia Pacific, high income	54	15	16 (15 to 17)	7	8 (7 to 8)
Asia, central	7588	1000	1111 (1049 to 1150)	158	184 (170 to 196)
Asia, east	12 527	2227	2443 (2322 to 2525)	499	571 (532 to 605)
Asia, south	488 551	155 947	170 817 (162 480 to 176 508)	54 436	62 153 (57 958 to 65 857)
Asia, south-east	45 733	11 681	12 446 (12 017 to 12 786)	4127	4510 (4299 to 4702)
Australasia	7	3	3 (3 to 3)	1	1 (1 to 1)
Caribbean	6302	1206	1278 (1237 to 1310)	190	207 (198 to 216)
Europe, central	84	9	10 (9 to 10)	2	2 (2 to 2)
Europe, eastern	299	25	28 (26 to 29)	6	7 (6 to 7)
Europe, western	71	22	24 (23 to 35)	10	11 (11 to 12)
Latin America, Andean	3406	554	603 (575 to 623)	89	101 (94 to 106)
Latin America, central	7646	1558	1667 (1606 to 1714)	258	285 (270 to 298)
Latin America, southern	136	18	19 (18 to 20)	3	3 (3 to 3)
Latin America, tropical	2575	276	295 (285 to 303)	41	46 (43 to 48)
North America, high income	38	17	18 (17 to 19)	10	11 (10 to 12)

[Continues]

[Continued]

Region	2008	2030		2050	
		No climate change	With climate change	No climate change	With climate change
North Africa/ Middle East	35 453	14 648	15 971 (15 230 to 16 498)	6256	7068 (6625 to 7462)
Oceania	740	365	387 (375 to 397)	174	189 (181 to 197)
Sub-Saharan Africa, central	139 770	83 642	89 968 (86 416 to 92 588)	47 863	53 336 (50 336 to 56 037)
Sub-Saharan Africa, eastern	288 036	150 319	161 316 (155 130 to 165 904)	62 948	69 899 (66 086 to 73 340)
Sub-Saharan Africa, southern	13 155	5416	5905 (5631 to 6101)	2045	2312 (2166 to 2441)
Sub-Saharan Africa, western	297 885	181 690	194 427 (187 271 to 199 800)	104 420	115 594 (109 459 to 121 143)
World	1 350 055	610 638	658 752 (631 735 to 678 340)	283 544	316 498 (298 458 to 332 695)

a Mid-estimates based on the mid exposure–response relationship are given; low and high estimates are shown in brackets and are based on the low and high exposure–response relations (see Table 4.3)

b With climate change, estimates are based on the median temperature anomaly across the five global climate scenarios

Table 4.5 High growth scenario: estimated number of deaths[a] due to diarrhoeal disease in children aged under 15 years by region, for 2008, 2030 and 2050, with and without climate change[b]

Region	2008	2030		2050	
		No climate change	With climate change	No climate change	With climate change
Asia Pacific, high income	54	14	16 (15 to 16)	7	8 (7 to 8)
Asia, central	7588	864	959 (906 to 993)	121	141 (130 to 150)
Asia, east	12 527	1816	1991 (1893 to 2058)	330	377 (351 to 400)
Asia, south	488 551	147 283	161 306 (153 445 to 166 677)	52 456	59 968 (55 887 to 63 568)
Asia, south-east	45 733	8893	9475 (9148 to 9733)	2385	2606 (2484 to 2717)
Australasia	7	2	3 (3 to 3)	1	2 (1 to 2)
Caribbean	6302	802	850 (823 to 871)	117	128 (122 to 133)
Europe, central	84	7	8 (7 to 8)	1	1 (1 to 1)
Europe, eastern	299	21	23 (22 to 24)	4	5 (4 to 5)
Europe, western	71	22	24 (23 to 25)	11	12 (11 to 13)

[Continues]

[Continued]

Region	2008	2030		2050	
		No climate change	With climate change	No climate change	With climate change
Latin America, Andean	3406	409	445 (425 to 460)	66	74 (70 to 78)
Latin America, central	7646	1092	1169 (1126 to 1202)	207	229 (217 to 239)
Latin America, southern	136	13	14 (13 to 14)	4	4 (4 to 5)
Latin America, tropical	2575	197	211 (203 to 217)	42	47 (44 to 49)
North America, high income	38	17	19 (18 to 20)	12	13 (12 to 14)
North Africa/ Middle East	35 453	13 035	14 201 (13 548 to 14 666)	4664	5254 (4932 to 5541)
Oceania	740	262	278 (269 to 285)	93	101 (97 to 105)
Sub–Saharan Africa, central	139 770	85 022	91 459 (87 845 to 94 125)	28 148	31 371 (29 605 to 32 962)
Sub–Saharan Africa, eastern	288 036	151 722	162 835 (156 593 to 167 472)	48 705	54 108 (51 145 to 56 781)
Sub–Saharan Africa, southern	13 155	4222	4603 (4389 to 4756)	572	645 (605 to 681)
Sub–Saharan Africa, western	297 885	165 526	177 124 (170 608 to 182 019)	57 930	64 142 (60 372 to 67 227)
World	1 350 055	581 241	627 011 (601 321 to 645 644)	195 878	219 237 (206 463 to 230 680)

a Mid-estimates based on the mid exposure–response relationship are given; low and high estimates are shown in brackets and are based on the low and high exposure–response relations (see Table 4.3)

b With climate change, estimates are based on the median temperature anomaly across the five climate scenarios

Table 4.6 Low growth scenario: estimated number of deaths[a] due to diarrhoeal disease in children aged under 15 years by region, for 2008, 2030 and 2050, with and without climate change[b]

Region	2008	2030		2050	
		No climate change	With climate change	No climate change	With climate change
Asia Pacific, high income	54	13	14 (14 to 15)	5	6 (6 to 6)
Asia, central	7588	1399	1554 (1467 to 1609)	293	340 (315 to 363)
Asia, east	12 527	4219	4627 (4398 to 4793)	1987	2271 (2117 to 2407)
Asia, south	488 551	237 097	259 520 (246 948 to 268 128)	132 326	150 996 (140 845 to 159 960)

[Continues]

[Continued]

Region	2008	2030		2050	
		No climate change	With climate change	No climate change	With climate change
Asia, south-east	45 733	16 370	17 443 (16 841 to 17 919)	7422	8110 (7731 to 8456)
Australasia	7	2	2 (2 to 2)	1	1 (11)
Caribbean	6302	1448	1535 (1486 to 1573)	305	332 (317 to 345)
Europe, central	84	13	14 (13 to 14)	3	3 (3 to 3)
Europe, eastern	299	38	43 (40 to 45)	7	9 (8 to 9)
Europe, western	71	20	22 (21 to 23)	9	10 (9 to 10)
Latin America, Andean	3406	700	763 (728 to 788)	143	162 (152 to 171)
Latin America, central	7646	1830	1959 (1887 to 2015)	394	435 (412 to 455)
Latin America, southern	136	23	25 (24 to 25)	5	5 (5 to 5)
Latin America, tropical	2575	363	387 (373 to 398)	71	78 (74 to 81)
North America, high income	38	12	13 (13 to 14)	6	6 (6 to 7)
North Africa/ Middle East	35 453	19 275	21 025 (20 045 to 21 720)	10 614	12 003 (11 246 to 12 676)
Oceania	740	450	477 (462 to 490)	249	271 (259 to 282)
Sub-Saharan Africa, central	139 770	109 175	117 440 (112 799 to 120 863)	73 114	81 480 (76 895 to 85 608)
Sub-Saharan Africa, eastern	288 036	211 502	226 990 (218 290 to 233 450)	142 591	158 349 (149 to 705 to 166 150)
Sub-Saharan Africa, southern	13 155	7402	8070 (7695 to 8339)	4381	4951 (4640 to 5229)
Sub-Saharan Africa, western	297 885	227 037	242 929 (234 001 to 249 639)	164 364	181 914 (172 278 to 190 631)
World	1350 055	838 389	904 852 (867 549 to 931 852)	538 290	601 731 (567 022 to 632 856)

a Mid-estimates based on the mid exposure–response relationship are given; low and high estimates are shown in brackets and are based on the low and high exposure–response relations (see Table 4.3)

b With climate change, estimates are based on the median temperature anomaly across the five climate scenarios

The impact of climate change on diarrhoeal disease is concentrated in the world regions in Asia and sub-Saharan Africa, reflecting the current and future high burden of diarrhoeal disease in these populations.

4.6 Climate uncertainty

We estimated climate uncertainty in climate change-attributable diarrhoeal deaths by holding the exposure–response relationship constant as the mid-estimate (see Table 4.3). We looked at this for the two future time slices and for the three socioeconomic scenarios (Table 4.7).

Table 4.7 Number of additional diarrhoeal deaths globally in children aged 0–15 years due to climate change relative to the same future without climate change based on the mid exposure–response relationship

Temperature change	2030			2050		
	Base case	High growth	Low growth	Base case	High growth	Low growth
Minimum	37 084	35 346	51 032	28 503	19 803	54 110
Median	48 115	45 770	66 463	32 954	23 359	63 442
Maximum	62 618	59 574	86 275	42 430	29 789	81 330

Reading down any column in Table 4.7 shows uncertainty in the number of deaths associated with climate for a given time slice and for a given socioeconomic scenario. That is, in any column, the estimates are based on the minimum, median and maximum temperature anomalies across the five global climate models. For example, in the base case in 2030, and based on the mid-estimate of the exposure–response relationship, our lower and upper estimates are 37 084 and 62 618 climate change-attributable deaths respectively (based on the minimum and maximum temperature anomalies).

Reading across any row shows the influence of the socioeconomic scenario on additional deaths, for a given time slice, for a given estimate of the temperature anomaly (and based on the mid-estimate of the exposure–response relationship). For example, based on the minimum temperature anomaly in 2030, our estimates are 37 084 additional deaths in the base case scenario, reducing to 35 346 additional deaths in the high growth scenario and increasing to 51 032 additional deaths in the low growth scenario.

The range of uncertainty related to the climate scenarios is large and is roughly of the same order of magnitude of differences in estimates across the economic growth scenarios.

4.7 Discussion

This assessment indicates that higher temperatures may have significant effects on future diarrhoeal disease transmission, even when taking into account significant improvements in child health. The results show that the impact of climate change on diarrhoeal disease is likely to be a significant contribution to the overall burden on health of climate change. The impacts are particularly concentrated in south Asia and eastern Africa.

Climate change is likely to have significant effects on water availability. The direct temperature effects are not the only, or even the main, mechanism by which climate change may affect future diarrhoeal transmission. Reduction in water availability is a major concern for sustainable development. Only 10% of total global freshwater is used, and about 70% of this is used for irrigated agriculture, underpinning global food production (Rosegrant et al., 2009). Water security is challenged further by climate change, agricultural and biofuel production, and increased demand for domestic use (Gerbens-Leenes et al., 2009). Future research should focus on a better description of the pathways by which climate change may affect health through changes in water scarcity.

4.7.1 Limitations of this study

There are several limitations to this model that are discussed above, relating to the lack of information on temperature–diarrhoeal associations in a wide range of settings. The use of relative risks for all types of diarrhoeal disease is a conservative approach when there is emerging evidence that different pathogens have different temperature profiles. A more robust approach to modelling should consider developing models for individual pathogens, such as cholera.

There is the potential for double counting with deaths in children aged under 5 years from malnutrition. The interactions between diarrhoeal disease and undernutrition have been well described, with either condition increasing the risk of the other (Guerrant et al., 2008).

Malaria

5

Andreas Béguin, Joacim Rocklöv, Christofer Åström, Rainer Sauerborn, Valerie Louis, Simon Hales

5.1 Background

Plasmodium falciparum malaria, transmitted predominantly by the *Anopheles gambiae* mosquito, is the vector-borne disease with the largest health effects worldwide. Every year 1.1–1.27 million people die from malaria, most of them children aged under 5 years. The global geographical distribution of malaria has contracted over the 20th century due to human interventions following the strong economic development, particularly in the United States and Europe (Gething et al., 2010).

Seasonality of malaria transmission was recognized at an early stage in the epidemiological research (Gubler et al., 2001). This led to the reasoning that climate change can affect the areas where malaria is transmitted. The development of *P. falciparum* is highly dependent on temperature and ceases when the temperature is below 16°C (Macdonald, 1953). Larvae of *A. gambiae* will not develop into adults when the temperature is below 16°C (Jepson et al., 1947), and the mosquito's survival is limited to areas with ambient temperatures below 40°C (Lindsay & Martens, 1998). Higher ambient temperatures increase the metabolic rate of the insect, thereby leading to more frequent blood meals. In addition, higher temperatures support faster development of the malaria parasite within the mosquito, increasing the probability that vectors will become infective before they die. As a result, human–vector contact – and the frequency of infective bites – are increased at higher temperatures; beyond temperatures of 35°C, however, the survival of the vector declines. The transmission potential of the vector appears optimal around 28–30°C. Many vector species other than *A. gambiae* can transmit malaria, some of which are less restrained by ambient climatic conditions (Chaves & Koenraadt, 2010).

Several studies have found rainfall to be an important predictor of vector density, with a lag time of 1–2 weeks (Koenraadt et al., 2004). The onset of the rainy season has been associated with increasing incidence of malaria, leading to the development of seasonal forecasts and early warning systems in Africa (Thomson et al., 2006). It has been found that humidity determines the lifespan of the mosquito in some regions (Chaves & Koenraadt, 2010).

Several studies have estimated the impact of climate change on malaria (Rogers & Randolph, 2000; Patz et al., 2002; Tanser et al., 2003; van Lieshout et al., 2004; Ebi et al., 2005; Caminade et al., 2014). Climate conditions are by no means the only important factors contributing to malaria proliferation, however. For example, Hay and colleagues (2006) highlight the importance of taking into account population changes, climate change and urban risk reduction from urbanization and change in land use. Urbanization is often associated with economic growth, and it has been argued that economic development strongly influences the geography of malaria (van Lieshout et al., 2004). Malaria prevalence tends to be lower

in urban areas, where there are fewer breeding sites suitable for the most effective malaria vectors, treatment is easier to reach and prevention measures such as insecticide-treated bednets are more widely available (Noor et al., 2009). The importance of global transport networks on the spread of infectious diseases in general is widely accepted (Tatem et al., 2006).

Few studies projecting the effect of climate change on malaria have accounted for different levels of adaptive capacity. In this assessment, climate change adaptation, for example, refers to the level of societal and health system changes manifested through land use changes, disease prevention and treatment, and vector control. These measures are believed to be highly associated with socioeconomic development. In this assessment, we estimate future impacts of climate change based on three different socioeconomic scenarios (see Chapter 1). Unlike in other chapters of this assessment, GDP per capita is used as an empirical predictor of an intermediate outcome (the population at risk of malaria) rather than directly as a predictor of future mortality.

5.2 Description of the model

The malaria model is an empirical-statistical model created at the Umeå University (Béguin et al., 2011). The model uses climate and socioeconomic factors to estimate the spatial distribution of endemic malaria transmission. Population data were used together with the risk areas from the climate and socioeconomic malaria model to estimate the future population at risk of malaria. The climate change-attributable component is the difference between the population at risk under climate scenarios compared with the population at risk in a future world without climate change. To calculate a simplified estimate of the future mortality associated with malaria infections, national current malaria mortality estimates were multiplied by the national ratio of projected population at risk to the present population at risk.

5.2.1 Malaria data

We used data on global malaria risk from the Malaria Atlas Project (Hay et al., 2009). The data consist of a map of prevalence of malaria parasites in children aged 2–10 years. The data were taken from 7953 surveys and interpolated to a map using a geostatistical model. All areas where children were predicted to have parasites in their blood were classified as areas with malaria present.

5.2.2 Climate data (observed)

Global climate data as grids of 0.5° × 0.5° latitude and longitude for the time period 1991–2005 were provided by the Climate Research Unit, University of East Anglia (Mitchell & Jones, 2005) for 15-year averages of annual means, and monthly means of temperature and precipitation. From these data, several climate variables were calculated:

- mean temperature of the coldest month;
- mean temperature of the warmest month;

- mean annual temperature;
- mean precipitation of the driest month;
- mean precipitation of the wettest month;
- mean annual precipitation.

5.2.3 GDP data

The GDP data were downscaled to a grid (0.5° × 0.5°) by the IMAGE modelling group at the Netherlands Environmental Assessment Agency (Bouwman et al., 2006). The baseline period was the year 2000, and for future projections the years 2030 and 2050 were used.

5.2.4 Population data

Gridded population data for the A1B scenario were obtained from IIASA (2009) for the years 2000, 2030 and 2050.

5.3 Estimating model parameters and validation

We used generalized additive logistic regression models to empirically estimate the relationship between endemic malaria fever transmission and climatic factors on a global scale. To allow flexible relationship and interaction between climate factors on the probability of malaria transmission areas, we fitted linear models (allowing for interaction) and models using multidimensional spline functions as implemented in the mgcv package of the statistical software R (R Development Core Team, 2010).

The model was evaluated using 10-fold cross-validation, leaving 10% of data out of model fitting (out-of-bag samples) for validation purpose, and repeating the procedure 10 times, alternating the out-of-bag samples each time. External cross-validation allows investigation of over fitting of the model as observations not used in setting up the model can be used to evaluate its prediction performance.

The predictive performance of statistical models can be calculated in several different ways. We computed measures of predictive accuracy according to classification sensitivity (proportion of malaria presence areas correctly classified) and specificity (proportion of malaria absence correctly classified), and total error rate. The approach taken allows careful investigation of the underlying classification rationale as plots of the log odds as a function on climate.

Some observations in this dataset hold very similar information, especially when large malaria-free or malaria-positive areas have a similar climate. This raises a question about the independence of observations. If the observations from which a statistical model is built are not sufficiently independent, then this could lead to smaller standard deviations of the coefficients, thereby raising the significance level and increasing the confidence in the parameter estimates. This problem has been described as the issue of spatial autocorrelation in ecological prediction (Koenig, 1999; Araujo et al., 2005). Spatial autocorrelation in the climatic and health datasets was not adjusted for in our approach. The model parameter

estimates are supposed to be robust to such dependencies. Confidence intervals are small, however, when the similarity of observations is high. If the observations and outcomes are spatially autocorrelated, then the variance of the effect estimates is likely to be negatively biased. To quantify this effect, we clustered the observations by country and built models using only a subset of the data. The similarity between the models using spatially clustered observations and all observations was used to assess the generalizability of the model and its behaviour with respect to spatial autocorrelation.

5.3.1 Final model

The model providing the best fit in terms of predictive accuracy to discriminate the malaria presence and absence areas on out-of-bag samples was identified. The best-fitting model was found to be

$$\text{logit}(Malaria_i) = \beta_0 + \beta_1 T\_min_i + \beta_2 PR\_max_i + \beta_3 \sqrt{(GDPpc_i)}$$

where the index *i* indicates the spatial grid location, *Malaria* is the probability of malaria, β_0, β_1, β_2 and β_3 are regression coefficients, *T_min* is the mean temperature of the coldest month, *PR_max* is the mean precipitation of the wettest month, and *GDPpc* is the GDP per capita.

The inclusion of GDP per capita in the model increased the percentage of correctly classified observations.

5.4 Scenario data

The climate scenarios used in this assessment are described in Chapter 8. All climate scenarios were forced with the A1b medium-high emissions scenario.

For each dataset, climatologies of the temperature and precipitation variables were calculated for three 30-year periods: 1961–1990, 2016–2045 and 2036–2065. Subsequently, differences between the scenario and baseline climatologies of these variables were calculated for each dataset. These differences were interpolated on to a 0.5° grid by assigning the values of each 1° × 1° grid box to the four underlying 0.5° × 0.5° grid boxes and added to the Climate Research Unit baseline dataset to obtain model estimates of future climate.

This procedure minimizes problems arising from model biases towards warmer or cooler climates by evaluating changes of model future with respect to the model present and combining them with the best available estimates of baseline climate.

The IMAGE model produces GDP values for the A1B scenario that do not vary within each country and do not incorporate differences between urban and rural areas.

5.5 Results

5.5.1 Model parameters

The model with the best performance for modelling the present-day climate was a linear logistic regression model using the mean temperature of the coldest month, the maximum monthly precipitation, and a GDP per capita variable as a predictor.

The odds ratios for the model are given in Table 5.1. The effect of an incremental increase in temperature and precipitation is an increase in the risk of malaria. An increase in average GDP per capita of a given area results in lowered probability of malaria presence.

Table 5.1 Model parameters (odds ratios) for the logistic regression model for malaria[a]

Model parameter	Odds ratio	*P*
T_min: mean temperature of the coldest month (°C)	1.48	<0.0001
PR_min: maximum monthly precipitation (mm/day)	1.99	<0.0001
√(GDP per capita) (billion US$)	0.82	<0.0001

a 66 000 observations (grid points) were used to construct the model

Based on the 10-fold cross-validation on out-of-bag samples, the model correctly predicts 92% of the grids observed to be malaria presence or malaria absence. Around 85% of grids are predicted correctly as being malaria-positive (sensitivity). The proportion of correctly predicted absences is slightly higher and estimated at 95% (specificity). The classification probability threshold in the logistic model was set to 0.5.

There are omission errors (malaria presence areas predicted to be malaria-free) in Africa, in particular in the African highlands. There are also commission errors (malaria-free areas predicted to be malaria presence areas) in South America and south-east Asia. The effects of these errors on the estimated population at risk are quantified in Table 5.2 and Table 5.3.

Modelled probabilities of transmission were similar in South America and Africa. This illustrates the effect of using malaria presence or absence only as a response variable, rather than the parasite rates supplied in the Malaria Atlas Project. The similarity of modelled probabilities does not reflect so well the findings from the Malaria Atlas Project (Hay et al., 2009) due to the dichotomization into presence and absence of the response. Models of the continuous response were attempted, however, without great success. This perhaps results from the parasite prevalence being much more sensitive to local interventions and land use rather than the global climate.

Table 5.2 Population at risk (millions of people) in the 21 Global Burden of Disease regions considering climate change and GDP effects[a]

Region	1961–1990		2030					2050				
	Baseline	Bias to observed baseline	Population change only – observed areas	Population change only – modelled areas	Climate change – mean predicted	Climate change – lowest predicted	Climate change – highest predicted	Population change only – observed areas	Population change only – modelled areas	Climate change – mean predicted	Climate change – lowest predicted	Climate change – highest predicted
Asia Pacific, high income	1.75	1.75	0.00	1.68	1.65	1.54	1.68	0.00	1.54	1.57	1.54	1.68
Asia, central	0.00	0.00	0.00	0.00	0.00	0.00	0.00	0.00	0.00	0.00	0.00	0.00
Asia, east	0.00	–13.41	11.94	0.00	0.00	0.00	0.00	10.41	0.00	0.00	0.00	0.00
Asia, south	259.43	–156.43	558.19	360.48	134.16	106.85	143.96	567.89	379.02	112.66	96.22	135.37
Asia, south-east	216.69	41.71	221.46	276.90	41.52	21.83	48.23	231.43	290.06	27.05	19.52	50.27
Australasia	0.02	0.02	0.00	0.01	0.01	0.01	0.01	0.00	0.01	0.01	0.01	0.01
Caribbean	1.08	–4.86	8.69	1.10	0.76	0.60	0.91	9.60	0.94	0.85	0.41	2.51
Europe, central	0.00	0.00	0.00	0.00	0.00	0.00	0.00	0.00	0.00	0.00	0.00	0.00
Europe, eastern	0.00	0.00	0.00	0.00	0.00	0.00	0.00	0.00	0.00	0.00	0.00	0.00
Europe, western	0.00	0.00	0.00	0.00	0.00	0.00	0.00	0.00	0.00	0.00	0.00	0.00
Latin America, Andean	3.19	–1.95	6.95	4.99	2.13	1.70	2.30	7.22	5.41	1.78	1.59	2.43
Latin America, central	33.99	27.82	12.62	61.48	28.40	26.22	30.44	15.02	72.00	22.93	15.80	32.10
Latin America, southern	0.00	0.00	0.00	0.00	0.00	0.00	0.00	0.00	0.00	0.00	0.00	0.00
Latin America, tropical	11.20	6.63	3.65	11.01	6.39	4.48	7.24	2.79	9.58	4.05	3.04	7.34
North America, high income	0.04	0.04	0.00	0.16	0.12	0.10	0.16	0.00	0.22	0.12	0.10	0.13
North Africa/Middle East	1.10	–9.46	32.50	4.76	4.48	3.88	6.90	52.61	8.39	4.39	4.17	4.77
Oceania	4.66	0.90	6.57	8.27	4.25	2.96	4.78	8.06	10.32	3.18	2.79	4.51
Sub-Saharan Africa, central	34.68	–29.27	142.30	76.07	79.08	76.11	89.92	181.04	93.63	78.79	77.41	81.12
Sub-Saharan Africa, eastern	60.39	–140.51	386.88	125.90	109.70	101.95	129.76	469.48	153.01	103.49	96.84	116.00
Sub-Saharan Africa, southern	0.00	–11.10	10.10	0.00	0.00	0.00	0.00	8.22	0.00	0.00	0.00	0.00
Sub-Saharan Africa, western	199.97	–53.12	486.40	404.56	313.57	301.23	334.82	578.88	490.02	290.04	256.43	344.17
World	828.19	–341.24	1888.26	1337.38	726.22	716.24	744.06	2142.65	1514.15	650.91	599.60	781.42

a The lowest and highest predictions refer to the populations in the smallest and largest predicted risk areas out of the five futures obtained per time horizon from the statistical model. The mean, lowest and highest predicted/projected values correspond to the mean and range of the projected values among the five global climate model runs

Table 5.3 Population at risk of malaria (millions of people) in the 21 Global Burden of Disease regions considering climate change effects only[a]

Region	1961–1990		2030					2050				
	Baseline	Bias to observed baseline	Population change only – observed areas	Population change only – modelled areas	Climate change – mean predicted	Climate change – lowest predicted	Climate change – highest predicted	Population change only – observed areas	Population change only – modelled areas	Climate change – mean predicted	Climate change – lowest predicted	Climate change – highest predicted
Asia Pacific, high income	1.75	1.75	0.00	1.68	1.81	1.74	1.82	0.00	1.54	1.76	1.74	1.82
Asia, central	0.00	0.00	0.00	0.00	0.00	0.00	0.00	0.00	0.00	0.00	0.00	0.00
Asia, east	0.00	–13.41	11.94	0.00	0.00	0.00	0.00	10.41	0.00	0.00	0.00	0.00
Asia, south	259.43	–156.43	558.19	360.48	425.31	387.95	505.49	567.89	379.02	462.87	427.72	516.24
Asia, south-east	216.69	41.71	221.46	276.90	336.22	317.15	380.50	231.43	290.06	361.83	333.08	375.27
Australasia	0.02	0.02	0.00	0.01	0.02	0.01	0.02	0.00	0.01	0.01	0.01	0.02
Caribbean	1.08	–4.86	8.69	1.10	5.90	3.57	11.25	9.60	0.94	6.28	5.91	6.50
Europe, central	0.00	0.00	0.00	0.00	0.00	0.00	0.00	0.00	0.00	0.00	0.00	0.00
Europe, eastern	0.00	0.00	0.00	0.00	0.00	0.00	0.00	0.00	0.00	0.00	0.00	0.00
Europe, western	0.00	0.00	0.00	0.00	0.00	0.00	0.00	0.00	0.00	0.00	0.00	0.00
Latin America, Andean	3.19	–1.95	6.95	4.99	7.89	5.93	10.62	7.22	5.41	9.34	8.22	10.17
Latin America, central	33.99	27.82	12.62	61.48	70.50	66.37	85.10	15.02	72.00	78.27	69.84	81.28
Latin America, southern	0.00	0.00	0.00	0.00	0.00	0.00	0.00	0.00	0.00	0.00	0.00	0.00
Latin America, tropical	11.20	6.63	3.65	11.01	14.53	13.43	15.15	2.79	9.58	14.77	13.97	15.55
North America, high income	0.04	0.04	0.00	0.16	0.17	0.16	0.22	0.00	0.22	0.21	0.16	0.22
North Africa/ Middle East	1.10	–9.46	32.50	4.76	10.22	7.89	19.21	52.61	8.39	13.60	8.58	15.22
Oceania	4.66	0.90	6.57	8.27	9.34	8.89	10.89	8.06	10.32	10.64	8.89	11.60
Sub-Saharan Africa, central	34.68	–29.27	142.30	76.07	100.34	89.87	137.23	181.04	93.63	121.40	99.60	130.43
Sub-Saharan Africa, eastern	60.39	–140.51	386.88	125.90	209.57	180.29	320.36	469.48	153.01	260.92	207.05	278.83
Sub-Saharan Africa, southern	0.00	–11.10	10.10	0.00	0.01	0.00	0.04	8.22	0.00	0.03	0.00	0.05
Sub-Saharan Africa, western	199.97	–53.12	486.40	404.56	461.45	434.68	560.11	578.88	490.02	520.72	441.78	548.06
World	828.19	–341.24	1888.26	1337.38	1653.27	1524.67	2057.68	2142.65	1514.15	1862.64	1627.14	1972.75

a The lowest and highest predictions refer to the populations in the smallest and largest predicted risk areas out of the five futures obtained per time horizon from the statistical model. The mean, lowest and highest predicted/projected values correspond to the mean and range of the projected values among the five global climate model runs

5.5.2 Change in malaria risk in 2030 and 2050

The model projected contraction of malaria presence areas when GDP variations are taken into account, and expansions when only changes in climatic variables are used to predict future disease areas.

In general, the changes in malaria presence areas occur at the borders of current transmission zones. The largest changes are predicted in Africa. At the northern border of the transmission areas, there is an extension of the transmission towards the desert areas. In the south of this transmission area, the predicted expansion occurs into areas that are already presence areas. There is also expansion into absence areas in South America and Asia.

5.6 Population at risk of malaria

The baseline and future populations at risk of malaria stratified by region are shown in Tables 5.2 and 5.3. The columns with population change only show the population change within areas modelled to be current malaria transmission areas and constitute a baseline against which the projections of population at risk should be examined. As discussed, there are some inconsistencies between the modelled and observed malaria regions. This has an effect on the modelled populations at risk in each region. Regions illustrating the effect of these differences on the modelled population at risk include southern sub-Saharan Africa, which

Figure 5.1 Changes in the global population at risk of malaria transmission in the five climate change datasets and in the cases of population change only within the model baseline and the observed baseline when evaluating climate and socioeconomic change

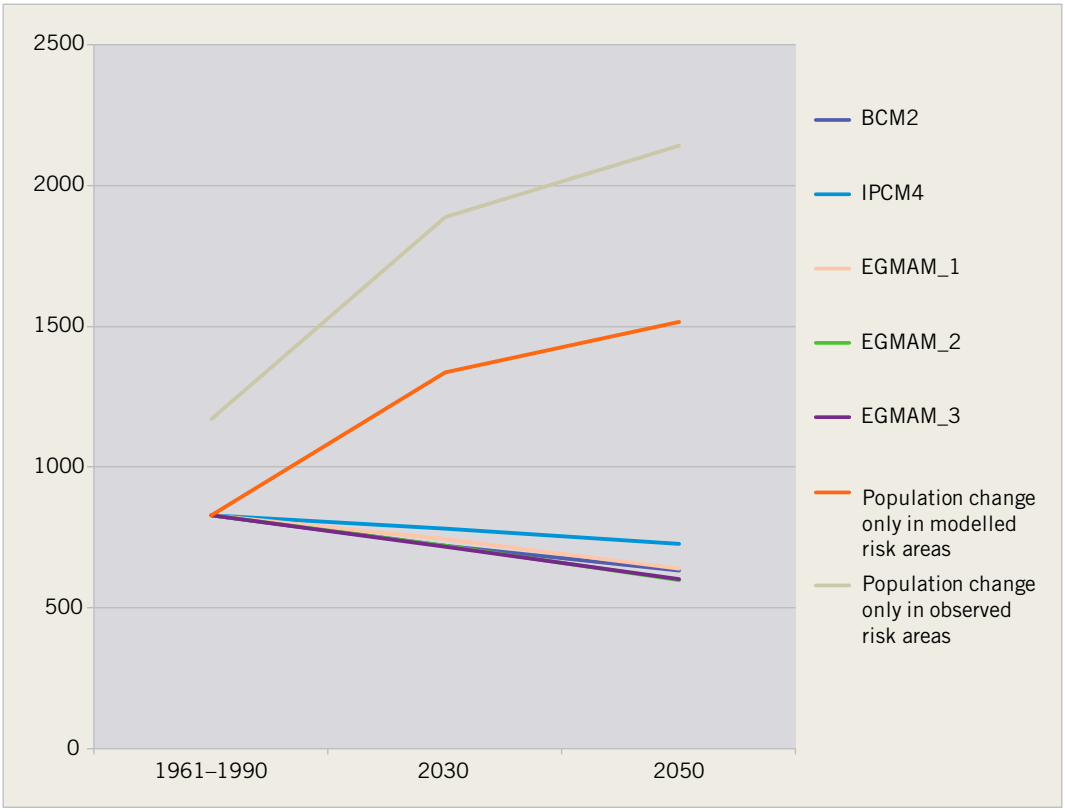

is not modelled to be a malaria presence area and therefore has a negative bias towards the baseline (–11 million people). Also, the predictions for south Asia and south-east Asia, which are modelled to be malaria presence areas more often than observed, result in a positive bias towards the observed baseline (527 million people and 331 million people, respectively).

Figure 5.1 shows the modelled global populations at risk of malaria transmission when GDP effects are included. The population at risk is projected to decrease by 2030 and to decrease further by 2050. Note that all five climate model runs use the same GDP dataset. This partly accounts for the low variation between the projected global populations at risk.

Figure 5.2 summarizes the data in Table 5.3 (climate change effects only) on a global level. The variability between the three runs of the same climate model, the ECHO-G Middle Atmosphere Model (EGMAM), is considerably smaller than the variability between the three different models. The difference between the populations at risk modelled with different climate change datasets is smaller than the difference between the populations at risk when climate change is taken into account and a population change only scenario is used.

5.7 Discussion

The recent spatial distribution of all-cause malaria can be modelled empirically with high accuracy, based on average climate and GDP per capita. If the global climate changes as

Figure 5.2 Changes in the global population at risk of malaria transmission in the five climate change datasets and in the cases of population change only within the model baseline and the observed baseline when evaluating climate change, keeping socioeconomic changes fixed

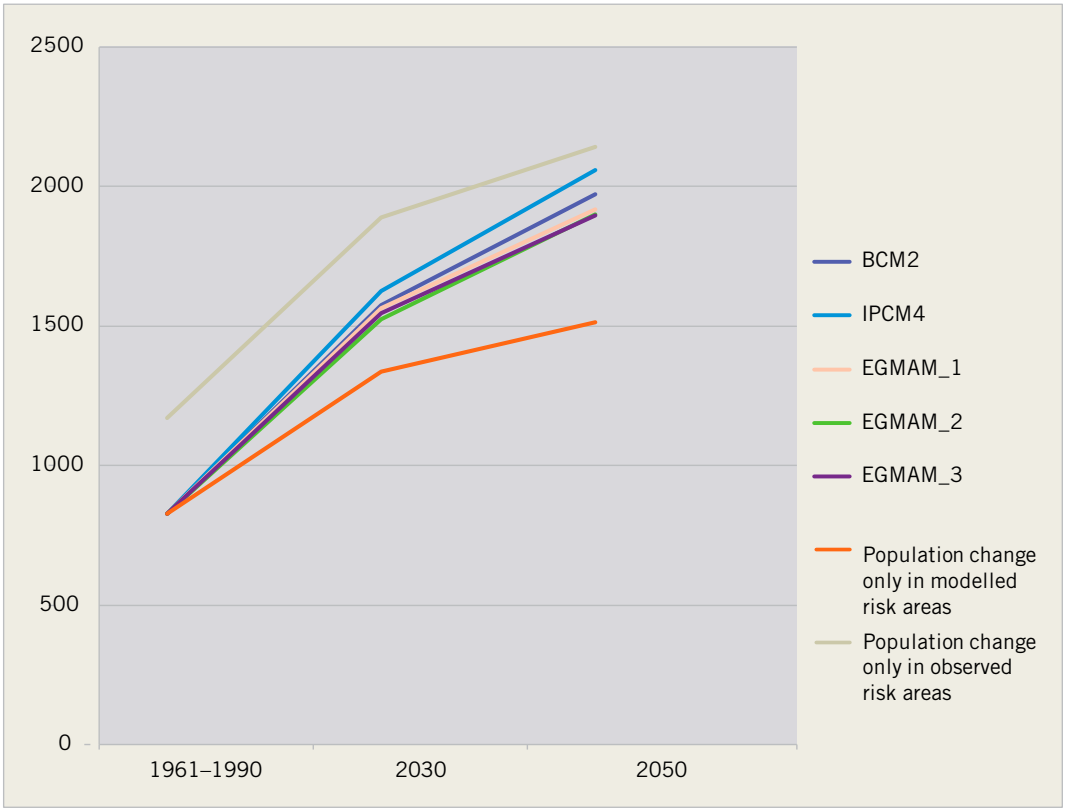

projected by global climate models but GDP remains constant, then a modest expansion of malaria risk is projected, mainly in South America and Asia, by the 2050s. If GDP changes as projected by economic models but the global climate remains constant, then much of the world, with the notable exception of Africa, is projected to become free from malaria by the 2050s. The projected geographical contraction in malaria is less marked, but still substantial, given simultaneous changes in GDP and climate in the 2050s.

We found a strong independent relationship between GDP per capita, climate and malaria risk. Empirically, climate factors have a substantial effect on malaria transmission in countries where GDP per capita is less than US$ 20 000. This study addresses the confounding effect of development on malaria presence geographically, thereby estimating the impact of climate change on the potential distribution of malaria transmission areas without confounding by socioeconomic factors.

The association between GDP per capita and malaria is not directly causal, however. GDP per capita is used as a proxy for many aspects of welfare and economic status in our analysis. As an example, GDP per capita can influence malaria by the amount households can spend on individual prevention measures such as insecticide-treated bednets and malaria drug treatment (Sachs & Malaney, 2002). A limitation of our study is that GDP per capita may not remain such a good proxy for socioeconomic factors affecting malaria risk in the future, since the relationships between malaria and development are complex and bidirectional.

The social burden of malaria has been proposed as an important factor retarding economic growth. In one study, countries with intensive malaria grew by 1.3% per year less than other countries (Gallup & Sachs, 2004). Our model was constructed on the basis of spatial patterns and does not account explicitly for dynamic effects such as year-to-year variability of transmission intensity. Therefore, the effects of climate change estimated in this study may be negatively biased.

Projections of GDP per capita are more uncertain than those for temperature or precipitation changes because of intrinsic differences between climatic and socioeconomic systems. Although the equations governing the climate system are known but highly nonlinear, the dynamics of socioeconomic systems are governed by processes that are little understood. Therefore, weather and climate are easier to model than future socioeconomic development, which can be influenced to a large degree by unanticipated factors. Projections of economic growth must therefore be interpreted cautiously. Surprises in the development of GDP per capita such as the recent financial crisis can alter future values of GDP per capita significantly.

Over the past century, socioeconomic development has had a dominant influence on the geographical contraction of malaria. We project further substantial geographical contraction of malaria by the 2050s. Under the A1B climate scenario, climate change has much weaker effects than GDP per capita increase. This outcome is, however, dependent on optimistic estimates of continued socioeconomic development. Even then, climate change has important effects on the projected distribution of malaria, leading to an increase in the projected population at risk compared with a scenario in which no climate change occurred.

Dengue

6

Christofer Åström, Joacim Rocklöv, Andreas Béguin, Rainer Sauerborn, Valerie Louis, Simon Hales

6.1 Background

Dengue, caused by a flavivirus, is transmitted by vector mosquitoes of the genus *Aedes*. The principal mosquito vector spreading dengue viruses is *Aedes aegypti*. *A. aegypti* is an efficient epidemic vector due mainly to its high susceptibility to dengue viruses, its preference to feed on humans, being a daytime feeder, and its capability of biting several people in a short period for one blood meal (Gibbons & Vaughn, 2002; Gubler, 2002). *A. aegypti* is well adapted to urban life because it breeds in manufactured containers that collect rainwater. *Aedes albopictus* is a less competent vector, resulting partly from differences in host preference (Lambrechts et al., 2010). *A. albopictus* is, however, less sensitive to temperature and is migrating into temperate regions (Gubler, 2003).

Climate affects dengue fever transmission in tropical areas related to the vectorial capacity, including survival, biting rate and the extrinsic incubation period. It has been shown that the vectorial capacity increases with warm temperatures up to 29°C, while further increases beyond this optimum limit transmission (Liu-Helmersson et al., 2014). From dengue surveillance data, several studies have found incidence correlated to weather, with the effect delayed up to weeks and months (Hii et al., 2009; Johansson et al., 2009); other studies have directly estimated the climatic constraints on endemic transmission of dengue fever in geographical models (Hales et al., 2002). Furthermore, attempts have been made to estimate the global distribution of dengue fever with respect to climate change on a longer-term timescale using empirical statistical models and deterministic virus transmission models (Patz et al., 1998; Hales et al., 2002).

The impact of climate and climate change on the distribution of dengue is still uncertain. This uncertainty is related partly to influences of several co-acting factors in addition to climate change, such as urbanization and population movements (Hales et al., 2002; Wilder-Smith & Gubler, 2008). Here we aim to describe the relationship between climate and the geographical distribution of dengue fever transmission in an attempt to better understand the future distributional changes, population at risk, and mortality associated with climate change and socioeconomic scenarios.

6.2 Description of the model

As for malaria, but unlike in other chapters of this assessment, GDP per capita is used as an empirical predictor of an intermediate outcome (the population at risk of dengue) rather than directly as a predictor of future mortality. The dengue model was developed further, as described by Åström and colleagues (2012).

6.2.1 Dengue distribution data (observed)

We collected data on dengue fever transmission for the world from a systematic review (van Kleef et al., 2010). The register was based on countries reporting dengue within their national boundaries from 1975 to the present day, plus countries where outbreaks have been reported in the peer-reviewed literature. The geographical resolution of the collected data varied but was mainly on a national scale.

6.2.2 Climate data (observed)

Global climate data as grids of 0.5° × 0.5° latitude and longitude for 1961–1990 were provided by the Climate Research Unit, University of East Anglia (Mitchell & Jones, 2005). The data comprised 30-year averages of annual means, and monthly means of temperature and precipitation. From these data, additional variables such as mean temperature of the warmest and coldest months and temperatures for different seasons were constructed.

6.2.3 GDP and population data

GDP per capita estimates for 2030 and 2050 were taken from the IMAGE 2.3 model produced by the Netherlands Environmental Assessment Agency (Bouwman et al., 2006). The process of downscaling from the 17 world regions modelled in the IMAGE model to the 0.5° resolution used in this assessment is described by van Vuuren and colleagues (2007).

The IMAGE model produces GDP values for the A1B scenario that do not vary within each country and that do not incorporate differences between urban and rural areas. The population projections are based on the A1B scenario from the IPCC special report on emission scenarios (Nakicenovic & Swart, 2000). Spatially explicit population projections for the A1B scenario were used in this study (IIASA, 2009).

6.3 Scenario data

The climate scenarios used in this assessment are described in Chapter 8. All climate scenarios were forced with the A1b medium-high emissions scenario.

For each dataset, climatologies of the temperature and precipitation variables were calculated for three 30-year periods: 1961–1990, 2016–2045 and 2036–2065. Subsequently, differences between the scenario and baseline climatologies of these variables were calculated for each dataset. These differences were interpolated on to a 0.5° grid by assigning the values of each 1° × 1° grid box to the four underlying 0.5° × 0.5° grid boxes and added to the Climate Research Unit baseline dataset to obtain model estimates of future climate.

This procedure minimizes problems arising from model biases towards warmer or cooler climates by evaluating changes of model future with respect to the present model and combining them with the best available estimates of baseline climate.

From these data, several climate variables were calculated:

- mean temperature of the coldest month;
- mean temperature of the warmest month;
- mean annual temperature;
- mean precipitation of the driest month;
- mean precipitation of the wettest month;
- mean annual precipitation.

6.4 Statistical analysis

We used a generalized additive modelling framework employing a logit link function to empirically estimate the probability of dengue transmission in each grid box on the basis of the climatic variables and GDP per capita. To allow a flexible relationship and interaction between the climate variables on the probability of dengue transmission areas, we applied thin plate splines as implemented in the mgcv package of the statistical software R. The spline functions allow the disease predictor relationship of disease presence to vary in a more complex way than in the logistic regression without splines, and they allow nonlinear synergies to be examined by visualization as three-dimensional fields. Nonparametric functions estimated in the generalized additive modelling framework are less sensitive to over fitting, as over fitted exposure–response relationships are penalized to become smoother using generalized cross-validation.

6.4.1 Validation of model

As the aim of this study was to develop a prediction model, model selection was based on the model prediction performance of the current geographical areas of dengue fever transmission. Prediction performance was evaluated using a six-fold country-wise cross-validation (Refaeilzadeh et al., 2009).

The predictive performance of statistical models can be calculated in several different ways. In medical research, two often used measures are sensitivity and specificity. In this case, sensitivity measures the probability of an area being predicted dengue-positive given that it is truly dengue-positive. The specificity is a measure of how well the model predicts the non-infected areas. We also calculated the total rate of correctly classified observations.

We did not adjust for spatial autocorrelation because the effect estimates are supposed to be robust to such dependencies. Confidence intervals are not presented because the variance of the effect estimates may become negatively biased due to the potential spatial covariance patterns in the data.

The analysis in this assessment assumes that everything except climate, population and GDP levels will stay the same. To calculate a simple best guess of the future mortality associated with dengue, national current dengue mortality estimates were multiplied by the national ratio of projected population at risk to the present population at risk (see Chapter 1).

6.5 Results: time periods and scenarios

6.5.1 Model

The model was chosen based on classification ability and by investigating the pattern of misclassifications. This model used a splined interaction between the annual mean temperature and the annual mean precipitation and a standalone variable of GDP per capita:

$$\text{logit}(Dengue_i) = \beta_0 + F(Temperature_i, Precipitation_i) + \beta_1 GDPpc_i \quad [6.1]$$

where the index i denotes a grid box; *Dengue* corresponds to the probability of dengue transmission; F denotes a spline function; *Temperature* is the annual mean temperature; *Precipitation* is the annual mean precipitation; and *GDPpc* is the GDP per capita.

The model classified 91% of the grid cells correctly and had a sensitivity and specificity of 87% and 81%, respectively, based on a cut-off probability value of 0.5. The generalizability measure based on the cross-validation results was 98%.

The relationship fitted between temperature and rainfall is presented graphically in Figure 6.1. The results show increasing probability for dengue presence when the temperature or rainfall increases.

6.5.2 Population at risk

On the basis of Equation [6.1], the future distribution of dengue was estimated for combinations of future projections of the explanatory variables. Estimates were generated by

Figure 6.1 Modelled relationship between dengue transmission and climate variables

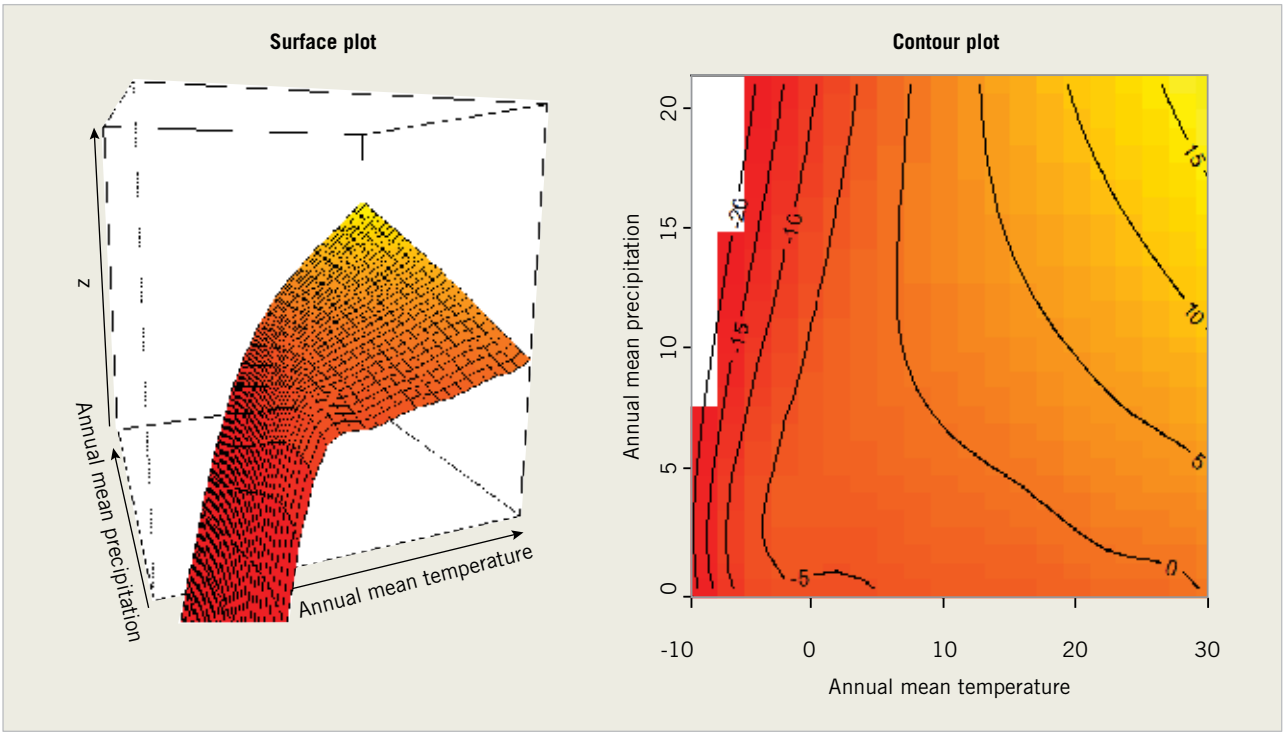

varying all factors. In addition, in separate runs we kept climate, population and GDP fixed, exploring the marginal influence of the other variables. Projections were used to produce estimates of the population at risk for each future scenario separately.

In 2050, a contraction was observed in most parts of the world, except sub-Saharan Africa, under scenarios of climate and socioeconomic change. The population at risk averaged 4.59 billion people in this scenario. We observed an overall expansion when holding socioeconomic development fixed under climate change. This resulted in a population at risk of approximately 5.16 billion people, an increase of around 0.52 billion people compared with the current distribution. A coherent contraction was observed when climate was fixed and socioeconomic development was assumed to follow the base case. Under the current distribution of dengue and with population growth, 4.64 billion people will be at risk of dengue in 2050 (Table 6.1). Detailed regional results are presented in Table 6.2.

Table 6.1 Population at risk of dengue infection in 2030 and 2050 under climate and socioeconomic change, for scenario 1

	Baseline (billions)[a]	Mean (billions)	Highest estimate (billions)[b]	Lowest estimate (billions)[b]
2030	4.26	4.39	4.42	4.29
2050	4.64	4.59	4.64	4.51

a Baseline refers to the population in the modelled current distribution

b Highest and lowest estimates represent the result from the climate model run estimating the highest and lowest population at risk

Table 6.2 Population at risk of dengue under climate and socioeconomic change in 2030 and 2050 under five global climate model runs

Region	2030				2050			
	Population change only (millions)	Mean estimate (millions)	Lowest prediction[a] (millions)	Highest prediction[a] (millions)	Population change only (millions)	Mean estimate (millions)	Lowest prediction[a] (millions)	Highest prediction[a] (millions)
Asia Pacific, high income	0.81	0.56	0.56	0.56	0.92	0.69	0.69	0.69
Asia, central	0.10	0.23	0.10	0.29	0.07	0.07	0.00	0.13
Asia, east	310.93	353.61	299.89	375.59	283.74	191.93	163.95	216.79
Asia, south	1637.54	1673.00	1651.94	1689.54	1729.20	1743.36	1710.93	1758.51
Asia, south-east	713.35	713.37	713.35	713.38	756.66	756.67	756.66	756.69
Australasia	0.20	0.01	0.01	0.01	0.19	0.00	0.00	0.00
Caribbean	41.54	41.54	41.54	41.54	41.10	40.32	40.15	40.83

[Continues]

[Continued]

Region	2030				2050			
	Population change only (millions)	Mean estimate (millions)	Lowest prediction[a] (millions)	Highest prediction[a] (millions)	Population change only (millions)	Mean estimate (millions)	Lowest prediction[a] (millions)	Highest prediction[a] (millions)
Europe, central	0.00	0.00	0.00	0.00	0.00	0.00	0.00	0.00
Europe, eastern	0.00	0.00	0.00	0.00	0.00	0.00	0.00	0.00
Europe, western	0.00	0.00	0.00	0.00	0.00	0.00	0.00	0.00
Latin America, Andean	16.52	17.21	15.94	18.79	18.00	16.68	13.92	20.27
Latin America, central	185.46	181.10	173.21	185.82	206.58	184.91	180.95	189.45
Latin America, southern	4.45	4.32	4.30	4.36	4.58	3.21	2.81	3.34
Latin America, tropical	232.12	230.52	226.90	231.90	242.58	223.78	220.98	227.39
North America, high income	15.67	0.03	0.03	0.03	16.92	0.02	0.02	0.02
North Africa/ Middle East	3.11	6.37	5.09	7.42	5.46	10.73	8.83	12.92
Oceania	9.86	9.84	9.84	9.85	11.95	11.95	11.95	11.95
Sub-Saharan Africa, central	155.03	156.05	155.70	156.17	198.44	199.41	199.23	199.61
Sub-Saharan Africa, eastern	438.57	490.14	474.34	498.05	534.73	610.69	595.26	623.69
Sub-Saharan Africa, southern	5.19	12.60	10.57	14.45	4.02	6.82	3.17	8.32
Sub-Saharan Africa, western	490.23	494.87	493.58	495.74	585.34	593.23	592.08	594.59
World	4260.68	4385.38	4291.88	4418.34	4640.49	4594.47	4506.27	4640.62

a The highest and lowest predictions are the estimates by the global climate models generating the highest and lowest projected populations at risk under scenario 1

6.5.3 Projection of mortality

The population at risk in a region under climate change and socioeconomic scenarios was used to estimate the future mortality burden of dengue by assuming the cumulative incidence stayed the same (see Chapter 1).

6.6 Discussion

We found that the recent geographical distribution of dengue depends strongly on climatic and socioeconomic variables. The findings suggest that social and economic factors appear most effective at preventing dengue at the border of the transmission areas where there are less favourable climatic conditions. According to our findings, climate change would contribute to expansion at the fringes of the current distribution of dengue, while socioeconomic developments may counteract this change in most parts of the world. We emphasize that future economic development is hard to predict, and the projected dengue estimates incorporating rapid economic growth should be assessed critically. Under the A1B scenario, it is assumed that the differences in GDP per capita in the world today will virtually disappear by the end of the 21st century. To test the sensitivity of this assumption, we provide estimates where there is assumed to be no economic growth (climate change only). The range of these estimates indicates the sensitivity of the model regarding the economic growth scenarios.

Socioeconomic development and related changes in water-storage practices appear to have influenced the distribution of dengue in the past (Russell et al., 2009). GDP per capita is a proxy for socioeconomic status, but in this assessment it does not describe the distribution of wealth within a country. It is used here as an indicator for several variables related to development, such as access to piped water supplies and vector control programmes. Reticulated water supplies reduce the need for water storage containers and may help to limit the distribution of dengue (WHO, 2009b).

The major limitation of this study is the coarse spatial resolution of the dengue data. The mostly national-scale observations will result in a less accurate specification of the current limits of the dengue distribution. When an entire country is classified as dengue-positive, climatically unsuitable subregions of that country will be misclassified. This is clear, for example, in Mali, where the northern area, located in the Sahara, has a climate highly unsuitable for dengue and the southern part has a climate that is very suitable for dengue. More detailed dengue data would make it possible to investigate the effect of additional variables such as population and urbanization on the dengue distribution on a global scale. Future studies should analyse global spatial patterns of dengue incidence rates (rather than presence/absence) in relation to climate and socioeconomic factors. Recent studies have assessed the evidence-based consensus on the dengue presence and absence in countries (Brady et al., 2012) and made estimates of the disease burdens in symptomatic and asymptomatic carriers (Bhatt et al., 2013), but they have not assessed the influence of climate and socioeconomic change on the global distribution.

Undernutrition

7

Simon Lloyd, Sari Kovats, Zaid Chalabi

7.1 Background

Hunger and undernutrition are major contributors to the global burden of disease and are the leading risk factors for death and morbidity in children aged under 5 years (IHME, 2013).

Around 1 billion people are thought to have insufficient food to meet their needs (FAO, 2009). In children aged under 5 years, 45% of deaths (3.1 million deaths) were attributed to undernutrition in 2011 (Black et al 2013). The reduction of hunger and undernutrition is one of the Millennium Development Goals, but although progress has been made, reductions lag behind aspirations, particularly following the food price and financial crises in 2008–2009 (UN, 2010). Box 7.1 defines the key terms used in this assessment.

Box 7.1 Definitions used in this assessment

Undernourishment, modelled using the FAO (2003) method, is defined as having a "dietary energy consumption [that] is continuously below a minimum dietary energy requirement for maintaining a healthy life and carrying out a light physical activity with an acceptable minimum body-weight for attained-height" (FAO, 2010). Undernourishment has one final cause: a lack of calories.

Undernutrition is conventionally measured using anthropometrics such as stunting (height for age) and underweight (weight for age) (WHO, 2010). It has multiple causes, of which lack of food is one. In this assessment, since we are looking at long-term average conditions such as average crop productivity, we focus on stunting, which best reflects these conditions (Black et al., 2008) and use the terms undernutrition and stunting synonymously.

The causes of undernutrition are complex, extending beyond food availability to include factors such as poverty, access to services (such as adequate water and sanitation), social conditions (such as women's access to education) and underlying population health (such as prevalence of diarrhoeal disease) (UNICEF, 1990). For example, Checkley and colleagues (2008) found that a quarter of irreversible stunting in young children could be attributed to having had five or more episodes of diarrhoea. Smith & Haddad (2000) attributed 43% of the reduction in child underweight between 1970 and 1995 to greater access of women to education, 26% of the reduction to greater food access, and 19% of the reduction to improved water and sanitation.

Climate change is expected to have significant impacts on cereal production, particularly at low latitudes. Crop models have been used to estimate changes in yield under a range of climate scenarios. The 4th IPCC assessment report concluded that although moderate warming may benefit crop yields in mid- to high-latitude regions, it is likely that there will be decreases in yields in seasonally dry and low-latitude regions (Meehl et al., 2007).

Methods for estimating the impacts of reduced average food yields on human health and welfare are complex, linking various models (such as crop, food trade and health) and using a range of metrics to estimate health impacts. Initial models were based on a threshold level of per capita calorie availability that meets an average individual's calorie estimated minimum requirements (FAO, 2003). Populations below the threshold were considered at risk of hunger. Thus, studies have estimated an additional 5 million to 170 million people may be at risk of hunger by the 2080s (Parry et al., 2004; Schmidhuber & Tubiello, 2007). More recent modelling efforts have quantified more direct outcome measures. For example, Nelson and colleagues (2009) estimated that under a medium-high emissions scenario (SRES A2), global reductions in crop productivity could increase the proportion of underweight children by around 20% in 2050.

Future climate change may also affect crop productivity through a range of mechanisms that are not included within current crop yield modelling, including increases in extreme weather events (such as droughts and heavy rainfall – although some climate variability is incorporated in some models), spatially remote conditions that influence local conditions (such as rainfall higher in a river catchment), sea-level rise (such as loss of crop land from inundation or salinization), changes in demand for water, and increases in pests and diseases (Gornall et al., 2010). Furthermore, climate change is likely to affect undernutrition through routes other than crop productivity. Livelihoods may be lost if formerly productive land ceases to be productive and poverty may increase. Infectious diseases such as diarrhoeal disease (see Chapter 4) and malaria (see Chapter 5) may become more prevalent. These factors, which may be anticipated to increase the risk of future undernutrition, are not accounted for in existing models.

Food security is defined as the "situation that exists when all people, at all times, have physical, social, and economic access to sufficient, safe, and nutritious food that meets their dietary needs and food preferences for an active and health life" (FAO, 2011) and is commonly considered along the dimensions of availability, access, stability and utility (Schmidhuber & Tubiello, 2007). Existing health impact modelling covers the dimensions of food availability (such as crop productivity) and access (such as global distribution via trade), but it does cover not stability (such as losses due to extreme weather) or utility (such as absorption of nutrients compromised in a child with chronic diarrhoea) or how these factors are affected via routes other than food production. For more details, see Schmidhuber & Tubiello (2007).

7.2 Assessment method: linking crop, trade and health impact models

The connections between climate change and undernutrition are many and complex. We used the output from a chain of models shown in Figure 7.1. We used the following steps to estimate climate change-attributable burden of undernutrition:

1. Future post-global food trade national calorie availability estimates for 2030 and 2050 with and without climate change were obtained from the dataset accompanying the report of Nelson and colleagues (2010).
2. Within-country food distribution estimates, represented as the proportion of population undernourished, were generated using the method of the Food and Agriculture Organization of the United Nations (FAO, 2003).
3. Estimates of regional-level child stunting were generated from national proportion of population undernourished values and projections of GDP per capita, using an undernutrition model (Lloyd et al., 2011).
4. Estimates of all-cause mortality attributable to child stunting were made using the methods of the WHO Burden of Disease Assessment, with population-attributable fractions. This used our stunting estimates, estimates of relative risk of mortality in stunted children from Black and colleagues (2008), and mortality projections (see Chapter 8).

7.2.1 Step 1: national calorie availability estimates

Nelson and colleagues (2010) estimated national calorie availability in future worlds with climate entering the model via crop productivity. Estimates were calculated in the absence of climate change and under two climate change scenarios (MIROC and CSIRO) driven by A1 emissions, for three socioeconomic futures (see Section 7.3). Future cereal production under particular scenarios was estimated using the Decision Support System for Agrotechnology Transfer (DSSAT) crop models for rice, wheat, maize, soy and groundnut (Jones et al., 2003). Crop production was assessed for average weather conditions and did not include extreme weather or other events such as potential pest invasions.

Figure 7.1 Schematic illustration of the modelled pathway from climate change to child undernutrition and its consequences

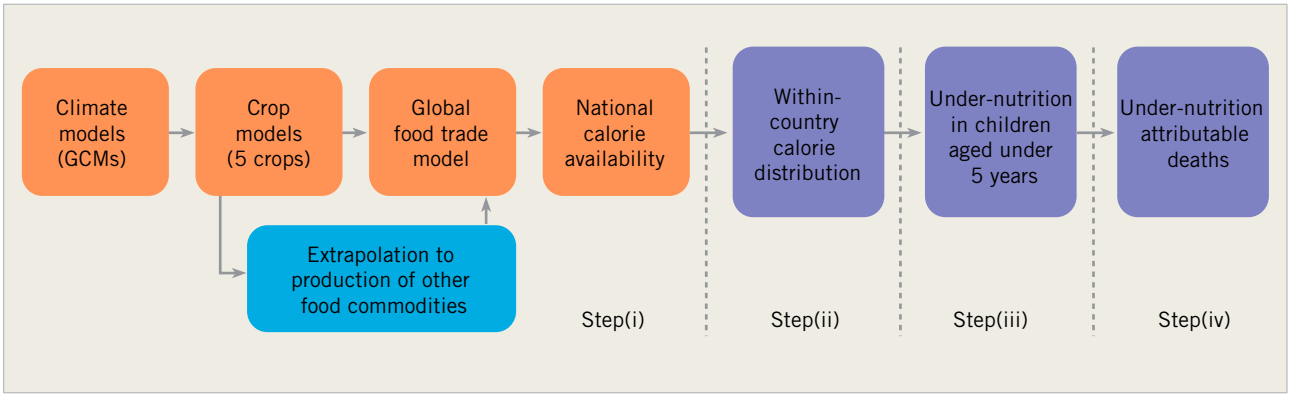

Changes in other food commodities were estimated by extrapolating from the five modelled crops (Nelson et al., 2010). Of note, using data from WHO (2010) and FAO (2010), we found that in the 34 countries that together account for 90% of all stunting, on average about 50% of calories come from wheat, rice, maize or soy, and the contribution of animal products to calorie intake is about 10% (unpublished results). Thus, the crop yield changes that were explicitly modelled in this assessment account for a significant portion of calorie intake in countries with the highest rates of undernutrition.

To estimate global food distribution, the food production estimates were used to drive the IMPACT model (Rosegrant et al., 2008), which in turn partially drives future crop production. IMPACT analyses 32 crop and livestock commodities in 281 world regions, covering all land surface except for Antarctica. Production and demand are linked via global trade; crop production is determined by factors including prices, area expansion, irrigation and water availability, and demand is based on food, feed, biofuels and other uses. In a globalized world, the trade model component is essential to estimate future food availability, as countries will either grow or import food. The assumptions about economic growth are therefore important, as this will determine whether or not a country can afford to purchase food in the model.

The final output was future national-level per capita calorie availability in 2030 and 2050, under two climate scenarios and without climate change, for each of the three socioeconomic scenarios. We used this as the basis for our undernutrition estimates.

The calorie availability data did not cover all countries and the spatial aggregations did not directly match the 21 world regions used in this assessment; therefore, we made estimates for 12 world regions (Box 7.2). Two of these regions are aggregated: tropical Latin America and Andean Latin America were combined into mid Latin America, and some countries from the Caribbean region where included in central Latin America.

Box 7.2 Countries[a] included in our regional projections based on output from the IMPACT model

Asia, central: Armenia, Azerbaijan, Georgia, Kazakhstan, Kyrgyzstan, Mongolia, Tajikistan, Turkmenistan, Uzbekistan

Asia, east: China, Democratic People's Republic of Korea

Asia, south: Afghanistan, Bangladesh, Bhutan, India, Nepal, Pakistan

Asia, southeast: Cambodia, Indonesia, Lao People's Democratic Republic, Malaysia, Myanmar, Philippines, Sri Lanka, Thailand, Viet Nam

Latin America, central: Belize,[b] Colombia, Costa Rica, El Salvador, French Guiana,[b] Guatemala, Guyana,[b] Honduras, Mexico, Nicaragua, Panama, Suriname,[b] Venezuela (Bolivarian Republic of)

Latin America, mid: Bolivia (Plurinational State of),[c] Brazil,[d] Ecuador,[c] Paraguay,[d] Peru[c]

Latin America, south: Argentina, Chile, Uruguay

North Africa and the Middle East: Algeria, Bahrain, Egypt, Iran (Islamic Republic of), Jordan, Kuwait, Lebanon, Libyan Arab Jamahiriya, Morocco, Oman, Qatar, Saudi Arabia, Syrian Arab Republic, Tunisia, Turkey, United Arab Emirates

Sub-Saharan Africa, central: Angola, Central African Republic, Congo, Democratic Republic of the Congo, Equatorial Guinea, Gabon

Sub-Saharan Africa, eastern: Burundi, Djibouti, Eritrea, Ethiopia, Kenya, Madagascar, Malawi, Mozambique, Rwanda, Somalia, Sudan, Uganda, United Republic of Tanzania, Zambia

Sub-Saharan Africa, southern: Botswana, Lesotho, Namibia, South Africa, Swaziland, Zimbabwe

Sub-Saharan Africa, western: Benin, Burkina Faso, Cameroon, Chad, Cote d'Ivoire, Gambia, Ghana, Guinea, Guinea-Bissau, Liberia, Mali, Mauritania, Niger, Nigeria, Senegal, Sierra Leone, Togo

[a] The list in this box has not been changed from the original study and does not comply with WHO style for country references

[b] Countries from the Caribbean region included in Latin America, central

[c] Countries from Latin America, Andean

[d] Countries from Latin America, tropical

For full details of the methods and assumptions underlying the calorie availability estimates, see the original paper by Nelson and colleagues (2010).

7.2.2 Step 2: within-country food distribution estimates

We used national calorie availability estimates from Step 1 to estimate the proportion of the population expected to be undernourished in each scenario combination using the FAO (2003) method. The method assumes that within a country, food distribution is described by a right-skewed log-normal distribution. The peak of the curve is determined by average calorie availability (calories/capita), the spread is determined by a measure of inequality of food distribution (similar to the commonly used Gini coefficient for income distribution), and the cut-off point for being undernourished is based on estimated average minimum calorie needs for a given population. The proportion undernourished is the area under the curve up to the minimum requirements cut-off point (Figure 7.2). For a full explanation of the method, see the original FAO (2003) document.

To use this method, in addition to national calorie available data, we required data on the within-country food distribution and the average minimum calorie requirement to avoid undernourishment. As projection data were not available for either of these, we obtained baseline (current) FAO data and assumed the values would remain constant in the future. We believe this approach is reasonable. For within-country food distribution, even at baseline, FAO country-level estimates are based on extrapolations of infrequently collected data from relatively few countries and are restricted to values between 0.2 and 0.35 (this is a convention of the FAO (2003) method). Variation within this range has been found to have little impact on changes in undernourishment in countries with low calorie availability (FAO, 1996; Svedberg, 2002). For average minimum calorie requirements across all countries, the mean change was 0.1% per year over the period 1990–1992 to 2004–2006 (FAO, 2010). Furthermore, Svedberg (2002) found that over a 20-year period, 88% of the change in regional undernourishment was explained by changes in per capita calorie availability.

Figure 7.2 FAO method for estimating the proportion of a population that is undernourished[a]

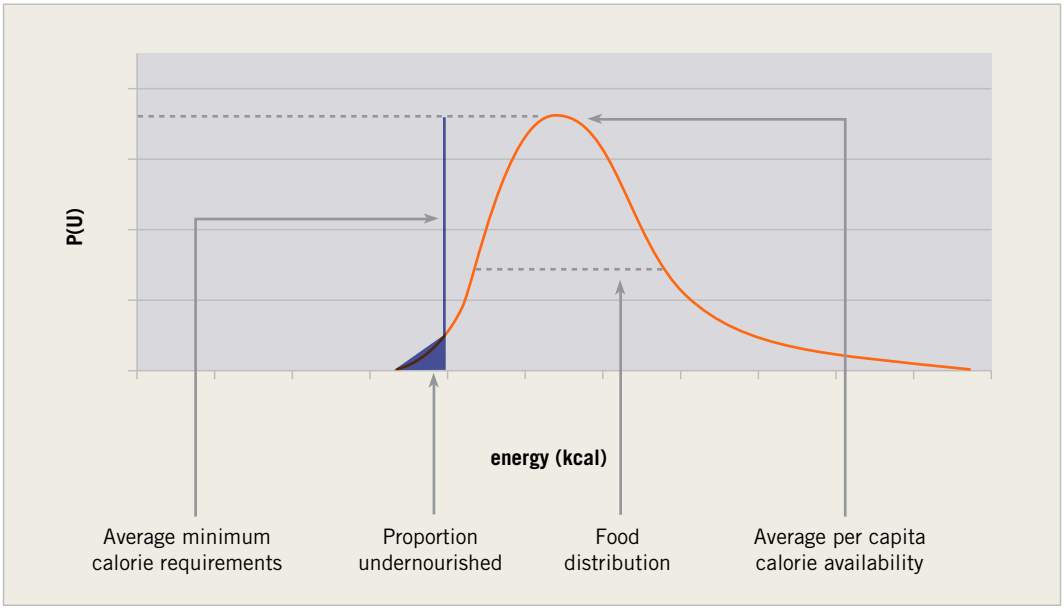

[a] *x*-axis is energy intake; *y*-axis is proportion of population with that energy intake

7.2.3 Step 3: estimates of child stunting

We used a model that we had previously developed to estimate future stunting attributable to global climate change (Lloyd et al., 2011). The model considers stunting to have two broad causes: a lack of food (food causes), which is represented as proportion of population undernourished, and non-food causes, which are a cluster of socioeconomic factors modelled using GDP per capita and the Gini coefficient for income distribution. The model also includes the interaction of food and non-food causes; for instance, a given intake of food will have different impacts on nutrition, depending on the presence and severity of diarrhoeal disease. See the original paper by Lloyd and colleagues (2011) for more details on the modelling method.

For model inputs, we used national-level estimates of the proportion of population undernourished derived from Step 2, national population and national GDP per capita projections (Nelson et al., 2010), and the current Gini coefficient for income distributions (World Bank, 2010a). (Projections for the Gini coefficient were not available. We used the most recent estimates available and assumed they remained constant in the future.)

The model output is the proportion of children moderately and severely stunted, as defined by the WHO (2006) child growth standards. A child is considered to be moderately stunted if they are more than two standard deviations below the mean expected height for age, and severely stunted if they are more than three standard deviations below the mean expected height for age.

To account for parameter uncertainty in the undernutrition model, stunting was estimated as probability density functions using a Monte Carlo simulation. We ran the simulation

100 000 times (each using a randomly selected combination of parameter values) for each scenario combination to obtain estimated distributions of the proportion stunted. We then combined the distributions for the two climate scenarios[2] to obtain a single distribution of proportion stunted under climate change for each scenario combination.

For each distribution of proportion stunted, we used the mean to represent our best estimate and represent the uncertainty interval as mean ± 1 standard deviation. We estimated stunting attributable to climate change by subtracting the mean estimate without climate change from the mean estimate with climate change, and combined their variances to estimate uncertainty,[3] reported as mean ± 1 standard deviation.

The undernutrition model has three underlying assumptions of relevance to our stunting estimates. First, the model estimates stunting specifically in children aged under 5 years, but the proportion undernourished is estimated for the entire population. As a result, estimates made with the model implicitly assume that, in all populations, the age distribution of undernourishment remains constant over time.

Second, the model is partly driven by an estimate of the physiological relationship between stunting and undernourishment; it is assumed that this estimate is representative of the true relationship and that it will be constant over the 50-year period included in this assessment. In terms of representativeness, the estimate is an approximation made for modelling purposes, and it gave a good fit between predicted and observed stunting in the model validation. Of note, the estimate suggests that about 60% of stunting could not be attributed directly to a lack of food, which is consistent with a previous estimate that around 40–60% of undernutrition could be attributed to environmental conditions (Pruss-Ustun & Corvalan, 2006).

Third, the undernutrition model accounts for socioeconomic conditions using an indicator based on GDP per capita and the Gini coefficient for income distribution (the "development score"). We assume that the Gini coefficient remains at baseline levels, although it may change significantly over the next 50 years. Also, in using the development score, we effectively assumed that the current relationship between GDP and socioeconomic conditions (such as access to adequate water supplies, health-care provision and education) will hold in the future. As this relationship is determined by many factors that may change, such as those shaped by politics and cultural norms, the relationship may change over the assessment period.

Due to a lack of data, we were unable to quantify the implications of the above assumptions.

---

2 We combined the distributions of proportion stunted for the MIROC and CSIRO scenarios based on their means and variances using the formulae $mean_{combined} = \frac{mean_{MIROC} + mean_{CSIRO}}{2}$ and $variance_{combined} = \frac{variance_{MIROC} + variance_{CSIRO}}{4}$

3 To estimate climate change-attributable proportion of stunting, we used the formulae $mean_{attributable} = mean_{with\ climate\ change} - mean_{without\ climate\ change}$ and $variance_{attributable} = variance_{with\ climate\ change} + variance_{without\ climate\ change}$

7.2.4 Step 4: estimates of all-cause mortality attributable to stunting

We combined our estimates of the future proportion of children who are moderately and severely stunted with odds ratios for all-cause mortality associated with each level of stunting from Black and colleagues (2008) to estimate population-attributable fractions of deaths due to stunting. The odds ratios were estimated using data from eight low-income countries considered to be broadly representative of all low-income countries and were adjusted for confounding due to socioeconomic factors (Table 7.1). For more details, see the paper by Black and colleagues (2008).

Table 7.1 Odds ratio for all-cause mortality associated with moderate and severe stunting

Cause	Moderate stunting[a]	Severe stunting[a]
All causes	1.6 (1.3 to 2.2)	4.1 (2.6 to 6.4)

a Odds ratios shown as central estimates with 95% confidence intervals in brackets
Source: Black et al. (2008)

Following the method of Black and colleagues (2008), we assumed that the odds ratios were a reasonable first-order approximation of the equivalent relative risks. We estimated population-attributable fractions using

$$PAF = \frac{\sum_{i=1}^{n}[P_i(RR_i - 1)]}{\sum_{i=1}^{n}[P_i(RR_i - 1)] + 1} \quad [7.1]$$

where PAF is the population-attributable fraction; P_i is the proportion affected by the exposure of interest at level i; RR_i is the relative risk for a given outcome when exposed at level i; and i is a level exposure, where there are n levels of exposure, with $1 \leq i \leq n$.

Specifically in our use, $i = 1$ for moderate stunting and $i = 2$ for severe stunting; P_i is the proportion stunted at level i; and RR_i is the relative risk of all-cause mortality associated with stunting at level i (compared with being not stunted).

When estimating the population-attributable fractions, we accounted for uncertainty in the proportion stunted and the mortality odds ratios as follows: for the proportion stunted, using our regional-level mean estimates and standard deviations generated in Step 3, we ran a standard Monte Carlo simulation to estimate 100 000 plausible values of the true proportion stunted at each level in each region. Similarly, for the odds ratios, using the central estimates and 95% confidence intervals, we estimated 100 000 plausible estimates of the true odds ratio.[4] Thus, we estimated population-attributable fractions for each region with and without climate change as distributions (probability density functions), based on 100 000 plausible estimates. The climate change-attributable population-attributable fractions were

4 The odds ratios in Table 7.1 were estimated in the log scale and then transformed to the natural scale. Therefore, the confidence intervals are asymmetrical about the means. Thus, we logged the odds ratios and confidence intervals and then calculated the averages of the upper and lower confidence intervals. We estimated the standard deviation for use in the Monte Carlo simulation. After running the simulation, we exponentiated the results.

estimated by subtracting the vectors of population-attributable fraction estimates without climate change from the vectors of population-attributable fraction estimates with climate change.

To estimate the number of deaths due to stunting in each scenario, we applied the population-attributable fractions directly to the projections of the all-cause mortality in children aged under 5 years (see Chapter 8 for discussion of mortality projections). We obtained probability density functions of stunting-attributable deaths for each region and used the mean as our best estimate and one standard deviation to describe the uncertainty interval.

7.3 Scenario data

As this chapter was dependent on input data produced outside this project (national-level calorie availability estimates), it uses a different set of scenarios from the other chapters.

7.3.1 Observed climate data

The current climate was represented using the WorldClim current conditions dataset, which represents the period 1950–2000 and provides monthly averages for minimum and maximum temperature and precipitation (Hijmans et al., 2005). The data were generated by interpolating average monthly data for weather stations to a 1 km^2 grid. For details of how the data were used to drive the crop models, see the paper by Nelson and colleagues (2010).

7.3.2 Climate scenarios

Two climate scenarios were used to drive the DSSAT model, both forced by the A1b emissions scenario:

- CSIRO model: by 2050, the mean change in annual average minimum and maximum temperatures is 1.6°C and 1.4°C, respectively, with a 0.7% increase in average annual precipitation.
- MIROC model: by 2050, the mean change in annual average minimum and maximum temperatures is 3.0°C and 2.8°C change, respectively, with a 4.7% increase in average annual precipitation.

7.3.3 GDP and population projections

The estimates of calorie availability from Step 1 (Nelson et al., 2010) were made under three socioeconomic scenarios intended to represent pessimistic, baseline (business as usual) and optimistic futures (Table 7.2). We note that these scenarios are quantitatively different from those used elsewhere in the CCRA project (see Chapter 8).

Of particular note, as seen in Table 7.2, the GDP data used in this chapter were in a different metric from the GDP data used in other chapters (market exchange rate versus purchasing power parity); thus, the data are not directly comparable. In general, purchasing power parity may better reflect conditions within a given country. The estimates tend to be of

Table 7.2 Socioeconomic scenarios subsequently used to estimate future national calories availability, showing global totals of GDP per capita and population for 2050[a] and socioeconomic scenarios used in the other chapters of the CCRA

Scenario	GDP			Population		
	Nelson et al. (2010)		CCRA	Nelson et al. (2010)		CCRA
	Source	Global GDP per capita, 2050[b]	Global GDP per capita, 2050[c]	Source	Global population, 2050[d]	Global population, 2050[d]
Pessimistic/ low growth	Low scenario from Millennium Ecosystem Assessment,[e] with growth rates used in base	8779	9191	UN high variant, 2008 revision	10 99	9130
Baseline/ base case	Based on rates from World Bank EACC study,[f] updated for sub-Saharan Africa and south Asia	17 23	29 84	UN medium variant, 2008 revision	9906	9130
Optimistic/ high growth	High scenario from Millennium Ecosystem Assessment,[e] with growth rates used in base	23 60	44 94	UN low variant, 2008 revision	7913	9130

a Based on Tables 1.1 and 1.3 in Nelson et al. (2010)
b GDP per capita in constant US$ 2000 as market exchange rate
c GDP per capita in 2005 international dollars as purchasing power parity
d Population totals in millions
e Millennium Ecosystem Assessment (2005)
f Margulis et al. (2010)

greater magnitude as they reflect the relative cost of living within a particular country, which tends to be lower in low-income compared with high-income countries. In contrast, market exchange rates may better reflect relative currency values, critical to global food trade, which is of major importance to estimates in this chapter. We assume that the purchasing power parity and market exchange rate data are roughly equivalent in each of the three socioeconomic scenarios; it is not, however, possible to test this assumption. The assumption is stronger for the baseline/base case and optimistic/high growth cases: in both studies, GDP continues to grow over the century. For the pessimistic/low growth scenarios, growth continues over the century in the purchasing power parity estimates (pessimistic scenario), but with the market exchange rate data used in other chapters (low growth scenario), GDP growth tapers towards zero and ceases to grow in any country after 2015.

As we have assumed equivalence between Nelson and colleagues' (2010) and the CCRA scenarios, for consistency with other chapters, we refer to our estimates as being for low growth, base case and high growth scenarios.

For population, the CCRA uses a common population projection for all three socioeconomic scenarios, while Nelson and colleagues use different projections for each scenario. In the optimistic and baseline scenarios, Nelson and colleagues use a higher population than

the CCRA (for high growth and base case) (see Table 7.2). Compared with using a lower population estimate (as in the CCRA), the use of the higher populations could have two opposing effects within the calorie availability model: having more people to feed may mean more people are undernourished (that is, the proportion of population undernourished would be higher than if the population were lower); but having more people to feed may lead to greater demand and thus production, resulting in increased food availability. The degree to which one effect is offset by the other is unknown; when scaling the results to be consistent with the CCRA population (see below), we assume the offset is complete – in effect, we assume that the proportion of population undernourished is independent of population (providing population total or growth is not excessively high) and that any additional risk of hunger due to a higher population is balanced by the accompanying decrease in risk due to increased demand-driven production). The same argument applies to the lower population (compared with the CCRA) in Nelson and colleagues' pessimistic scenario.

7.3.4 Scaling output for consistency with other health outcomes in the global assessment

It is important that all outcomes in this climate change assessment are based on a consistent set of assumptions about future worlds (particularly for economic growth and population growth). However, the future calorie estimates used in this chapter were based on a different set of scenarios. To bring our results in line with other chapter estimates as far as possible, we used the following strategies and assumptions:

- We estimated national-level stunting using data for the countries shown in Box 7.2, based on the population scenarios used by Nelson and colleagues (2010). This ensured within-model consistency between the calorie estimates and the undernutrition estimates.
- We aggregated the national-level stunting estimates to estimate the proportion stunted at regional level, using the regional definitions shown in Box 7.2. As noted in Step 1, these regional definitions do not match the regional definitions used in the other chapters of this assessment; in particular, due to missing data, fewer countries are included in the regions in Box 7.2. Hence, we assumed that our regional estimates of proportion stunted were representative of regional stunting when all countries in the region are included (that is, based on the world regions).
- To estimate the number stunted or number of deaths, we used population totals consistent with the CCRA population. This ensured comparability between estimates of number stunted and number of deaths in this chapter, and numbers estimated in other chapters of this assessment. We note that this assumes that the calorie availability estimates (which underlie the stunting estimates) are relatively independent of total population (that is, the two effects outlined above balance each other).

7.4 Results

Climate change is expected to cause a significant increase in the number of children with severe stunting, regardless of the socioeconomic scenario considered (Figure 7.3). In the base case, in a future without climate change, we estimate there will be 142.4 million

Figure 7.3 Additional number[a] of children aged under 5 years stunted due to climate change in 2030 and 2050 in the 12 study regions under low growth (L), base case (B) and high growth (H) socioeconomic scenarios

[a] Bars show additional number of children stunted due to climate change as a mean of the probability density function for the combined climate change scenario estimates minus the mean of the probability density function for the estimates without climate change

(uncertainty interval 139.8 million to 144.6 million) moderately stunted children and 58.2 million (uncertainty interval 56.3 million to 59.9 million) severely stunted children in 2030. The corresponding figures for 2050 are 101.9 million (uncertainty interval 100.1 million to 103.4 million) for moderate stunted children and 31.5 million (uncertainty interval 30.5 million to 32.5 million) for severely stunted children. We estimate that climate change will result in an additional 3.6 million (uncertainty interval 2.9 million to 4.4 million) moderately stunted children and 3.9 million (uncertainty interval 3.5 million to 4.4 million) severely stunted children by 2030; in total, this is 7.5 million (uncertainty interval 6.7 million to 8.4 million) additional stunted children. In 2050, additional severe stunting is estimated to remain at 3.9 million (uncertainty interval 3.6 million to 4.1 million), but moderate stunting is expect to rise to 6.2 million (uncertainty interval 5.4 million to 7.0 million), giving a total of 10.1 million (uncertainty interval 9.2 million to 11.0 million) additional stunted children.

Under the low growth scenario, without climate change we estimate that in 2030 there will be 162.3 million (uncertainty interval 159.5 million to 165.1 million) moderately stunted children and 73.6 million (uncertainty interval 71.7 million to 75.9 million) severely stunted children. For 2050, the corresponding estimates are 213.5 million (uncertainty interval 210.2 million to 216.4 million) and 112.6 million (uncertainty interval 109.6 million to 115.7 million), respectively. Our estimates suggest climate change will lead to a large increase in severe stunting. Climate change is projected to increase moderate stunting by 3.3 million (uncertainty interval 2.4 million to 4.1 million) by 2030, but then reduce it by 4.9 million (uncertainty interval 5.9 million to 3.9 million) (compared with a future without climate

change). This apparent benefit, however, is offset as severe stunting is expected to increase by 5.2 million (uncertainty interval 4.5 million to 5.9 million) by 2030 and 8.2 million (uncertainty interval 6.9 million to 9.5 million) by 2050. Total climate change-attributable stunting is expected to be 8.5 million (uncertainty interval 7.4 million to 9.5 million) in 2030 and 3.3 million (uncertainty interval 1.6 million to 4.9 million) in 2050.

For the high growth scenario without climate change, moderate and severe stunting in 2030 are estimated to be 123.1 million (uncertainty interval 121 million to 125.1 million) and 43.5 million (uncertainty interval 42.1 million to 45.2 million), respectively. In 2050 our estimates are 70.1 million (uncertainty interval 68.8 million to 71.6 million) for moderate stunting and 14.3 million (uncertainty interval 13.5 million to 15.2 million) for severe stunting. Climate change is expected to increase moderate stunting by 3.3 million (uncertainty interval 2.7 million to 4.0 million) in 2030, and 3.8 million (uncertainty interval 3.3 million to 4.3 million) by 2050. Severe stunting is estimated to increase by 3.1 million (uncertainty interval 2.7 million to 3.6 million) and 1.4 million (uncertainty interval 1.3 million to 1.6 million) in 2030 and 2050, respectively. Total stunting is expected to increase by 6.5 million (uncertainty interval 5.7 million to 7.2 million) in 2030 and 5.2 million (uncertainty interval 4.7 million to 5.7 million) in 2050.

Figure 7.4 shows additional severe stunting attributable to climate change in the sub-Saharan African regions, which are, along with south Asia, expected to be the most affected[5] by climate change (in terms of stunting). Table 7.3 shows the estimated number of children with stunting attributable to climate change in sub-Saharan Africa and south Asia.

Table 7.3 Estimated number[a] of children aged under 5 years with climate change-attributable stunting in 2030 and 2050 in sub-Saharan Africa[b] and south Asia

Region	Climate change–attributable stunting (millions of children aged < 5 years)						
	Stunting level	Base case		Low growth		High growth	
		2030	2050	2030	2050	2030	2050
Sub-Saharan Africa	Moderate	0.8 (0.4 to 1.1)	1.8 (1.6 to 2.1)	0.4 (–0.06 to 0.8)	–2.6 (–3.0 to –2.1)	0.7 (0.4 to 1.1)	1.2 (1.0 to 1.4)
	Severe	2.3 (2.0 to 2.6)	2.4 (2.2 to 2.5)	2.9 (2.6 to 3.2)	3.9 (3.5 to 4.3)	1.9 (1.7 to 2.2)	1.1 (9.7 to 1.2)
Asia, south	Moderate	1.1 (0.6 to 1.6)	1.8 (1.6 to 2.1)	1.1 (0.6 to 1.6)	–1.5 (–2.1 to –0.9)	1.1 (0.8 to 1.5)	1.3 (1.1 to 1.5)
	Severe	0.9 (0.6 to 1.3)	0.9 (0.8 to 1.0)	1.4 (0.9 to 1.9)	2.1 (1.2 to 3.1)	0.6 (3.5 to 0.9)	0.2 (0.1 to 0.3)

a Numbers are mean estimate (millions of children aged under 5 years) with uncertainty interval (mean ± 1 standard deviation) in brackets

b Sub-Saharan Africa is the sum of estimates for central, eastern, southern and western sub-Saharan Africa. The mean estimate is the sum of the mean estimates from each region; the uncertainty interval is based on the uncertainty interval in each region (and was calculated by summing the variances in each region)

5 With the exception of southern sub-Saharan Africa, which has lower rates of stunting than the other regions in sub-Saharan Africa.

Figure 7.4 Number[a] of children with severe stunting, with and without climate change (CC), in 2030 and 2050 in four African regions under (a) base case, (b) low growth and (c) high growth scenarios

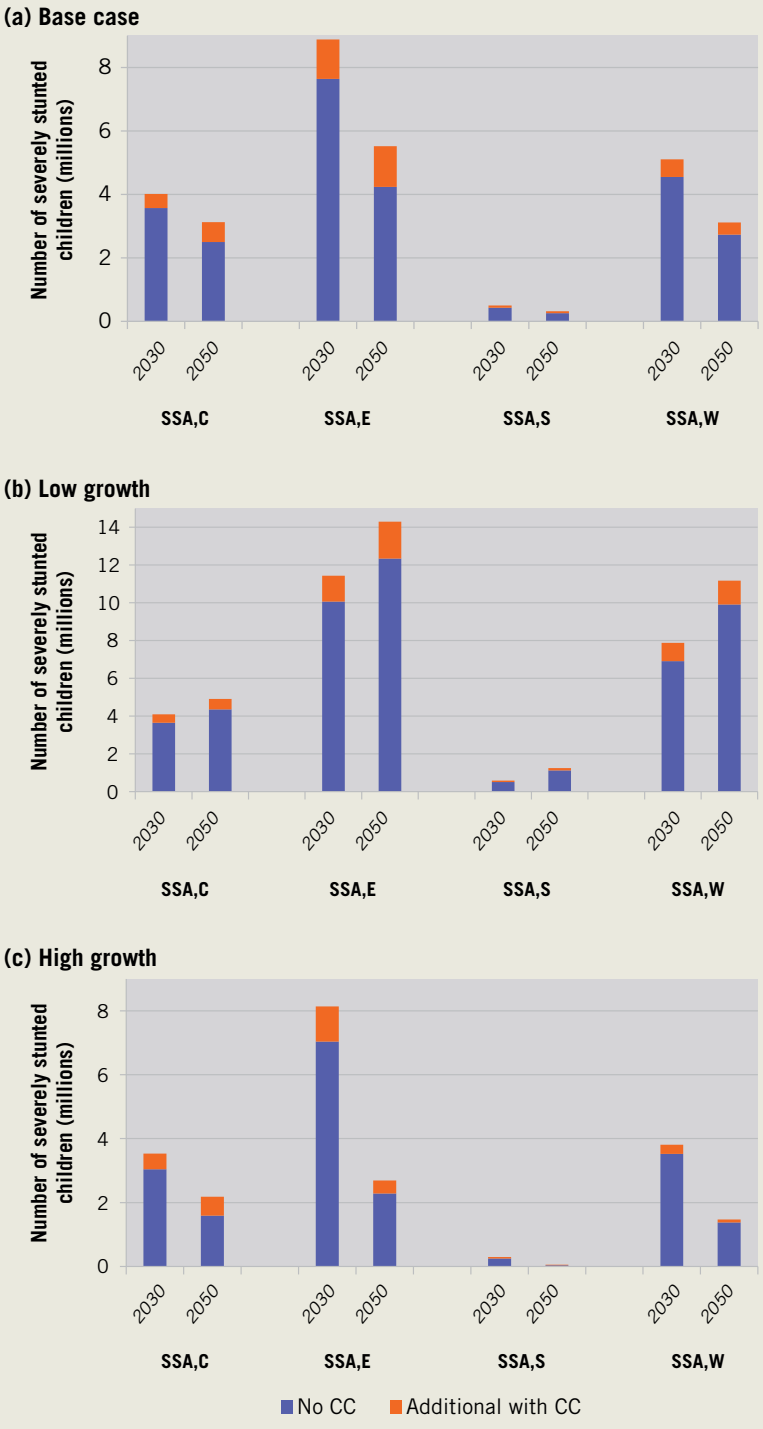

SSA,C – sub-Saharan Africa, central; SSA,E – sub-Saharan Africa, eastern; SSA,S – sub-Saharan Africa, southern; SSA,W – sub-Saharan Africa, western

[a] Note y-axis scale is different for each graph; bars show number of children severely stunted as mean of the probability density function for the estimates without climate change and the mean additional number stunted with climate change based on the probability density function of the combined climate change scenario estimates

7.5 Regional estimates of children with stunting due to climate change

Table 7.4 gives regional estimates of the number of children with stunting due to climate change in 2030 and 2050.

Table 7.4 Percentage of children aged under 5 years estimated to be moderately or severely stunted in 2030 and 2050, with and without climate change, for (a) base case, (b) low growth and (c) high growth scenarios[a]

(a) Base case

Region	Stunting level	2030			2050		
		No climate change	With climate change	Climate change-attributable	No climate change	With climate change	Climate change-attributable
Asia, central	Moderate	11.9 (11.7 to 12.1)	13.1 (13.0 to 13.3)	1.2 (1.0 to 1.5)	7.9 (7.8 to 8.0)	9.9 (9.8 to 10.0)	2.0 (1.8 to 2.1)
	Severe	3.4 (3.3 to 3.5)	4.1 (4.1 to 4.2)	0.8 (0.6 to 0.9)	1.3 (1.2 to 1.3)	2.1 (2.0 to 2.1)	0.8 (0.7 to 0.9)
Asia, east	Moderate	9.0 (8.8 to 9.2)	9.6 (9.5 to 9.8)	0.6 (0.5 to 0.8)	4.1 (4.0 to 4.2)	5.1 (5.0 to 5.2)	1.1 (0.9 to 1.2)
	Severe	1.9 (1.8 to 2.0)	2.1 (2.0 to 2.2)	0.2 (0.0 to 0.4)	0.2 (0.2 to 0.3)	0.4 (0.3 to 0.4)	0.1 (0.1 to 0.2)
Asia, south	Moderate	13.7 (13.5 to 13.9)	14.4 (14.3 to 14.6)	0.7 (0.5 to 1.0)	8.1 (8.0 to 8.2)	9.4 (9.2 to 9.5)	1.3 (1.1 to 1.4)
	Severe	4.4 (4.2 to 4.6)	5.0 (4.9 to 5.1)	0.6 (0.4 to 0.8)	1.5 (1.5 to 1.6)	2.1 (2.1 to 2.2)	0.6 (0.5 to 0.7)
Asia, south-east	Moderate	10.8 (10.6 to 10.9)	11.7 (11.5 to 11.8)	0.9 (0.7 to 1.1)	6.7 (6.6 to 6.8)	8.3 (8.2 to 8.4)	1.6 (1.4 to 1.7)
	Severe	2.8 (2.7 to 2.9)	3.3 (3.2 to 3.3)	0.5 (0.4 to 0.6)	1.1 (1.0 to 1.1)	1.6 (1.5 to 1.6)	0.5 (0.4 to 0.6)
Latin America, central and Caribbean	Moderate	9.7 (9.5 to 9.8)	10.8 (10.6 to 10.9)	1.1 (0.9 to 1.3)	6.1 (6.0 to 6.1)	7.8 (7.7 to 7.9)	1.7 (1.6 to 1.9)
	Severe	2.1 (2.0 to 2.2)	2.5 (2.4 to 2.5)	0.4 (0.3 to 0.5)	0.6 (0.5 to 0.6)	1.1 (1.0 to 1.1)	0.5 (0.4 to 0.6)

[Continues]

[Continued]

Region	Stunting level	2030			2050		
		No climate change	With climate change	Climate change-attributable	No climate change	With climate change	Climate change-attributable
Latin America, mid	Moderate	7.0 (6.9 to 7.1)	7.8 (7.7 to 7.9)	0.8 (0.7 to 1.0)	5.2 (5.1 to 5.3)	6.4 (6.3 to 6.5)	1.2 (1.1 to 1.3)
	Severe	1.0 (1.0 to 1.1)	1.3 (1.3 to 1.3)	0.3 (0.2 to 0.3)	0.4 (0.4 to 0.4)	0.7 (0.7 to 0.8)	0.3 (0.3 to 0.4)
Latin America, south	Moderate	3.2 (3.1 to 3.3)	3.5 (3.4 to 3.6)	0.3 (0.2 to 0.5)	2.9 (2.8 to 3.0)	3.3 (3.3 to 3.4)	0.4 (0.3 to 0.5)
	Severe	0.0 (0.0 to 0.1)	0.1 (0.0 to 0.1)	0.0 (0.0 to 0.0)	0.0 (0.0 to 0.0)	0.0 (0.0 to 0.1)	0.0 (0.0 to 0.0)
North Africa/Middle East	Moderate	8.4 (8.3 to 8.5)	9.0 (8.9 to 9.1)	0.6 (0.5 to 0.8)	5.3 (5.2 to 5.4)	6.1 (6.0 to 6.2)	0.8 (0.7 to 0.9)
	Severe	1.6 (1.5 to 1.6)	1.8 (1.7 to 1.8)	0.2 (0.1 to 0.3)	0.5 (0.5 to 0.5)	0.7 (0.6 to 0.7)	0.2 (0.1 to 0.2)
Sub-Saharan Africa, central	Moderate	19.7 (19.2 to 20.1)	19.7 (19.3 to 20.1)	0.0 (–0.5 to 0.6)	18.2 (17.8 to 18.5)	19.1 (18.8 to 19.5)	1.0 (0.5 to 1.5)
	Severe	17.3 (16.7 to 17.8)	19.4 (19.0 to 19.8)	2.1 (1.5 to 2.8)	12.3 (11.9 to 12.8)	15.4 (15.1 to 15.8)	3.1 (2.5 to 3.6)
Sub-Saharan Africa, eastern	Moderate	19.8 (19.5 to 20.1)	20.3 (20.1 to 20.6)	0.5 (0.1 to 0.9)	15.6 (15.4 to 15.8)	17.0 (16.9 to 17.2)	1.4 (1.2 to 1.7)
	Severe	10.8 (10.6 to 10.9)	12.5 (12.4 to 12.6)	1.8 (1.5 to 2.0)	5.8 (5.7 to 5.9)	7.5 (7.4 to 7.6)	1.8 (1.6 to 1.9)
Sub-Saharan Africa, southern	Moderate	11.6 (11.4 to 11.8)	12.4 (12.2 to 12.6)	0.8 (0.5 to 1.1)	8.4 (8.2 to 8.5)	9.7 (9.5 to 9.8)	1.3 (1.1 to 1.5)
	Severe	5.8 (5.6 to 5.9)	6.6 (6.5 to 6.7)	0.8 (0.6 to 1.0)	3.7 (3.6 to 3.8)	4.6 (4.5 to 4.7)	0.9 (0.7 to 1.1)
Sub-Saharan Africa, western	Moderate	17.6 (17.3 to 17.8)	18.1 (17.9 to 18.3)	0.5 (0.2 to 0.8)	13.4 (13.2 to 13.6)	14.1 (14.0 to 14.3)	0.8 (0.5 to 1.0)
	Severe	7.1 (6.9 to 7.3)	8.0 (7.9 to 8.1)	0.9 (0.6 to 1.1)	4.1 (4.0 to 4.2)	4.7 (4.6 to 4.8)	0.6 (0.4 to 0.7)

[Continues]

[Continued]

(b) Low growth

Region	Stunting level	2030			2050		
		No climate change	With climate change	Climate change-attributable	No climate change	With climate change	Climate change-attributable
Asia, central	Moderate	13.6 (13.4 to 13.8)	14.8 (14.6 to 14.9)	1.2 (0.9 to 1.5)	26.7 (26.4 to 27.0)	25.6 (25.4 to 25.9)	–1.1 (–1.5 to –0.6)
	Severe	4.2 (4.1 to 4.3)	5.1 (5.0 to 5.2)	0.9 (0.8 to 1.1)	14.1 (13.7 to 14.4)	15.6 (15.4 to 15.9)	1.5 (1.1 to 2.0)
Asia, east	Moderate	12.0 (11.8 to 12.2)	12.7 (12.6 to 12.8)	0.7 (0.5 to 0.9)	26.9 (26.5 to 27.2)	26.1 (25.8 to 26.3)	–0.8 (–1.2 to –0.4)
	Severe	3.2 (3.0 to 3.4)	3.6 (3.4 to 3.7)	0.4 (0.1 to 0.7)	13.8 (13.1 to 14.5)	15.0 (14.4 to 15.5)	1.1 (0.2 to 2.0)
Asia, south	Moderate	16.4 (16.2 to 16.6)	17.1 (16.9 to 17.3)	0.7 (0.4 to 1.0)	26.0 (25.7 to 26.4	25.0 (24.7 to 25.2)	–1.0 (–1.4 to –0.6)
	Severe	6.4 (6.2 to 6.7)	7.3 (7.1 to 7.5)	0.9 (0.6 to 1.2)	15.1 (14.5 to 15.6)	16.6 (16.2 to 16.9)	1.5 (0.8 to 2.1)
Asia, south-east	Moderate	12.6 (12.4 to 12.8)	13.5 (13.3 to 13.6)	0.9 (0.7 to 1.1)	23.3 (22.9 to 23.6)	22.5 (22.3 to 23.7)	–0.7 (–1.1 to 0.4)
	Severe	3.9 (3.8 to 4.0)	4.5 (4.4 to 4.5)	0.6 (0.5 to 0.7)	12.9 (12.6 to 13.2)	14.3 (14.0 to 14.5)	1.4 (1.0 to 1.28)
Latin America, central and Caribbean	Moderate	10.0 (9.9 to 10.2)	11.1 (10.9 to 11.2)	1.0 (0.8 to 1.2)	15.0 (14.8 to 15.1)	15.6 (15.5 to 15.8)	0.7 (0.5 to 0.9)
	Severe	2.3 (2.2 to 2.4)	2.7 (2.6 to 2.8)	0.4 (0.3 to 0.5)	6.4 (6.1 to 6.6)	7.1 (6.9 to 7.3)	0.8 (0.5 to 1.0)
Latin America, mid	Moderate	8.8 (8.6 to 8.9)	9.6 (9.4 to 9.7)	0.8 (0.6 to 1.0)	11.5 (11.3 to 11.6)	11.9 (11.8 to 12.0)	0.4 (0.2 –0.6)
	Severe	1.7 (1.7 to 1.8)	2.1 (2.0 to 2.1)	0.3 (0.2 to 0.4)	4.3 (4.1 to 4.4)	4.8 (4.7 to 4.9)	0.5 (0.3 to 0.7)

[Continues]

[Continued]

Region	Stunting level	2030			2050		
		No climate change	With climate change	Climate change-attributable	No climate change	With climate change	Climate change-attributable
Latin America, south	Moderate	3.3 (3.2 to 3.4)	3.7 (3.6 to 3.7)	0.4 (0.3 to 0.5)	3.2 (3.1 to 3.3)	3.8 (3.7 to 3.8)	0.6 (0.5 to 0.7)
	Severe	0.0 (0.0 to 0.1)	0.1 (0.1 to 0.1)	0.0 (0.0 to 0.1)	0.0 (0.0 to 0.1)	0.1 (0.1 to 0.1)	0.0 (0.0 to 0.1)
North Africa/Middle East	Moderate	10.5 (10.3 to 10.6)	11.2 (11.0 to 11.3)	0.7 (0.5 to 0.9)	25.6 (25.3 to 25.9)	25.5 (25.3 to 25.7)	–0.2 (–0.5 to 0.2)
	Severe	2.4 (2.3 to 2.4)	2.7 (2.6 to 2.7)	0.3 (0.2 to 0.4)	11.3 (11.1 to 11.6)	12.0 (11.8 to 12.2)	0.7 (0.3 to 1.0)
Sub-Saharan Africa, central	Moderate	19.8 (19.3 to 20.3)	19.8 (19.4 to 20.1)	0.0 (–0.6 to 0.5)	22.0 (21.5 to 22.4)	20.3 (19.9 to 20.7)	–1.6 (–2.3 to –1.1)
	Severe	17.6 (17.1 to 18.2)	19.8 (19.4 to 20.2)	2.2 (1.5 to 2.8)	21.5 (20.8 to 22.1)	24.2 (23.8 to 24.7)	2.8 (2.0 to 3.5)
Sub-Saharan Africa, eastern	Moderate	21.0 (20.6 to 21.4)	21.2 (20.9 to 21.5)	0.2 (–0.3 to 0.7)	24.8 (24.4 to 25.2)	23.1 (22.8 to 23.3)	–1.7 (–2.2 to –1.3)
	Severe	14.2 (14.0 to 14.4)	16.1 (16.0 to 16.3)	1.9 (1.7 to 2.2)	16.9 (16.6 to 17.1)	19.5 (19.3 to 19.7)	2.7 (2.3 to 3.0)
Sub-Saharan Africa, southern	Moderate	14.1 (13.9 to 14.4)	15.0 (14.8 to 15.2)	0.9 (0.6 to 1.3)	25.2 (24.8 to 25.4)	23.9 (23.7 to 24.1)	–1.2 (–1.6 to –0.9)
	Severe	6.9 (6.7 to 7.1)	7.8 (7.6 to 7.9)	0.9 (0.6 to 1.1)	16.5 (16.0 to 17.0)	18.4 (18.0 to 18.7)	1.9 (1.3 to 2.5)
Sub-Saharan Africa, western	Moderate	20.2 (19.9 to 20.5)	20.5 (20.3 to 20.7)	0.3 (–0.1 to 0.7)	26.2 (25.8 to 26.5)	24.9 (24.6 to 25.1)	–1.3 (–1.7 to –0.9)
	Severe	10.8 (10.6 to 11.1)	12.4 (12.2 to 12.5)	1.5 (1.2 to 1.8)	14.8 (14.5 to 15.1)	16.7 (16.5 to 17.0)	1.9 (1.5 to 2.3)

[Continues]

[Continued]

(c) High growth

Region	Stunting level	2030			2050		
		No climate change	With climate change	Climate change-attributable	No climate change	With climate change	Climate change-attributable
Asia, central	Moderate	9.3 (9.1 to 9.4)	10.4 (10.2 to 10.5)	1.1 (0.9 to 1.3)	3.5 (3.5 to 3.6)	4.4 (4.4 to 4.5)	0.9 (0.8 to 1.0)
	Severe	1.9 (1.8 to 1.9)	2.4 (2.3 to 2.4)	0.5 (0.4 to 0.6)	0.1 (0.0 to 0.1)	0.2 (0.2 to 0.2)	0.1 (0.1 to 0.1)
Asia, east	Moderate	6.7 (6.6 to 6.8)	7.2 (7.1 to 7.3)	0.5 (0.4 to 0.7)	3.2 (3.0 to 3.3)	3.7 (3.6 to 3.8)	0.6 (0.4 to 0.7)
	Severe	0.8 (0.7 to 0.9)	1.1 (1.0 to 1.1)	0.3 (0.2 to 0.4)	0.0 (0.1 to 0.1)	0.1 (0.0 to 0.1)	0.0 (0.0 to 0.1)
Asia, south	Moderate	12.3 (12.1 to 12.5)	13.0 (12.9 to 13.1)	0.7 (0.5 to 0.9)	5.1 (5.0 to 5.2)	6.0 (5.9 to 6.1)	0.9 (0.8 to 1.0)
	Severe	3.3 (3.1 to 3.4)	3.7 (3.6 to 3.8)	0.4 (0.2 to 0.6)	0.4 (0.3 to 0.4)	0.5 (0.5 to 0.5)	0.2 (0.1 to 0.2)
Asia, south-east	Moderate	7.4 (7.2 to 7.5)	8.1 (8.0 to 8.2)	0.7 (0.6 to 0.8)	3.6 (3.6 to 3.7)	4.4 (4.3 to 4.4)	0.8 (0.7 to 0.8)
	Severe	1.1 (1.1 to 1.2)	1.4 (1.4 to 1.5)	0.3 (0.2 to 0.4)	0.1 (0.1 to 0.1)	0.2 (0.2 to 0.2)	0.1 (0.1 to 0.1)
Latin America, central and Caribbean	Moderate	7.0 (6.9 to 7.1)	7.9 (7.8 to 8.0)	1.0 (0.8 to 1.1)	3.5 (3.4 to 3.6)	4.4 (4.3 to 4.4)	0.9 (0.8 to 1.0)
	Severe	1.0 (0.9 to 1.0)	1.2 (1.2 to 1.3)	0.2 (0.2 to 0.3)	0.0 (0.0 to 0.1)	0.1 (0.1 to 0.1)	0.1 (0.0 to 0.1)
Latin America, mid	Moderate	5.9 (5.8 to 6.0)	6.6 (6.5 to 6.7)	0.7 (0.6 to 0.8)	3.3 (3.2 to 3.4)	3.9 (3.9 to 4.0)	0.6 (0.5 to 0.7)
	Severe	0.6 (0.6 to 0.7)	0.8 (0.7 to 0.8)	0.2 (0.1 to 0.2)	0.0 (0.0 to 0.1)	0.1 (0.1 to 0.1)	0.0 (0.0 to 0.1)

[Continues]

[Continued]

Region	Stunting level	2030			2050		
		No climate change	With climate change	Climate change-attributable	No climate change	With climate change	Climate change-attributable
Latin America, south	Moderate	3.1 (3.1 to 3.2)	3.5 (3.4 to 3.6)	0.3 (0.2 to 0.5)	2.8 (2.7 to 2.9)	3.0 (3.0 to 3.1)	0.3 (0.1 to 0.4)
	Severe	0.0 (0.0 to 0.1)	0.1 (0.0 to 0.1)	0.0 (0.0 to 0.0)	0.0 (0.0 to 0.0)	0.0 (0.0 to 0.0)	0.0 (0.0 to 0.0)
North Africa/Middle East	Moderate	8.0 (7.9 to 8.1)	8.5 (8.5 to 8.6)	0.6 (0.4 to 0.7)	3.4 (3.3 to 3.4)	3.7 (3.7 to 3.7)	0.4 (0.3 to 0.4)
	Severe	1.4 (1.4 to 1.7)	1.6 (1.5 to 1.6)	0.1 (0.1 to 0.2)	0.1 (0.0 to 0.1)	0.1 (0.1 to 0.1)	0.0 (0.0 to 0.0)
Sub-Saharan Africa, central	Moderate	20.1 (19.6 to 20.5)	20.4 (20.0 to 20.7)	0.3 (–0.2 to 0.9)	15.6 (15.4 to 15.9)	16.9 (16.7 to 17.2)	1.3 (1.0 to 1.7)
	Severe	14.7 (14.2 to 15.2)	17.1 (16.7 to 17.5)	2.4 (1.8 to 3.0)	7.8 (7.5 to 8.2)	10.8 (10.5 to 11.1)	2.9 (2.5 to 3.4)
Sub-Saharan Africa, eastern	Moderate	19.2 (18.9 to 19.5)	19.7 (19.5 to 20.0)	0.5 (0.1 to 0.9)	11.8 (11.6 to 12.0)	12.8 (12.6 to 12.9)	1.0 (0.8 to 1.2)
	Severe	9.9 (9.7 to 10.1)	11.5 (11.3 to 11.6)	1.5 (1.3 to 1.8)	3.1 (3.0 to 3.2)	3.7 (3.6 to 3.7)	0.6 (0.5 to 0.7)
Sub-Saharan Africa, southern	Moderate	8.4 (8.3 to 8.6)	9.2 (9.1 to 9.3)	0.8 (0.6 to 1.0)	4.7 (4.6 to 4.8)	5.4 (5.3 to 5.5)	0.7 (0.6 to 0.8)
	Severe	3.3 (3.2 to 3.3)	4.0 (3.9 to 4.1)	0.7 (0.5 to 0.8)	0.6 (0.5 to 0.6)	0.8 (0.8 to 0.8)	0.2 (0.2 to 0.3)
Sub-Saharan Africa, western	Moderate	15.7 (15.5 to 15.9)	16.1 (16.0 to 16.3)	0.4 (0.1 to 0.6)	9.6 (9.5 to 9.8)	9.9 (9.8 to 10.0)	0.3 (0.1 to 0.5)
	Severe	5.5 (5.4 to 5.7)	6.0 (5.9 to 6.1)	0.5 (0.3 to 0.6)	2.1 (2.0 to 2.2)	2.2 (2.1 to 2.3)	0.1 (0.0 to 0.2)

a All numbers are percentages as a mean of the probability density function and uncertainty interval (in brackets), defined as mean ± 1 standard deviation

7.6 Mortality due to climate change-attributable undernutrition

Climate change is estimated to increase mortality due to undernutrition, compared with a world without climate change (Figure 7.5).

Figure 7.5 Estimated additional deaths in children aged under 5 years attributable to climate change in 2030 and 2050, in the 12 study regions, under low growth (L), base case (B) and high growth (H) scenarios[a]

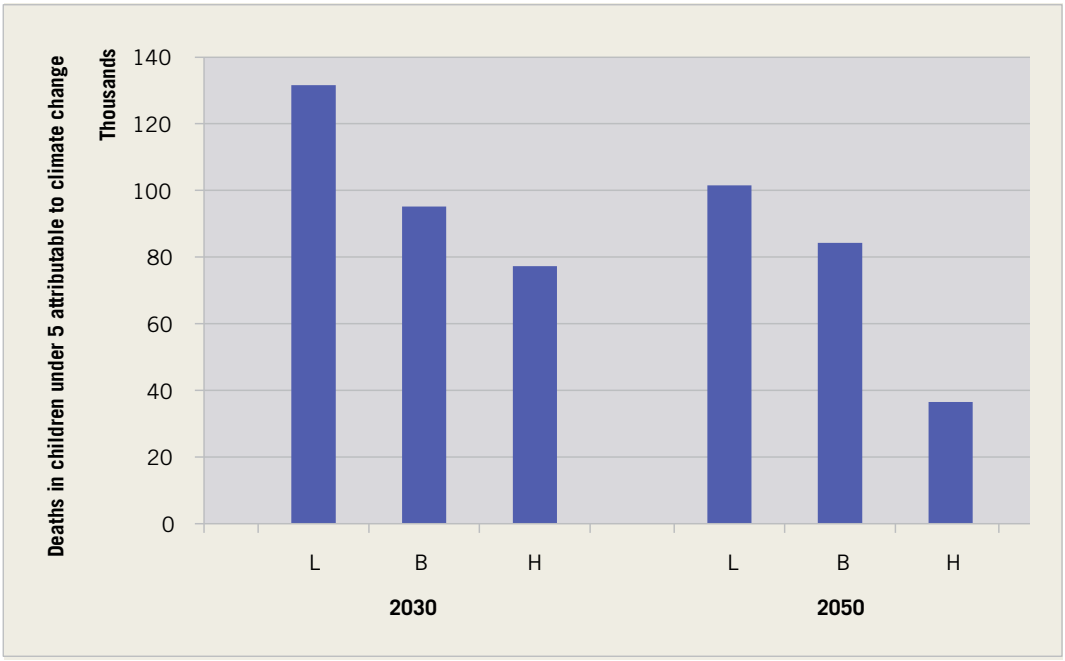

[a] Bars show additional numbers of deaths in children attributable to climate change as mean of the probability density function for the combined climate change scenario estimates minus the mean of the probability density function for the estimates without climate change

There are important differences in mortality impacts, depending on the economic growth scenario. In the base case, we estimate there will be an additional 95 175 (uncertainty interval −3586 to 193 937) deaths in 2030 and 84 695 (uncertainty interval 29 815 to 139 576) deaths in 2050. The corresponding numbers for the low growth scenario are 131 634 (uncertainty interval −11 273 to 274 541) deaths in 2030 and 101 484 (uncertainty interval −32 326 to 235 294) deaths in 2050; and for the high growth scenario 77 205 (uncertainty interval −12 491 to 166 900) deaths in 2030 and 36 524 (uncertainty interval 2518 to 70 530) deaths in 2050.

The regional distribution of mortality is shown in Table 7.5.

Table 7.5 Estimated number of deaths in children aged under 5 years attributable to moderate and severe stunting in 2030 and 2050, with and without climate change for (a) base case, (b) low growth and (c) high growth scenarios[a]

(a) Base case

Region	2030			2050		
	No climate change	With climate change	Climate change-attributable	No climate change	With climate change	Climate change-attributable
Asia, central	3149 (2328 to 3970)	3622 (2820 to 4423)	473 (–215 to 1161)	846 (589 to 1102)	1160 (873 to 1446)	314 (66 to 563)
Asia, east	15 734 (9711 to 21 756)	16 888 (11 606 to 22 171)	1155 (–5313 to 7622)	2363 (1345 to 3381)	3063 (1957 to 4169)	700 (–427 to 1828)
Asia, south	240 492 (174 541 to 306 443)	261 185 (201 266 to 321 103)	20 692 (–39 019 to 80 404)	66 908 (47 388 to 86 428)	83 438 (62 739 to 104 137)	16 530 (–1582 to 34 642)
Asia, south-east	29 989 (22 349 to 37 629)	33 337 (25 917 to 40 756)	3348 (–2635 to 9331)	9562 (6762 to 12 362)	12 611 (9566 to 15 656)	3049 (605 to 5494)
Latin America, central and Caribbean	6526 (4634 to 8418)	7385 (5584 to 9185)	859 (–837 to 2554)	1657 (1085 to 2230)	2363 (1689 to 3037)	706 (100 to 1311)
Latin America, mid	2700 (1856 to 3544)	3145 (2311 to 3979)	445 (–327 to 1218)	937 (599 to 1275)	1267 (895 to 1638)	330 (–6 to 665)
Latin America, south	154 (86 to 221)	168 (104 to 231)	14 (–49 to 76)	89 (49 to 129)	100 (61 to 138)	11 (–27 to 49)
North Africa/Middle East	17 151 (12 515 to 21 788)	18 769 (14 275 to 23 262)	1617 (–2030 to 5264)	5693 (3818 to 7568)	6860 (4926 to 8794)	1167 (–480 to 2813)
Sub-Saharan Africa, central	212 737 (165 285 to 260 189)	227 121 (186 129 to 268 113)	14 385 (–27 448 to 56 217)	131 831 (98 655 to 165 007)	150 104 (121 101 to 179 106)	18 273 (–12 372 to 48 918)
Sub-Saharan Africa, eastern	332 128 (269 769 to 394 487)	360 127 (298 601 to 421 654)	27 999 (–8701 to 64 699)	152 953 (120 400 to 185 507)	179 433 (145 544 to 213 322)	26 480 (4936 to 48 024)
Sub-Saharan Africa, southern	12 779 (9476 to 16 082)	14 024 (10 970 to 17 077)	1245 (–1505 to 3994)	5632 (3957 to 7306)	6663 (5064 to 8262)	1032 (–516 to 2580)
Sub-Saharan Africa, western	324 418 (252 177 to 396 659)	347 362 (279 731 to 414 993)	22 944 (–31 728 to 77 616)	176 163 (132 115 to 220 211)	192 267 (150 862 to 233 673)	16 105 (–19 500 to 51 709)

[Continues]

[Continued]

(b) Low growth

Region	2030			2050		
	No climate change	With climate change	Climate change-attributable	No climate change	With climate change	Climate change-attributable
Asia, central	4569 (3457 to 5682)	5188 (4094 to 6283)	619 (–268 to 1507)	5522 (4480 to 6563)	5775 (4813 to 6737)	253 (–522 to 1029)
Asia, east	33 309 (20 895 to 45 722)	35 996 (25 248 to 46 744)	2687 (–10 707 to 16 082)	63 415 (45 215 to 81 614)	66 312 (51 584 to 81 040)	2897 (–16 284 to 22 079)
Asia, south	403 558 (294 010 to 513 105)	437 660 (340 635 to 534 684)	34 102 (–68 345 to 136 548)	490 521 (381 807 to 599 235)	513 270 (419 341 to 607 200)	22 749 (–76 357 to 121 856)
Asia, south-east	45 141 (34 172 to 56 110)	49 726 (39 100 to 60 351)	4585 (–3841 to 13 010)	68 288 (54 671 to 81 906)	71 700 (59 132 to 84 268)	3412 (–7033 to 13 857)
Latin America, central and Caribbean	7814 (5592 to 10 036)	8799 (6682 to 10 916)	985 (–992 to 2962)	9060 (6605 to 11 515)	9773 (7611 to 11 936)	713 (–1528 to 2954)
Latin America, mid	4413 (3027 to 5800)	4976 (3698 to 6255)	563 (–732 to 18 58)	5003 (3677 to 6330)	5379 (4158 to 6600)	376 (–755 to 1506)
Latin America, south	186 (105 to 267)	207 (129 to 284)	21 (–54 to 95)	136 (76 to 196)	163 (102 to 223)	26 (–31 to 83)
North Africa/Middle East	27 155 (20 276 to 34 034)	29 493 (22 860 to 36 125)	2338 (–2827 to 7503)	57 523 (46 658 to 68 387)	59 111 (49 054 to 69 168)	1588 (–5840 to 9016)
Sub-Saharan Africa, central	260 373 (203 148 to 317 597))	277 273 (227 695 to 326 851)	16 901 (–33 191 to 66 993)	232 162 (185 407 to 278 918)	245 642 (204 704 to 286 580)	13 480 (–26 491 to 53 451)
Sub-Saharan Africa, eastern	474 650 (391 172 to 558 129)	506 556 (424 377 to 588 735)	31 906 (–14 849 to 78 660)	449 793 (375 099 to 524 487)	477 993 (405 041 to 550 944)	28 200 (–13 843 to 70 244)
Sub-Saharan Africa, southern	17 047 (13 000 to 21 095)	18 506 (14 720 to 22 292)	1458 (–1746 to 4663)	21 210 (16 827 to 25 593)	22 300 (18 445 to 26 155)	1089 (–2645 to 4824)
Sub-Saharan Africa, western	486 798 (388 603 to 584 993)	522 268 (429 362 to 615 174)	35 470 (–34 802 to 105 742)	518 904 (425 297 to 612 511)	545 604 (457 297 to 633 611)	26 700 (–37 825 to 91 235)

[Continues]

[Continued]

(c) High growth

Region	2030			2050		
	No climate change	With climate change	Climate change-attributable	No climate change	With climate change	Climate change-attributable
Asia, central	1977 (1404 to 2550)	2325 (1763 to 2888)	348 (–163 to 859)	204 (128 to 281)	270 (178 to 361)	65 (–5 to 136)
Asia, east	8709 (4933 to 12 485)	9916 (6426 to 13 405)	1207 (–3031 to 5444)	1281 (640 to 1923)	1484 (879 to 2088)	202 (–460 to 865)
Asia, south	193 269 (134 936 to 251 603)	209 274 (157 373 to 261 175)	16 005 (–39 902 to 71 912)	30 312 (19 489 to 41 136)	36 847 (25 141 to 48 553)	6535 (–4076 to 17 145)
Asia, south-east	14 139 (10 010 to 18 268)	16 325 (12 273 to 20 377)	2186 (–1240 to 5611)	2590 (1653 to 3527)	3237 (2190 to 4283)	646 (–141 to 1434)
Latin America, central and Caribbean	3177 (2147 to 4207)	3714 (2699 to 4730)	537 (–432 to 1506)	545 (331 to 759)	687 (443 to 930)	141 (–58 to 341)
Latin America, mid	1647 (1098 to 2197)	1906 (1362 to 2450)	259 (–243 to 760)	362 (209 to 516)	421 (267 to 576)	59 (–83 to 201)
Latin America, south	119 (67 to 172)	130 (80 to 179)	11 (–38 to 59)	58 (31 to 85)	62 (37 to 87)	4 (–21 to 29)
North Africa/ Middle East	14 837 (10 723 to 18 951)	15 995 (12 075 to 19 914)	1158 (–2135 to 4451)	2295 (1460 to 3129)	2518 (1658 to 3379)	224 (–394 to 842)
Sub-Saharan Africa, central	188 709 (144 726 to 232 691)	205 167 (167 101 to 243 233)	16 458 (–22 983 to 55 900)	71 966 (50 263 to 93 668)	87 345 (68 203 to 106 488)	15 379 (–6274 to 37 033)
Sub-Saharan Africa, eastern	307 504 (248 677 to 366 330)	332 996 (275 109 to 390 883)	25 492 (–9248 to 60 233)	85 365 (64 811 to 105 919)	95 226 (74 838 to 115 614)	9861 (–5158 to 24 881)
Sub-Saharan Africa, southern	6668 (4697 to 8639)	7650 (5800 to 9499)	982 (–826 to 2790)	907 (573 to 1241)	1117 (775 to 1460)	210 (–140 to 560)
Sub-Saharan Africa, western	246 894 (188 621 to 305 167)	259 457 (205 791 to 313 124)	12 563 (–33 392 to 58 518)	75 617 (53 967 to 97 267)	78 813 (59 431 to 98 196)	3196 (–15 451 to 21 844)

a All numbers are absolute number of deaths as mean of the probability density function and uncertainty interval in brackets defined as mean ± 1 standard deviation

7.7 Uncertainty

7.7.1 Parameter uncertainty in the health model

To account for parameter uncertainty in stunting model, we used a standard Monte Carlo approach (see also Lloyd et al., 2011). Each parameter was assumed to be distributed either normally or uniformly about its point estimate (for details, see Lloyd et al., 2011). Figure 7.6 shows the histograms proportional to the probability density functions of future stunting for selected regions in the base case.

Figure 7.6 Histograms proportional to probability density functions for the proportion of children estimated to be stunted in 2050 under the base case scenario, for selected regions[a]

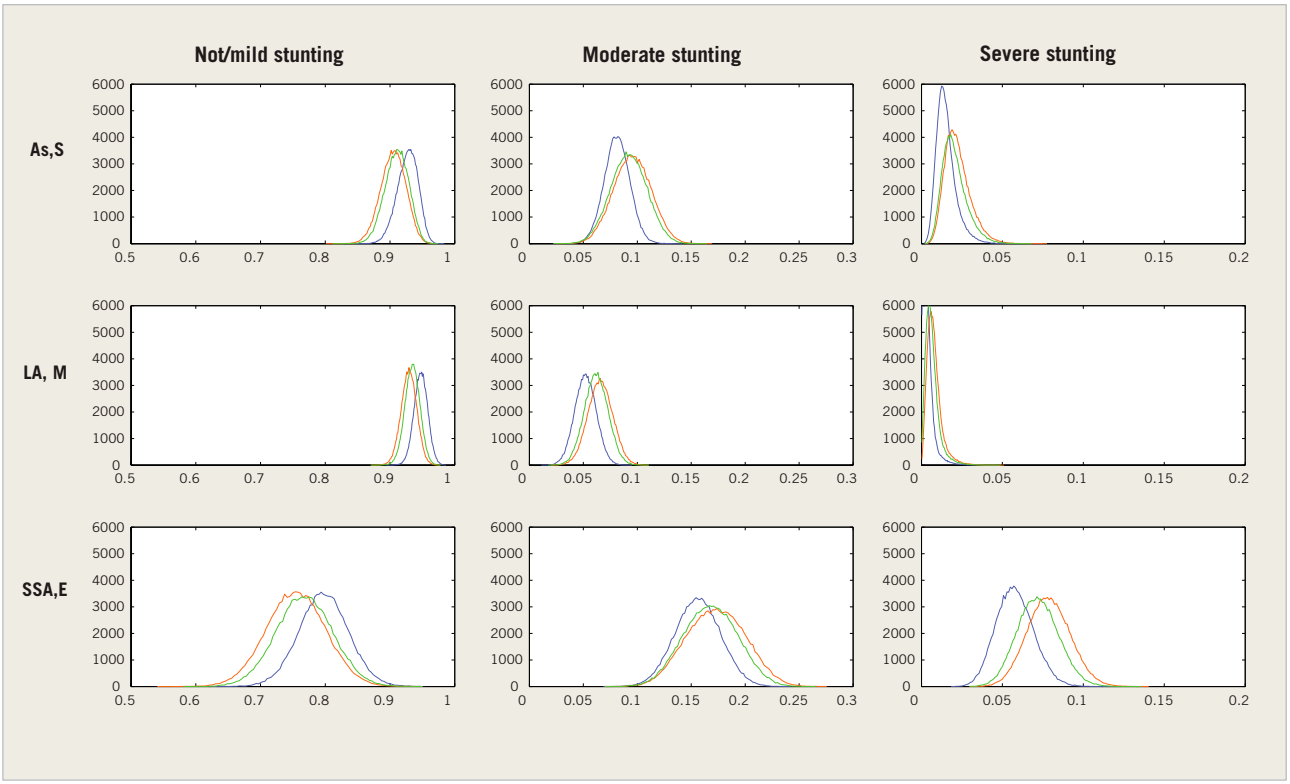

As,S – Asia, south; LA,M – Latin America, mid; SSA,E – sub-Saharan Africa, eastern

[a] Histograms were derived from 100 000 Monte Carlo runs. The *x*-axes show proportion of children stunted at a given level. Note that the *x*-axis scale runs from 0.5 to 1 in column 1, from 0 to 0.3 in column 2, and from 0 to 0.2 in column 3. The *y*-axes show number of estimates. The curves are blue for no climate change, red for MIROC and green for CSIRO

7.7.2 Uncertainty in stunting-attributable death

To estimate stunting-attributable deaths, we required data on the proportion of children stunted and the relative risk of death in moderate and severe stunting (relative to not stunted). For the stunting data, we used the probability density functions for stunting with and without climate change. For the relative risk estimates, we used the odds ratios shown in Table 7.1. Using the mean and standard deviations of the probability density functions for stunting and odds ratios, we estimated the population-attributable fractions using a standard Monte Carlo simulation (100 000 runs).

It was not possible to assess the uncertainty in the upstream models (such as climate, crop and trade models) that drive our model as we lacked the necessary information. This assessment has included two climate scenarios and three health futures.

The large uncertainty is a natural consequence of propagating uncertainties in a chain of models. More important than presenting uncertainty is taking into account the uncertainty of making robust decisions, such as in terms of prioritizing interventions to reduce the impact of climate change on health. This can be done using decision-analytical methods. Calculating uncertainty is a necessary first step to support policy-makers making robust decisions under uncertainty.

7.8 Discussion

Previous studies have shown that climate change is likely to increase future hunger and undernutrition (Rosenzweig & Parry, 1994; Parry et al. 1999, 2004; Nelson et al., 2009, 2010). A previous assessment using the same undernutrition model but under different climate and socioeconomic scenarios estimated that moderate stunting in sub-Saharan Africa and south Asia would increase by 1–29% by 2050, with increases of 23–62% in severe stunting (Lloyd et al., 2011). At the time of writing, no other studies have estimated future mortality attributable to undernutrition as a result of climate change, and therefore a direct comparison cannot be attempted.

According to this assessment, regardless of the future socioeconomic scenario considered, climate change will result in millions more children being stunted. In the base case scenario, our mean estimate suggests an additional 7.5 million children will be stunted by 2030, increasing to an additional 10.1 million by 2050. In the low growth scenario, moderate stunting is estimated to be 4.9 million (mean estimate) lower by 2050 in a future with climate change (compared with a future without climate change), but severe stunting is expected to increase by 8.2 million (mean estimate). This poses a major health risk: moderate stunting has an all-cause mortality odds ratio (compared with not being stunted) of 1.6; the odds ratio for severe stunting is 4.1 (Black et al., 2008). Furthermore, severe stunting brings a higher risk of morbidity (Black et al., 2008) and has a greater impact on future potential, such as education and earning potential (Victora et al., 2008).

In the high growth scenario, climate change is expected to increase severe stunting by 3.1 million in 2030 and 1.4 million in 2050 (mean estimates). This is despite the considerable income growth in this scenario, which (due to assumed accompanying lowering of the non-food risks of stunting such as those related to physical infrastructure and education) lowers the risk of stunting. This scenario assumes that high income growth can be achieved without increasing climate change (that is, the amount of climate change in this scenario is the same as in the base and optimistic scenarios); in other words, it is optimistic in terms of the development of green technology.

Geographically, the areas expected to be most affected (in terms of numbers of children stunted) by climate change are sub-Saharan Africa (with the exception of southern sub-Saharan Africa) and south Asia. That these regions are also expected to have a generally

high burden of disease magnifies the likely impacts of stunting, which acts synergistically with many infectious diseases and increases the risk of some chronic diseases (Black et al., 2008; Victora et al., 2008).

In terms of the proportion of children stunted, regardless of the presence or absence of climate change, economic growth is expected to reduce child stunting. Over time, the proportion of children stunted drops considerably in the high growth scenario; it drops less so, but still considerably, in the base case scenario. In contrast, in the low growth scenario, the proportion of children stunted increases over time. Despite the potential benefits of economic growth, climate change leads to an increase in the proportion stunted in all scenarios.

These results may appear to suggest that high economic growth (as in the high growth scenario) is the optimal pathway to reduce stunting; in our results, stunting in the base case scenario without climate change exceeds stunting in the high growth case with climate change. We caution against such an interpretation for the following reasons. First, the high growth scenario assumes that additional economic growth brings no increase in climate change; this is highly unlikely. In reality, unless there is a rapid advance in the availability and use of green technology, the likely increase in emissions and accompanying climate change will have negative impacts on food production that are not accounted for in this assessment. Second, the undernutrition model we used assumes that the relationship between national income and stunting risk remains constant over time at baseline levels. This relationship has been estimated at a time (currently) when there are vast inequalities between and within countries, and there are many initiatives aimed at improving the situation. These initiatives, from the standpoint of the undernutrition model, aim to change the relationship between national income and stunting risk; that is, although one possible path to reducing stunting is to maximize national income (which may have unforeseen or unconsidered consequences that offset the expected benefits, such as greater climate change), another possible path is to reduce inequalities and improve living conditions.

We estimate that in the base case scenario, climate change-attributable stunting will result in about 95 000 extra child deaths in 2030 and 80 000 extra child deaths in 2050 (mean estimates). This finding is not insignificant, but it is lower than may have been anticipated given that we estimate climate change will result in millions more stunted children in all three socioeconomic scenarios. We believe our estimates should be considered very conservative for the following two reasons. First, the burden of disease projections assume that with time and development, there is a shift away from communicable diseases and towards noncommunicable diseases. The population projections assume the population of children aged under 5 years is declining in all but three countries included in our analysis, despite growth in total population. Considered together, this means over time there are fewer communicable disease deaths in fewer children; this shrinking group is the particular group at risk of stunting associated mortality. Furthermore, stunting in childhood has been associated with a greater risk of noncommunicable diseases and lower economic productivity in adulthood (Victora et al., 2008); this is not accounted for in our model. It is reasonable to expect that an increase in stunting of the magnitude we estimate would lead to an increase in rates of (and death rates due to) noncommunicable disease and reduce national income.

Second, our modelling does not include the impact of shocks; it considers stunting due only to expected average conditions. Climate shocks may occur in the form of acute food production decreases due to extensive and prolonged droughts, or increased food price instability leading to rapid price increases. Relevant shocks need not be related directly to food access; for example, there may be an epidemic of diarrhoea associated with changed temperature regimes. In the face of such shocks, stunting can be considered as a cause of vulnerability: if an already stunted child has a sudden decrease in food access, or a sudden increase in disease risk, then the risk of further morbidity or mortality is considerably higher than in non-stunted children. At the population level, if there are large numbers of already stunted children, then it will be considerably more difficult for a nation to cope with shocks.

Future worlds and scenario data

8

Sari Kovats, Simon Lloyd, Sophie Bonjour, Colin Mathers

8.1 Introduction

This chapter describes in more detail the scenarios used in this global climate change risk assessment. We have used three global climate models to generate five climate scenarios representing one emissions scenario (A1b) (Nakicenovic & Swart, 2000) and three economic futures (base case, low growth, high growth) to describe impacts across a range of plausible futures. An overview of the scenarios is given in Table 8.1.

Table 8.1 Summary of scenarios used in the assessment

Scenario name	Climate data	Population data	Mortality data	GDP data
Base case	A1b	UN 2010 revision, medium variant	Base case	Base case
Low growth	A1b	UN 2010 revision, medium variant	Low growth	Low growth
High growth	A1b	UN 2010 revision, medium variant	High growth	High growth

8.2 Climate data: observed

Observed climate data are used to represent the current climate. This was based on the Climate Research Unit TS 2.1 monthly time series for 1961–1990, which has a spatial resolution of 0.5° × 0.5° (Mitchell & Jones, 2005). We refer to this as baseline climate.

The baseline climate serves two purposes. First, it is used in combination with output from climate models to estimate future climate. The output of the climate models was not used directly. The temperature change (delta) was extracted as the difference between the projected future climate (for example, the 2030s) and the baseline time period (1961–1990), this change in temperature was then added to the observed baseline climate to represent future climate change. Second, the baseline climate is used to represent the future climate in a world without climate change – that is, it is used as the counterfactual climate.

8.3 Climate scenario data

There is much uncertainty about the future climate arising from the possible greenhouse gas emission pathways that society will follow and how a given level of emissions will influence climate. In terms of emissions, the effect of different pathways on global mean temperature is not significant before around 2040; as health impact estimates are made out to 2050, it was agreed to use a single emissions scenario: A1b from the SRES (Nakicenovic & Swart, 2000). The A1 scenario family comprises three groups that describe alternative directions of technological change in the energy system. The groups are distinguished by their technological emphasis: fossil-intensive (A1FI), non-fossil energy sources (A1T), and a balance across all sources (A1B) (where balanced is defined as not relying too heavily on one particular energy source, on the assumption that similar improvement rates apply to all energy supply and end-use technologies). Figure 8.1 shows the emissions trajectory under A1b.

Figure 8.1 A1b emissions trajectory; for comparison, an optimistic mitigation scenario known as E1 is also shown

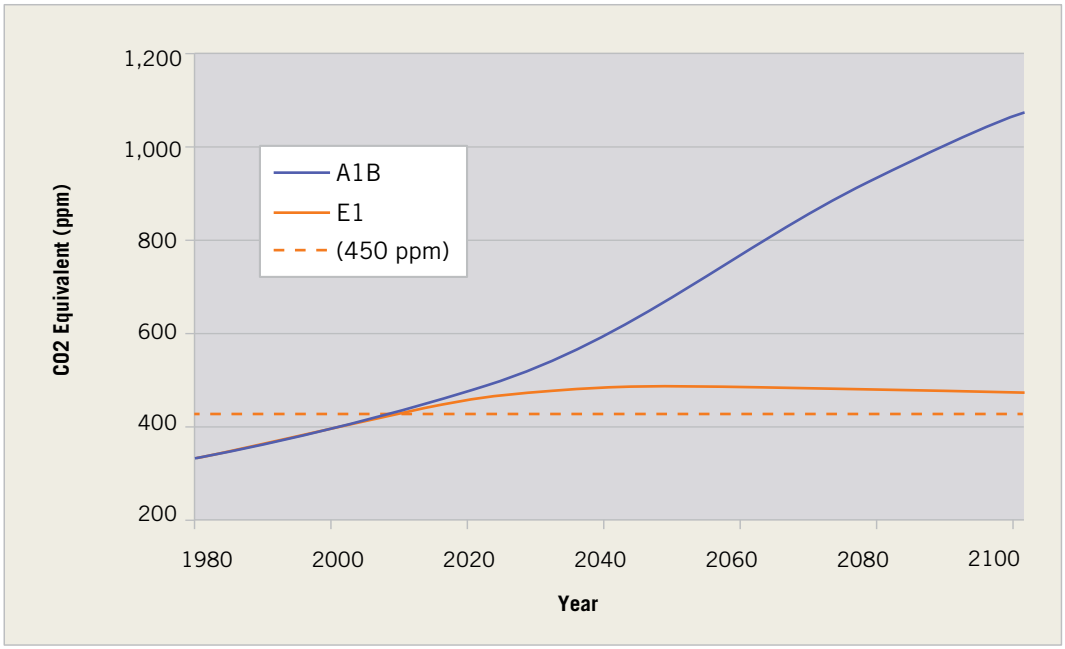

To account for uncertainty in how emissions will affect climate, the outputs of several different climate model runs were used. The model runs used were selected based on the availability of the following variables: temperature, humidity and precipitation. Table 8.2 describes the five climate scenarios used.

Table 8.2 Climate model descriptions for the runs used in this assessment

	BCM	EGMAM	CM4
Modelling centre	Bjerknes Centre for Climate Research, University of Bergen, Norway	Freie Universitaet Berlin, Institute for Meteorology, Berlin, Germany	Institut Pierre Simon Laplace, Paris, France
Model version	BCM 2.0	EGMAM (2006)	IPSL-CM4_v1
Scenarios	20C3M, SRA1B	20C3M, SRA1B	20C3M, SRA1B
Run numbers	1	1, 2, 3	1
Original grid	64 × 128	48 × 96	72 × 96
References	Otterå, OH et al (2009)	Roeckner et al. (1996); Manzini & McFarlane (1998); Legutke & Maier-Reimer (1999)	Marti O et al. (2004)

The climate models used do not share a common spatial grid, with grid resolutions ranging from 48 × 96 to 160 × 320. All runs were therefore regridded (interpolated) to a 1° × 1° global grid (180 × 360). This was carried out using a bilinear interpolation routine, linint2 from the NCAR Command Language package (http://www.ncl.ucar.edu/Document/Functions/Built-in/linint2.shtml). Spherical harmonic-based regridding routines were available but are not advised for bounded parameters such as precipitation. It was felt that the same technique should be used across all parameters, so bilinear interpolation was chosen. Data processing was carried out by Ian Harris at the Climate Research Unit, University of East Anglia. The underlying data were from the ENSEMBLES project (Hewitt, 2004).

New post-SRES emissions scenarios (Representative Concentration Pathways) were developed for the IPCC fifth assessment report, but scenario data for these were not available at the time the estimates in this project were made.

8.4 Population projections

To represent future population totals and patterns, we used the UN 2010 revision, medium variant (UN, 2011). As analysis suggests that fertility and life expectancy are currently higher in many countries than was expected in the UN revisions made immediately before the 2010 revision, and expectations are that these will remain higher than previously anticipated in coming decades, future population totals exceed those made in the years immediately before this revision. The 2010 revision projects that in 2050, the world population will be around 9 billion people and will continue to grow to reach about 10 billion people by 2100 (Figure 8.2).

We have used the above projections as they were the most recent estimates (at the time of this analysis) of the most likely future trends. Totals differ from those used in previous climate change impact assessments for A1 worlds – particularly in the long term – and these differences must be borne in mind when interpreting our health impact estimates. Global total populations in the UN 2010 revision projections compared with IIASA A1 projections are 9.3 billion and 8.7 billion in 2050; 10.0 billion and 8.1 billion in 2080; and 10.1 billion

Figure 8.2 World population projections by year to 2100 for the UN 2010 revision (medium variant) and IIASA A1

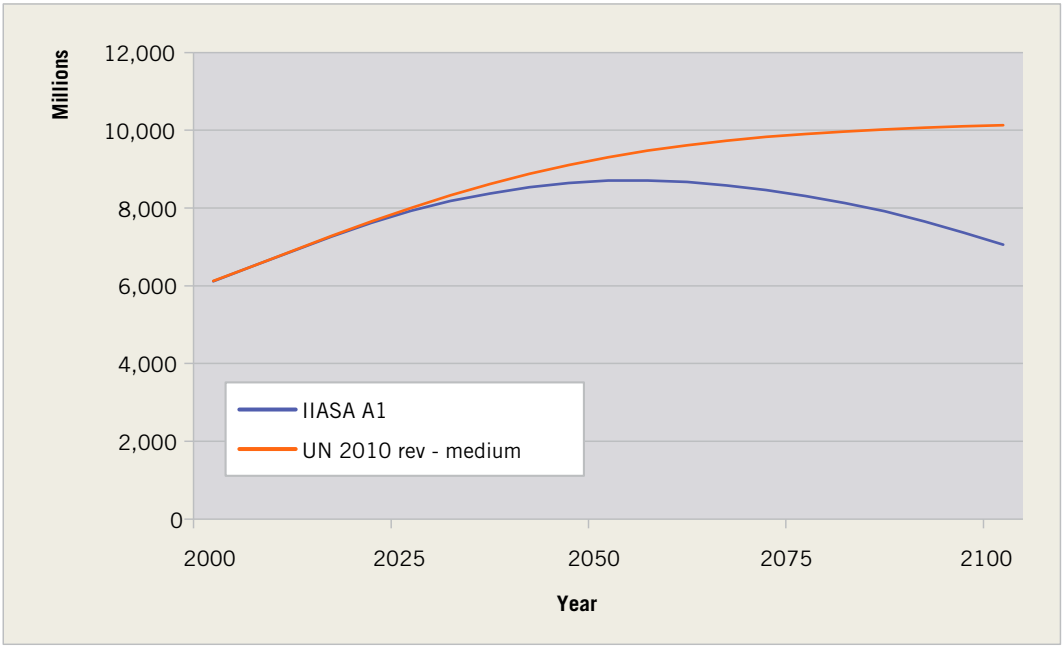

and 7.1 billion in 2100. Previous work has generally coupled A1b emissions with population projections specifically made to accompany these emissions (van Vuuren et al., 2007), and these population projections were in turn based on low variants of the UN population projections from 2003 and 2004, which may, in light of the findings of the UN 2010 revision, be considered out of date.

Figure 8.2 compares the UN 2010, medium variant and one set of A1 population projections produced by IIASA (Grubler et al., 2007), with the A1 population peaking around 2050 and then declining to around 7 billion in 2100.

The implication of using the higher UN (2011) population projections in this assessment than in previous A1-based assessments is that the number of climate change-attributable deaths is likely to be higher. This is because there are more people potentially affected by climate change, and the countries with the highest population growth are, in general, those with high pre-existing disease burdens and thus most vulnerable to the health impacts of climate change.

8.5 GDP data

The GDP data are in 2005 international dollars as purchasing power parity. Three sets of historical estimates and projections were made, drawing on data from sources including the World Bank, International Monetary Fund (IMF), International Futures and the Organisation for Economic Co-operation and Development (OECD) (Table 8.3). Figure 8.3 shows the global level GDP per capita projections for the three scenarios. A high growth set of GDP projections was built based on the GDP country estimates developed for the emission scenario A1b (CIESIN, 2002). A low growth set of GDP projection was constructed in which growth tapers to zero in all countries by 2015.

Table 8.3 Data used in mortality projections[a]

Scenario	Base case	High growth	Low growth
Population	UN (2011)	UNDP (2010); UN (2011)	UNDP (2010); UN (2011)
GDP per capita	World Bank, OECD, IMF, International Futures	SRES A1	Growth from 2010 to 2015 tapers to zero at country level; country-level growth zero from 2015 to 2100
Human capital (average years of schooling at age 25 years)	International Futures base case with some adjustments	As for base scenario	As for base scenario
HIV/AIDS	UN (2010) for 48 countries, UNAIDS extended for others	UNAIDS projections, extended with optimistic trends	As for base scenario
Tuberculosis	Base scenario from previous projections extended to 2080	Base scenario	Base scenario
Malaria	Global Fund to Fight AIDS, Tuberculosis and Malaria scenario 2 (scale up to 147 million bednets per year by 2020)	Global Fund scenario 2 (scale up to 190 million bednets per year by 2020)	Global Fund scenario 2 (scale up to 110 million bednets per year by 2020)
Smoking	Base scenario updated projections (lower than previous projections)	Base scenario	Base scenario
Body mass index	Projections based on estimated trends for 1990–2010 regressed against GDP and time	Base scenario	Base scenario

a Projected changes in GDP/capita and human capital (years of education at age 25 years) and time (as a proxy for technological development) are used to drive the equations for estimating future mortality. In addition, specific assumptions are made when making estimates for HIV/AIDS, tuberculosis, malaria, and outcomes associated with smoking and body mass index

Figure 8.3 Global level GDP per capita for three future worlds

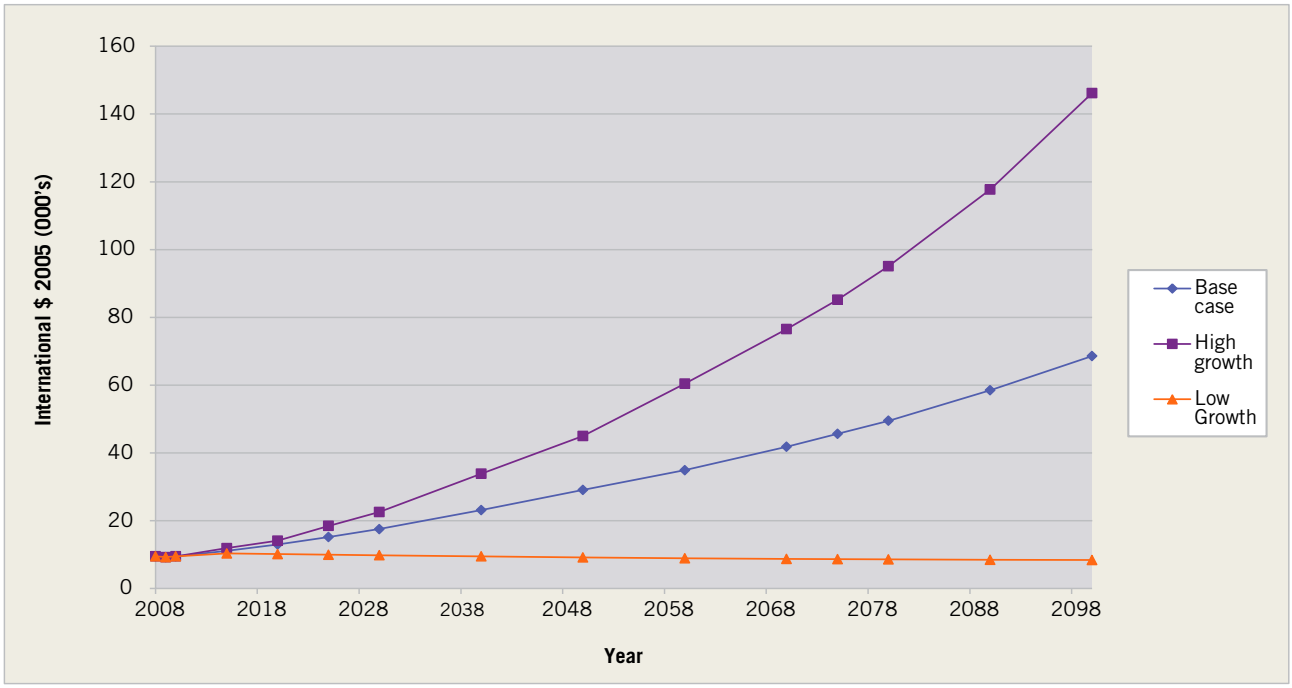

8.6 Mortality projections

The health impacts of climate change will depend on the underlying health of affected populations, which in turn will depend on future socioeconomic conditions. A set of mortality projections was developed for this project. The cause- and age-specific projections for each world region were generated using a regression model and using the assumptions and scenarios described in Table 8.3 (consistent with those used to drive the climate change impact models). The models built upon previous methods (Mathers & Loncar, 2006; WHO, 2008, 2012). The method uses a series of equations that quantify the current and historical relationships between mortality and a set of independent variables. The major independent variables (which were shown to be structurally related to mortality) are GDP per capita, human capital (as years of education at age 25 years), and time, which is assumed to be a proxy for health benefits arising from technological developments. In addition, specific assumptions are made regarding future patterns of HIV/AIDS, tuberculosis and malaria, and for outcomes associated with smoking and body mass index.

These updated projections have been prepared using the WHO cause of death estimates for the year 2008 as a starting point (WHO, 2011a). The methods used are essentially the same as those published previously (Mathers & Loncar, 2006; WHO, 2008, 2012), with the following changes:

- GDP projections were revised to take account of World Bank revisions to purchasing power parity conversion rates and updated using recent projections of real growth per annum in income per capita from the World Bank (2010c,d), IMF (2010) and OECD (2009). Longer-term projections of GDP per capita to the year 2100 were taken from the International Futures project (Hughes, 2010) and converted from base year 2000 to 2005 for purchasing power parity dollars. Country-specific GDP per capita growth rates were varied smoothly from the World Bank and OECD estimates for 2015 to the International Futures estimates for 2030.
- Human capital (average years of schooling for adults) estimates and projections were updated using the latest update of the Barro & Lee (2010) time series and projections from the International Futures project base case (Hughes, 2010).
- The projection regression equations were recalibrated so that back projections of child mortality rates to 1990 matched observed trends for World Bank regions. In the recalibrated projections, the regression coefficient for human capital was left unchanged and the regression coefficient for time (a proxy for technological change) was set to zero for low-income countries in the WHO African, European, South-East Asia and Western Pacific regions.
- Smoking impact projections were updated to take into account more recent regional trends in tobacco smoking (WHO, 2011b).

Figure 8.4 shows the trends in mortality for diseases grouped as communicable diseases (this category includes maternal conditions, perinatal causes, and nutritional deficiencies), noncommunicable diseases and injuries, by age group. Each of the three scenarios is in a separate plot.

Figure 8.4 Trends in mortality for communicable diseases (Comm D), noncommunicable diseases (NCD) and injuries (Inj), by age group, from 2008 to 2080 under (a) base case, (b) low growth and (c) high growth scenarios

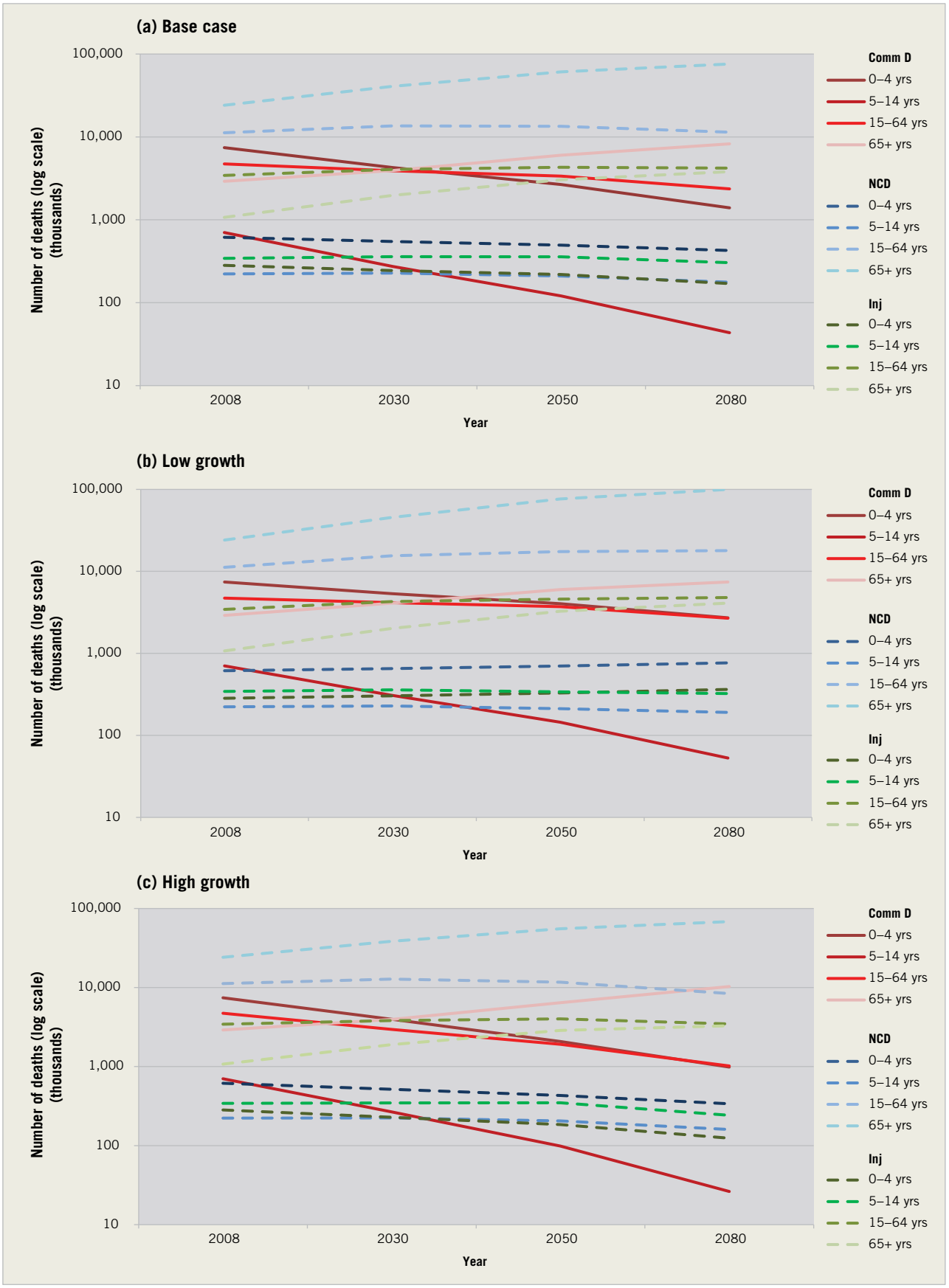

References

9

Ahern M, Kovats RS, Wilkinson P, Few R, Matthies F (2005). Global health impacts of floods: epidemiologic evidence. Epidemiol Rev. 27:36–46.

Araujo MB, Pearson RG, Thuiller W, Erhard M (2005). Validation of species–climate impact models under climate change. Glob Chang Biol. 11:1504–13.

Armstrong B (2006). Models for the relationship between ambient temperature and daily mortality. Epidemiology. 17:624–31.

Åström C, Rocklöv J, Hales S, Béguin A, Louis V, Sauerborn R (2012). Potential distribution of dengue fever under scenarios of climate change and economic development. Ecohealth. 9:448–54.

Baccini M, Biggeri A, Accetta G, Kosatsky T, Katsouyanni K, Analitis A, et al. (2008). Heat effects on mortality in 15 European cities. Epidemiology. 19:711–19.

Bai L, Cirendunzhu D, Woodward A, Dawa D, Xiraoruodeng D, Liu Q (2014). Temperature and mortality on the roof of the world: a time-series analysis in three Tibetan counties, China. Sci Total Environ. 485–6:41–8.

Barnett AG, Hajat S, Gasparrini A, Rocklöv J (2012). Cold and heat waves in the United States. Environ Res. 112:218–24.

Barro RJ, Lee J-W (2010). International data on educational attainment. Cambridge, MA: Centre for International Development at Harvard University.

Bartram J, Cairncross S (2010). Hygiene, sanitation, and water: forgotten foundations of health. PLoS Med. 7:e1000367.

Béguin A, Hales S, Rocklöv J, Angstrom C, Louis V, Sauerborn R (2011). The opposing effects of climate change and socio-economic development on the global distribution of malaria. Glob Environ Chang. 21: 1209–14.

Bell ML, O'Neill MS, Ranjit N, Borja-Aburto VH, Cifuentes L, Gouveia N (2008). Vulnerability to heat-related mortality in Latin America: a case-crossover study in Sao Paolo, Brazil, Santiago, Chile, and Mexico City, Mexico. Int J Epidemiol. 37:796–804.

Bhaskaran K, Gasparrini A, Hajat S, Smeeth L, Armstrong B (2013). Time series regression studies in environmental epidemiology. Int J Epidemiol. 42:1187–95.

Bhatt S, Gething PW, Brady OJ, Messina JP, Farlow AW, Moyes CL, et al. (2013). The global distribution and burden of dengue. Nature. 496:504–7.

Black RE, Morris S, Bryce J (2003). Where and why are 10 million children dying every year? Lancet. 361:2226–34.

Black RE, Allen LH, Bhutta ZA, Caulfield LE, de Onis M, Ezzati M, et al. (2008). Maternal and child undernutrition: global and regional exposures and health consequences. Lancet. 371:243–60.

Black RE, Victora CG, Walker SP, Bhutta ZA, Christian P, de Onis Met al. (2013). Maternal and child undernutrition and overweight in low-income and middle-income countries. Lancet. 382;427–51.

Bouwman AF, Kram T, Klein Goldewijk K (2006). Integrated modelling of global environmental change: an overview of IMAGE 2.4. The Hague: Netherlands Environmental Assessment Agency.

Brady OJ, Gething PW, Bhatt S, Messina JP, Brownstein JS, Hoen AG, et al. (2012). Refining the global spatial limits of dengue virus transmission by evidence-based consensus. PLoS Negl Trop Dis. 6:e1760.

Brown S, Nicholls RJ, Vafeidis A, Hinkel J, Watkiss P (2011). The impacts and economic costs of sea-level rise in Europe and the costs and benefits of adaptation. Summary of results from the EC RTD Climate Cost project. In: Watkiss P, editor. The Climate Cost project: final report. Vol. 1: Europe. Stockholm: Stockholm Environment Institute.

Brown S, Nicholls RJ, Lowe JA, Hinkel J (2013). Spatial variations of sea-level rise and impacts: an application of DIVA. Clim Chang. 1–14. DOI: 10.1007/s10584–013–0925-y.

Caminade C, Kovats S, Rocklöv J, Tompkins AM, Morse AP, Colón-González F et al. (2014). Impact of climate change on global malaria distribution. Proc Natl Acad Sci U S A. 111:3286–91.

Campbell-Lendrum D, Woodruff R (2006). Comparative risk assessment of the burden of disease from climate change. Environ Health Persp. 114:1935.

Campbell-Lendrum D, Corvalan CF, Neira M (2007). Global climate change: implications for international public health policy. Bull World Health Organ. 85:235–7.

Chaves LF, Koenraadt CJ (2010). Climate change and highland malaria: fresh air for a hot debate. Q Rev Biol. 85:27–55.

Checkley W, Epstein LD, Gilman RH, Figueroa D, Cama R, Patz JA, et al. (2000). Effects of El Nino and ambient temperature on hospital admissions for diarrhoeal diseases in Peruvian children. Lancet. 355:442–50.

Checkley W, Buckley G, Gilman RH, Assis AM, Guerrant RL, Morris SS, et al. (2008). Multi-country analysis of the effects of diarrhoea on childhood stunting. Int J Epidemiol. 37:816–30.

Chou W-C, Wu J-L, Wanf Y-C, Huang H, Sung F-C, Chuang C-Y (2010). Modeling the impact of climate variability on diarrhea-associated diseases in Taiwan (1996–2007). Sci Total Environ. 409:43–51.

Church JA, Clark PU, Cazenave A, Gregory JM, Jevrejeva S, Levermann A, et al. (2013). Sea level change. In: Stocker TF, Qin D, Plattner G-K, Tignor M, Allen SK, Boschung J, et al., editors. Climate change 2013: the physical science basis. Contribution of working group I to the fifth assessment report of the Intergovernmental Panel on Climate Change. Cambridge and New York: Cambridge University Press.

CIESIN (2002). Country-level GDP and downscaled projections based on the A1, A2, B1, and B2 marker scenarios, 1990–2100. Palisades, NY: Center for International Earth Science Information Network.

Collier P (2007). Poverty reduction in Africa. Proc Natl Acad Sci U S A. 104:16 763–8.

Costello A, Abbas M, Allen A, Ball S, Bell S, Bellamy R, et al. (2009). Managing the health effects of climate change. Lancet. 373:1693–733.

CRED (2011). EM-DAT: the International Disaster Database. Louvain: Centre for Research on the Epidemiology of Disasters (http://www.emdat.be/).

Curriero F, Heiner KS, Samet J, Zeger S, Strug L, Patz JA (2002). Temperature and mortality in 11 cities of the Eastern United States. Am J Epidemiol. 155:80–87.

Dar OA, Khan MS (2011). Millennium development goals and the water target: details, definitions and debate. Trop Med Int Health. 16:540–544.

Dasgupta S, Laplante B, Murray S, Wheeler D (2009). Climate change and the future impacts of storm-surge disasters in developing countries. Washington, DC: Centre for Global Development.

De Haen H, Hemrich G (2007). The economics of natural disasters: implications and challenges for food security. Agric Econ. 37:31–45.

D'Souza RM, Becker N, Hall G, Moodie KB (2004). Does ambient temperature affect foodborne disease? Epidemiology. 15:86–92.

Ebi KL (2008). Adaptation costs for climate change-related cases of diarrhoeal disease, malnutrition, and malaria in 2030. Global Health. 4:9.

Ebi KL, Hartman J, Chan N, Mcconnell J, Schlesinger M, Weyant J (2005). Climate suitability for stable malaria transmission in Zimbabwe under different climate change scenarios. Clim Change. 73:375–93.

Egondi T, Kyobutungi C, Kovats S, Muindi K, Ettarh R, Rocklöv J (2012). Time-series analysis of weather and mortality patterns in Nairobi's informal settlements. Glob Health Action. 5:23–32.

Emanuel K (2005). Increasing destructiveness of tropical cyclones over the past 30 years. Nature. 436:686–8.

ESRL (1996). NCEP/NCAR reanalysis 1: summary. Boulder, CO: Physical Sciences Division, Earth System Research Laboratory (http://www.esrl.noaa.gov/psd/data/gridded/data.ncep.reanalysis.html).

Ezzati M, Lopez AD, Rodgers A, Vander Hoorn S, Murray CJL, Comparative Risk Assessment Collaborating Group (2002). Selected major risk factors and global and regional burden of disease. Lancet. 360:1347–60.

FAO (1996). The sixth world food survey. Rome: Food and Agriculture Organization of the United Nations.

FAO (2003). FAO methodology for the measurement of food deprivation. Rome: Food and Agriculture Organization of the United Nations.

FAO (2009). State of food insecurity in the world: economic crises – impacts and lessons learned. Rome: Food and Agriculture Organization of the United Nations.

FAO (2010). FAOSTAT. Rome: Food and Agriculture Organization of the United Nations (http://faostat.fao.org/).

FAO (2011). State of food insecurity in the world, 2011. Rome: Food and Agriculture Organization of the United Nations.

Fewtrell L, Kay D (2008). An attempt to quantify the health impacts of flooding in the UK using an urban case study. Publ Health. 122:446–51.

Fritz HM, Blount CD, Thwin S, Thu MK, Chan N (2009). Cyclone Nargis storm surge in Myanmar. Nat Geosci. 2:448–9.

Gallup JL, Sachs JD (2004). The economic burden of malaria. Am J Trop Hyg Med. 64:85–96.

Gasparrini A, Armstrong B, Kenward MG (2010). Distributed lag non linear models. Stat Med. 29:2224–34.

Gasparrini A, Armstrong B, Kovats RS, Wilkinson P (2012). The effect of high temperatures on cause-specific mortality in England and Wales. Occupat Environ Med. 69:56–61.

Gerbens-Leenes W, Hoekstra AY, Meer THVD (2009). The water footprint of bioenergy. Proc Natl Acad Sci U S A. 106:10 219–23.

Gething PW, Smith DL, Patil AP, Tatem AJ, Snow RW, Hay SI (2010). Climate change and the global malaria recession. Nature. 465:342–5.

Gibbons RV, Vaughn DW (2002). Dengue: an escalating problem. BMJ. 324:1563–6.

Gornall J, Betts R, Burke E, Clark R, Camp J, Willett K et al. (2010). Implications of climate change for agricultural productivity in the early twenty-first century. Philos Trans R Soc Lond B Biol Sci. 365:2973–89.

Grubler A, O'Neill B, Riahi K, Chirkov V, Goujon A, Kolp P, et al. (2007). Regional, national and spatially explicit scenarios of demographic and economic change based on SRES. Technol Forecast Soc Change. 74:980–1029.

Gubler DJ (2002). The global emergence/resurgence of arboviral diseases as public health problems. Arch Med Res. 33:330–42.

Gubler DJ (2003). *Aedes albopictus* in Africa. Lancet Infect Dis. 3:751–2.

Gubler DJ, Reiter P, Ebi KL, Yap W, Nasci R, Patz JA (2001). Climate variability and change in the United States: potential impacts on vector- and rodent-borne diseases. Environ Health Perspect. 109(Suppl 2):223–33.

Guerrant RL, Oria RB, Moore SR, Oria MO, Lima AA (2008). Malnutrition as an enteric infectious disease with long-term effects on child development. Nutr Rev. 66:487–505.

Hajat S, Kosatky T (2010). Heat-related mortality: a review and exploration of heterogeneity. J Epidemiol Commun Health. 64:753–60.

Hales S, de Wet N, Maindonald J, Woodward A (2002). Potential effect of population and climate changes on global distribution of dengue fever: an empirical model. Lancet. 360:830–34.

Hashizume M, Armstrong B, Hajat S, Wagatsuma Y, Faruque ASG, Hayashi T, Sack DA (2007). Association between climate variability and hospital visits for non-cholera diarrhoea in Bangladesh: effects and vulnerable groups. Int J Epidemiol. 36:1030–37.

Hay B, Hay S, Marsh K (2006). Population at malaria risk in Africa 2005, 2015 and 2030. Foresight report series. London: Government Office for Science.

Hay SI, Guerra CA, Gething PW, Patil AP, Tatem AJ, Noor AM, et al. (2009). A world malaria map: *Plasmodium falciparum* endemicity in 2007. PLoS Med. 6:e1000048.

Hewitt CD (2004). ENSEMBLES-based predictions of climate changes and their impacts. Eos Trans Am Geophys Union. 85:566.

Hii YL, Rocklöv J, Ng N, Tang CS, Pang FY, Sauerborn R (2009). Climate variability and increase in intensity and magnitude of dengue incidence in Singapore. Glob Health Action. 2.

Hijmans R, Cameron S, Parra J, Jones P, Jarvis A (2005). Very high resolution interpolated climate surfaces for global land areas. Int J Climatol. 25:1965–78.

Hinkel J, Klein RJ (2009). Integrating knowledge to assess coastal vulnerability to sea-level rise: the development of the DIVA tool. Glob Environ Change. 19:384–95.

Honda Y, Ono M, Uchiyama I (2000). Humidity does not confound temperature-mortality relationship in Japan. Jpn J Biometeorol. 37:113–18.

Honda Y, Ono M, Kabuto M (2006). Do we adapt to a new climate as the globe warms? Epidemiology. 17:S204.

Honda Y, Kabuto M, Ono M, Uchiyama I (2007). Determination of optimum daily maximum temperature using climate data. Environ Health Prevent Med. 25:209–16.

Honda Y, Kondo M, McGregor G, Kim H, Guo YL, Hijioka Y, et al. (2014). Heat-related mortality risk model for climate change impact projection. Environ Health Prev Med. 19:56–63.

Howard G, Charles K (2010). Securing 2020 vision for 2030: climate change and ensuring resilience in water and sanitation services. J Water Clim Change. 1:2–16.

Huang C, Barnett AG, Wang X, Vaneckova P, Fitzgerald G, Tong S (2011). Projecting future heat-related mortality under climate change scenarios: a systematic review. Environ Health Perspect, 119:1681–90.

Hughes B (2010). The International Futures (IFs) modeling system, version 6.32. Denver, CO: Frederick S. Pardee Center for International Futures, Josef Korbel School of International Studies, University of Denver.

IHME (2010). Global burden of disease study: operations manual 2009. Seattle, WA: Institute for Health Metrics Evaluation.

IHME (2013). GBD arrow diagram. Seattle, WA: Institute for Health Metrics and Evaluation (http://vizhub.healthdata.org/irank/arrow.php).

IIASA (2009). GGI Scenario Database, version 2.0. Laxenburg, Austria: International Institute for Applied Systems Analysis.

IMF (2010). World economic outlook 2009 (update 2010). Washington, DC: International Monetary Fund.

Iniguez C, Ballester F, Ferrandiz J, Perez-Hoyos S, Saez M, Lopez A (2010). Relation between temperature and mortality in thirteen Spanish cities. Int J Environ Res Publ Health. 7:3196–210.

IPCC (2012) Managing the Risks of Extreme Events and Disasters to Advance Climate Change Adaptation. A Special Report of Working Groups I and II of the Intergovernmental Panel on Climate Change [Field, C.B., V. Barros, T.F. Stocker, D. Qin, D.J. Dokken, K.L. Ebi, M.D. Mastrandrea, K.J. Mach, G.-K. Plattner, S.K. Allen, M. Tignor, and P.M. Midgley (eds.)]. Cambridge University Press, Cambridge, UK, and New York, NY, USA, 582 pp.

IPCC (2013). Summary for policymakers. In: Stocker TF, Qin D, Plattner G-K, Tignor M, Allen SK, Boschung J, et al., editors. Climate Change 2013: The Physical Science Basis. Contribution of working group I to the fifth assessment report of the Intergovernmental Panel on Climate Change. Cambridge and New York: Cambridge University Press.

Ishigami A, Hajat S, Kovats RS, Bisanti L, Rognoni M, Paldy A (2008). An ecological time-series study of heat-related mortality in three European cities. Environ Health. 7:5.

Jepson WF, Moutia A, Courtois C (1947). The malaria problem in Mauritius: the bionomics of Mauritian anophelines. Bull Entomol Res. 38:177–208.

Johansson MA, Cummings DA, Glass GE (2009). Multiyear climate variability and dengue: El Nino southern oscillation, weather, and dengue incidence in Puerto Rico, Mexico, and Thailand – a longitudinal data analysis. PLoS Med. 6:e1000168.

Jones JW, Hoogenboom G, Porter CH, Boote KJ, Batchelor WD, Hunt LA, et al. (2003). The DSSAT cropping system model. Eur J Agron. 18:235–65.

Jonkman SN (2005). Global perspectives on loss of human life caused by floods. Nat Hazards. 342:151–75.

Jonkman SN, Vrijling JK, Vrouwenvelder ACWM (2008). Methods for the estimation of loss of life due to floods: a literature review and a proposal for a new method. Nat Hazards. 46:353–89.

Kellenberg DK, Mobarak AM (2008). Does rising income increase or decrease damage risk from natural disasters? J Urban Econ. 63:1315–37.

Kinney PL, O'Neill MS, Bell ML, Schwartz J (2008). Approaches for estimating effects of climate change on heat-related deaths: challenges and opportunities. Environ Sci Policy. 11:87–96.

Knabb RD, Rhome JR, Brown DP (2006). Tropical cyclone report: Hurricane Katrina, 23–30 August 2005. Miami, FL: National Hurricane Centre.

Koenig WD (1999). Spatial autocorrelation of ecological phenomena. Trends Ecol Evol. 14:22–6.

Koenraadt CJ, Githeko AK, Takken W (2004). The effects of rainfall and evapotranspiration on the temporal dynamics of *Anopheles gambiae* s.s. and *Anopheles arabiensis* in a Kenyan village. Acta Trop. 90:141–53.

Kolstad EW, Johansson KA (2011). Uncertainties associated with quantifying climate change impacts on human health: a case study for diarrhea. Environ Health Persp. 119:299–305.

Kovats RS, Hajat S (2008). Heat stress and public health: a critical review. Annu Rev Publ Health. 29:41–55.

Kovats RS, Edwards S, Hajat S, Armstrong B, Ebi KL, Menne B (2004). The effect of temperature on food poisoning: time series analysis in 10 European countries. Epidemiol Infect. 132:443–53.

Lama JR, Seas C, Leon-Barua R, Gotuzzo E, Sack RB (2004). Environmental temperature, cholera, and acute diarrhoea in adults in Lima, Peru. J Health Popul Nutr. 22:399–403.

Lambrechts L, Scott TW, Gubler DJ (2010). Consequences of the expanding global distribution of *Aedes albopictus* for dengue virus transmission. PLoS Negl Trop Dis. 4:e646.

Legutke S, Maier-Reimer E (1999). Climatology of the HOPE-G Global Ocean General Circulation Model. Technical report 21. Hamburg: German Climate Computing Centre.

Lim SS, Vos T, Flaxman AD, Danaei G, Shibuya K, Adair-Rohani H, et al. (2012). A comparative risk assessment of burden of disease and injury attributable to 67 risk factors and risk factor clusters in 21 regions, 1990–2010: a systematic analysis for the Global Burden of Disease Study 2010. Lancet. 380;2224–60.

Lindsay SW, Martens WJ (1998). Malaria in the African highlands: past, present and future. Bull World Health Organ. 76:33–45.

Liu-Helmersson J, Stenlund H, Wilder-Smith A, Rocklöv J (2014). Vectorial capacity of *Aedes aegypti*: effects of temperature and implications for global dengue epidemic potential. PLoS One. 9:e89783.

Lloyd S, Kovats RS, Armstrong B (2007). Global cross-sectional study of the association between diarrhoea morbidity, weather and climate. Clim Res. 34:119–27.

Lloyd S, Kovats RS, Chalabi Z (2011). Climate change, crop yields, and malnutrition: development of a model to quantify the impact of climate scenarios on child malnutrition. Environ Health Persp. 119:1817–23.

Lloyd SJ, Kovats RS, Chalabi Z, Brown S, Nicholls RJ (2014). Modelling the influences of climate change-associated sea-level rise and socioeconomic development on future storm surge mortality (under review).

Louis VR, Gillespie IA, O'Brien S, Russek-Cohen E, Pearson AD, Colwell R (2005). Temperature-driven Campylobacter seasonality in England and Wales. Appl Environ Microbiol. 71:85–92.

Lowe JA, Hewitt CD, van Vuuren DP, Johns TC, Stehfest E, Royer JF, van der Linden PJ (2009). New study for climate modeling, analyses, and scenarios. Eos Trans Am Geophys Union. 90:181–2.

Maaskant B, Jonkman SN, Bouwer LM (2009). Future risk of flooding: an analysis of changes in potential loss of life in South Holland (the Netherlands). Environ Sci Policy. 12:157–69.

Macdonald G (1953). The analysis of malaria epidemics. Trop Dis Bull. 50:871–89.

Manzini E, McFarlane NA (1998). The effect of varying the source spectrum of a gravity wave parameterization in a middle atmosphere general circulation model. J Geophys Res. 103:31 523–39.

Margulis S, Narain U, Chinowsky P, Cretegny G, Hughes G, Kirshen P, et al. (2010). Cost to developing countries of adapting to climate change: new methods and estimates. Washington, DC: World Bank.

Marti O, Braconnot P, Bellier J, Benshila R, Bony S, Brockmann P, et al. (2004) The new IPSL climate system model: IPSL-CM4. Note du pôle de modélisation. No. 26. Paris: Institut Pierre Simon Laplace.

Mathers CD, Loncar D (2006). Projections of global mortality and burden of disease from 2002 to 2030. PLoS Med. 3:2011–30.

McGranahan G, Balk D, Anderson B (2007). The rising tide: assessing the risks of climate change and human settlements in low elevation coastal zones. Environ Urban 19:17–37.

McMichael AJ (1999). Prisoners of the proximate: loosening the constraints on epidemiology in an age of change. Am J Epidemiol. 149:887–97.

McMichael AJ (2013). Impediments to comprehensive research on climate change and health. Int J Environ Res Public Health. 10:6096–105.

McMichael AJ, Campbell-Lendrum D, Kovats RS, Edwards S, Wilkinson P, Edmonds N, et al. (2004). Climate change. In: Ezzati M, Lopez AD, Rodgers A, Murray CJ, editors. Comparative quantification of health risks: global and regional burden of disease due to selected major risk factors. Vol. 2. Geneva: World Health Organization.

McMichael AJ, Wilkinson P, Kovats RS, Pattenden S, Hajat S, Armstrong B, et al. (2008). International study of temperature, heat and urban mortality: the "Isothurm" project. Int J Epidemiol. 37:1121–31.

Meehl GA, Stocker TF, Collins WD, Friedlingstein P, Gaye AT, Gregory JM, et al. (2007). Global climate projections. In: Solomon S, Qin D, Manning M, editors. Climate change 2007: the physical science basis. Contribution of working group I to the fourth assessment report of the Intergovernmental Panel on Climate Change. Cambridge: Cambridge University Press.

Millennium Ecosystem Assessment (2005). Ecosystems and human well-being. Vol II: scenarios. Washington, DC: Island Press.

Mitchell TD, Jones PD (2005). An improved method of constructing a database of monthly climate observations and associated high-resolution grids. Int J Climatol. 25:693–712.

Nakicenovic N, Swart R, editors (2000). IPCC Special Report on Emission Scenarios (SRES). Cambridge: Cambridge University Press.

Nelson G, Rosegrant MW, Koo J, Robertson R, Sulser T, Zhu T, et al. (2009). Climate change: impact on agriculture and costs of adaptation. Washington, DC: International Food Policy Research Institution.

Nelson G, Rosegrant M, Palazzo P, Gray I, Ingersoll C, Robertson R, et al. (2010). Food security, farming, and climate change to 2050. Washington, DC: International Food Policy Research Institution.

Ngo-Duc T, Polcher J, Laval K (2005). A 53-year forcing data set for land surface models. J Geophys Res. 110:27.

Nicholls RJ, Wong PP, Burkett VR, Codignotto JE, Hay JE, McLean RF, et al. (2007). Coastal systems and low-lying areas. In: Parry ML, Canziani OF, Palutikof JP, van der Linden PJ, Hansen CE, editors. Climate change 2007: impacts, adaptation and vulnerability. Contribution of working group II to the fourth assessment report of the Intergovernmental Panel on Climate Change. Cambridge: Cambridge University Press.

NOAA (2013). Storm Surge OverviewMiami, FL: NOAA/National Weather Service, National Hurricane Centre (2013)(http://www.nhc.noaa.gov/surge/).

Noor AM, Mutheu JJ, Tatem AJ, Hay SI, Snow RW (2009). Insecticide-treated net coverage in Africa: mapping progress in 2000–07. Lancet. 373:58–67.

OECD (2009). Economic outlook number 85. Paris: Organisation for Economic Co-operation and Development.

O'Neill MS, Zanobetti A, Schwartz J (2003). Modifiers of the temperature and mortality association in seven US cities. Am J Epidemiol. 157:1074–82.

Onozuka D, Hashizume M, Hagihara A (2010). Effects of weather variability on infectious gastroenteritis. Epidemiol Infect. 138:236–43.

Otterå OH, Bentsen M, Bethke I, Kvamstø NG (2009): Simulated pre-industrial climate in Bergen climate model (version 2): model description and large-scale circulation features, Geosci. Model Dev. 2; 197–212.

Pardaens AK, Lowe JA, Brown S, Nicholls RJ, Gusmão D (2011). Sea-level rise and impacts projections under a future scenario with large greenhouse gas emission. Geophys Res Lett. 38:L12 604–5.

Parry, ML, Rosenzweig, C, Iglesias, A, Fischer, G, Livermore, M (1999). Climate change and world food security: a new assessment. Glob Env Chang. 9;S51–6.

Parry ML, Rosenzweig C, Iglesias A, Livermore M, Fischer G (2004). Effects of climate change on global food production under SRES emissions and socioeconomic scenarios. Glob Environ Chang. 14:53–67.

Patt AG, Tadross M, Nussbaumer P, Asante K, Metzger M, Rafael J, et al. (2010). Estimating least-developed countries' vulnerability to climate-related extreme events over the next 50 years. Proc Natl Acad Sci U S A. 107:1333–7.

Patz JA, Martens WJ, Focks DA, Jetten TH (1998). Dengue fever epidemic potential as projected by general circulation models of global climate change. Environ Health Perspect. 106:147–53.

Patz JA, Hulme M, Rosenzweig C, Mitchell TD, Goldberg RA, Githeko AK, et al. (2002). Climate change: regional warming and malaria resurgence. Nature. 420:627–8.

Peduzzi P, Chatenoux B, Dao H, de Bono A, Herold C, Kossin J, et al. (2012). Global trends in tropical cyclone risk. Nat Clim Change. 2:289–94.

Peltier WR (2000a). Global glacial isostatic adjustment and modern instrumental records of relative sea level history. In: Douglas BC, Kearny MS, Leatherman SP, editors. Sea level rise: history and consequences. San Diego, CA: Academic Press.

Peltier WR (2000b). ICE4G (VM2) glacial isostatic adjustment corrections. In: Douglas BC, Kearny MS, Leatherman SP, editors. Sea level rise: history and consequences. San Diego, CA: Academic Press.

Penning-Roswell E, Floyd P, Ramsbottom D, Surendran S (2005). Estimating injury and loss of life in floods: a deterministic framework. Nat Hazards. 36:43–64.

Pruss-Ustun A, Corvalan C (2006). Preventing disease through healthy environments: towards an estimate of the environmental burden of disease. Geneva: World Health Organization.

Ramsdorf S (2010). Has the IPCC underestimated the risk of sea level rise? Nat Clim Change. 4:44–5.

R Development Core Team (2010). R: a language and environment for statistical computing. Vienna: R Foundation for Statistical Computing.

Refaeilzadeh P, Tang L, Liu H (2009). Cross validation. In: Özsu T, Liu L, editors. Encyclopedia of database systems. New York: Springer.

Rocklöv J, Ebi K, Forsberg B (2011). Mortality related to temperature and persistent extreme temperatures: a study of cause-specific and age-stratified mortality. Occup Environ Med. 68:531–6.

Roeckner E, Arpe K, Bengtsson L, Christoph M, Claussen M, Dümenil L, et al. (1996). The atmospheric general circulation model ECHAM4. MPI report no. 218. Hamburg: Max Planck Institute for Meteorology.

Rogers DJ, Randolph SE (2000). The global spread of malaria in a future, warmer world. Science. 289:1763–5.

Rogot E, Sorlie PD, Backlund E (1992). Air-conditioning and mortality in hot weather. Am J Epidemiol. 136:106–16.

Rosegrant MW, Ringler C, Msangi S, Sulser TB, Zhu T, Cline SA (2008). International Model for Policy Analysis of Agricultural Commodities and Trade (IMPACT): model description. Washington, DC: International Food Policy Research Institution.

Rosegrant MW, Ringler C, Zhu T (2009). Water for agriculture: maintaining food security under growing scarcity. Ann Rev Environ Resour. 34:205–22.

Rosenzweig, C, Parry, ML (1994). Potential impact of climate change on world food supply. Nature. 367;133–8.

Russell R, Currie B, Lindsay M, Mackenzie J, Ritchie S, Whelan P (2009). Dengue and climate change in Australia: predictions for the future should incorporate knowledge from the past. Med J Aust. 190:265–8.

Sachs JD, Malaney P (2002). The economic and social burden of malaria. Nature. 415:680–85.

Schifano P, Leone M, de Sario M, de'Donato F, Bargagli A, d'Ippoliti D, et al. (2012). Changes in the effects of heat on mortality among the elderly from 1998–2010: results from a multicenter time series study in Italy. Environ Health. 11:58.

Schmidhuber J, Tubiello FN (2007). Global food security under climate change. Proc Natl Acad Sci USA. 104:19 703–8.

Shultz JM, Russell J, Espinel Z (2005). Epidemiology of tropical cyclones: the dynamics of disaster, disease, and development. Epidemiol Rev. 27:21–35.

Silva HR, Phelan PE, Golden JS (2010). Modeling effects of urban heat island mitigation strategies on heat-related morbidity: a case study for Phoenix, Arizona, USA. Int J Biometeorol. 54:13–22.

Singh RBK, Hales S, Dewet N, Raj R, Hearnden M, Weinstein P (2001). The influence of climate variation and change on diarrhoeal disease in the pacific islands. Environ Health Persp. 109:155–9.

Smith L, Haddad L (2000). Explaining child malnutrition in developing countries: a cross-country analysis, Washington DC: International Food Policy Research Institution.

Smith K, Woodward A, Campbell-Lendrum D, Chadee D, Honda Y, Liu Q, et al. (2014). Human health: impacts, adaptation, and co-benefits. In: Field CB, Barros V, Dokken D, editors. Climate change 2014: impacts, adaptation, and vulnerability. Vol i: global and sectoral aspects. Contribution of working group II to the fifth assessment report of the Intergovernmental Panel on Climate Change. Cambridge: Cambridge University Press.

Sung T-I, Wu P-C, Lung S-C, Lin C-Y, Chen M-J, Su H-J (2013). Relationship between heat index and mortality of 6 major cities in Taiwan. Sci Total Environ. 442:275–81.

Svedberg P (2002). Undernutrition overestimated. Econ Dev Cult Change. 51:5–36.

Takahashi K, Honda Y, Emori S. Assessing mortality risk from heat stress due to global warming. J Risk Res. 10:339–54.

Tam CC, Rodrigues LC, O'Brien S, Hajat S (2006). Temperature dependence of reported *Campylobacter* infection in England, 1989–1999. Epidemiol Infect. 134:119–25.

Tanser FC, Sharp B, le Sueur D (2003). Potential effect of climate change on malaria transmission in Africa. Lancet. 362:1792–8.

Tatem AJ, Rogers DJ, Hay SI (2006). Global transport networks and infectious disease spread. Adv Parasitol. 62:293–343.

Thomson MC, Doblas-Reyes FJ, Mason SJ, Hagedorn R, Connor SJ, Phindela T, et al. (2006). Malaria early warnings based on seasonal climate forecasts from multi-model ensembles. Nature. 439:576–9.

UN (2010). The millennium development goals report 2010. New York: United Nations.

UN (2011). World population prospects: the 2010 revision. New York: United Nations (http://esa.un.org/unpd/wpp/index.htm).

UNDP (2010). The human development index. New York: United Nations Development Programme (http://hdr.undp.org/en/statistics/hdi/).

UNICEF (1990). Strategy for the improvement of nutrition in children and women in developing countries. New York: United Nations Children's Fund.

UNISDR (2011). GAR 2011: revealing risk, redefining development. Geneva: United Nations International Strategy for Disaster Reduction.

Vafeidis AT, Nicholls RJ, McFadden L, Tol RS, Hinkel J, Spencer T, et al. (2008). A new global coastal database for impact and vulnerability analysis to sea-level rise. J Coastal Res. 24:917–24.

Van Kleef E, Bambrick H, Hales S (2010). The geographic distribution of dengue fever and the potential influence of global climate change. Geneva: TropIKA.net.

Van Lieshout M, Kovats RS, Livermore MTJ, Martens P (2004). Climate change and malaria: analysis of the SRES climate and socio-economic scenarios. Global Environ Chang. 14:87–99.

Van Vuuren DP, Lucas PL, Hilderink H (2007). Downscaling drivers of global environmental change: enabling use of global SRES scenarios at the national and grid levels. Glob Environ Change. 17:114–30.

Victora CG, Adair L, Fall C, Hallal PC, Martorell R, Richter L, et al. (2008). Maternal and child undernutrition: consequences for adult health and human capital. Lancet. 371:340–57.

WHO (2006). WHO child growth standards: length/height for age, weight-for-age, weight-for-length, weight-for-height and body mass index-for-age: methods and development. Geneva: World Health Organization.

WHO (2008). The global burden of disease: 2004 update. Geneva: World Health Organization.

WHO (2009a). Global health risks: mortality and burden of disease attributable to selected major risk factors. Geneva: World Health Organization.

WHO (2009b). Dengue guidelines for diagnosis, treatment, prevention and control. Geneva: World Health Organization and the Special Programme for Research and Training in Tropical Diseases.

WHO (2010). WHO global database on child growth and malnutrition. Geneva: World Health Organization (http://www.who.int/nutgrowthdb/en/).

WHO (2011a). Deaths estimates for 2008 by cause for WHO Member States. Geneva: World Health Organization.

WHO (2011b). WHO report on the global tobacco epidemic, 2011: warning about the dangers of tobacco. Geneva: World Health Organization.

WHO (2012). Projections of mortality and causes of death, 2015 and 2030. Geneva: World Health Organization (http://www.who.int/healthinfo/global_burden_disease/projections/en/).

Wilder-Smith A, Gubler DJ (2008). Geographic expansion of dengue: the impact of international travel. Med Clin North Am. 92:1377–90, x.

Wisner B, Blaikie P, Cannon T, Davis I (2004). At risk: natural hazards, people's vulnerability and disasters. Oxford: Routledge.

World Bank (2010a). World development indicators. Washington, DC: World Bank (http://data.worldbank.org/products/wdi).

World Bank (2010b). World development report 2010. Washington, DC: World Bank.

World Bank (2010c). Global economic prospects 2010. Washington, DC: World Bank.

Zhang Y, Bi P, Hiller JE (2008). Weather and the transmission of bacillary dysentery in Jinan, northern China: a time-series analysis. Publ Health Rep. 123:61–6.

Annex[6]

Definition of regions used in this assessment

Estimates in this assessment were made for the 21 world regions defined for the Global Burden of Disease Study (IHME, 2010). The regions are:

ASIA PACIFIC, HIGH INCOME
Brunei Darussalam
Japan
Republic of Korea
Singapore

ASIA, CENTRAL
Armenia
Azerbaijan
Georgia
Kazakhstan
Kyrgyzstan
Mongolia
Tajikistan
Turkmenistan
Uzbekistan

ASIA, EAST
China
China, Hong Kong Special Administrative Region
China, Macao Special Administrative Region
China, Province of Taiwan
Democratic People's Republic of Korea

ASIA, SOUTH
Afghanistan
Bangladesh
Bhutan
India
Nepal
Pakistan

ASIA, SOUTH-EAST
Cambodia
Christmas Island
Cocos Islands
Indonesia
Lao People's Democratic Republic
Malaysia
Maldives
Mauritius
Myanmar
Philippines
Reunion
Seychelles
Sri Lanka
Thailand
Timor-Leste
Viet Nam

AUSTRALASIA
Australia
New Zealand

CARIBBEAN
Anguilla
Antigua and Barbuda
Aruba
Bahamas
Barbados
Belize
Bermuda
British Virgin Islands
Cayman Islands
Cuba
Dominica
Dominican Republic
French Guiana
Grenada
Guadeloupe
Guyana
Haiti
Jamaica
Martinique
Montserrat
Netherlands Antilles
Puerto Rico
Saint Barthelemy
Saint Kitts and Nevis
Saint Lucia
Saint Martin
Saint Vincent and the Grenadines
Suriname
Trinidad and Tobago
Turks and Caicos Islands
US Virgin Islands

EUROPE, CENTRAL
Albania
Bosnia and Herzegovina
Bulgaria
Croatia
Czech Republic
Hungary
Montenegro
Poland
Romania
Serbia

6 The list in this annex has not been changed from the Global Burden of Disease Study and does not comply with WHO style for country references.

Slovakia
Slovenia
The former Yugoslav Republic of Macedonia

EUROPE, EASTERN

Belarus
Estonia
Latvia
Lithuania
Republic of Moldova
Russian Federation
Ukraine

EUROPE, WESTERN

Akrotiri and Dhekelia
Aland Islands
Andorra
Austria
Belgium
Channel Islands
Cyprus
Denmark
Faeroe Islands
Finland
France
Germany
Gibraltar
Greece
Greenland
Guernsey
Holy See
Iceland
Ireland
Isle of Man
Israel
Italy
Jersey
Liechtenstein
Luxembourg
Malta
Monaco
Netherlands
Norway
Portugal
San Marino
Spain
Svalbard
Sweden
Switzerland
United Kingdom of Great Britain and Northern Ireland

LATIN AMERICA, ANDEAN

Bolivia (Plurinational State of)
Ecuador
Peru

LATIN AMERICA, CENTRAL

Colombia
Costa Rica
El Salvador
Guatemala
Honduras
Mexico
Nicaragua
Panama
Venezuela

LATIN AMERICA, SOUTHERN

Argentina
Chile
Falkland Islands (Malvinas)
Uruguay

LATIN AMERICA, TROPICAL

Brazil
Paraguay

NORTH AFRICA/ MIDDLE EAST

Algeria
Bahrain
Egypt
Iran (Islamic Republic of)
Iraq
Jordan
Kuwait
Lebanon
Libyan Arab Jamahiriya
Morocco
Occupied Palestinian territory
Oman
Qatar
Saudi Arabia
Syrian Arab Republic
Tunisia
Turkey
United Arab Emirates
Western Sahara
Yemen

NORTH AMERICA, HIGH INCOME

Canada
Saint Pierre et Miquelon
United States of America

OCEANIA

American Samoa
Cook Islands
Fiji
French Polynesia
Guam
Kiribati
Marshall Islands
Micronesia (Federated States of)
Nauru
New Caledonia
Niue
Norfolk Island
Northern Mariana Islands
Palau
Papua New Guinea
Pitcairn
Samoa
Solomon Islands
Tokelau

Tonga
Tuvalu
Vanuatu
Wallis and Futuna Islands

SUB-SAHARAN AFRICA, CENTRAL

Angola
Central African Republic
Congo
Democratic Republic of the Congo
Equatorial Guinea
Gabon

SUB-SAHARAN AFRICA, EAST

Burundi
Comoros
Djibouti
Eritrea
Ethiopia
Kenya
Madagascar
Malawi
Mayotte
Mozambique
Rwanda
Somalia
Sudan
Uganda
United Republic of Tanzania
Zambia

SUB-SAHARAN AFRICA, SOUTHERN

Botswana
Lesotho
Namibia
South Africa
Swaziland
Zimbabwe

SUB-SAHARAN AFRICA, WEST

Benin
Burkina Faso
Cameroon
Cape Verde
Chad
Cote d'Ivoire
Gambia
Ghana
Guinea
Guinea-Bissau
Liberia
Mali
Mauritania
Niger
Nigeria
Saint Helena
Sao Tome and Principe
Senegal
Sierra Leone
Togo

PUBLIC HEALTH AND ENVIRONMENT

Climate change is expected to affect many aspects of health. This report presents an assessment of the expected effects on a subset of these health outcomes, for which quantitative evidence is available at the global level; heat-related mortality, coastal flood mortality, diarrhoea, malaria, dengue and undernutrition. Although the assessment does not include all potential health risks, it makes clear that climate change is likely to have significant impacts in coming decades, and indicates the scale and nature of the challenges that need to be addressed through strengthening health resilience to climate risks, and mitigating climate change.

Public Health & Environment Department (PHE)
Health Security & Environment Cluster (HSE)
World Health Organization (WHO)
Avenue Appia 20 – CH-1211 Geneva 27 – Switzerland
www.who.int/phe/en/
http://www.who.int/globalchange/en/
E-mail: carbonfootprint@who.int

ISBN 978 92 4 150769 1